NTIS #PB97-142855

SSC-395

SHIP MAINTENANCE PROJECT

Phases II and III- Volume 4

Fatigue Classification of Critical Structural Details in Tankers

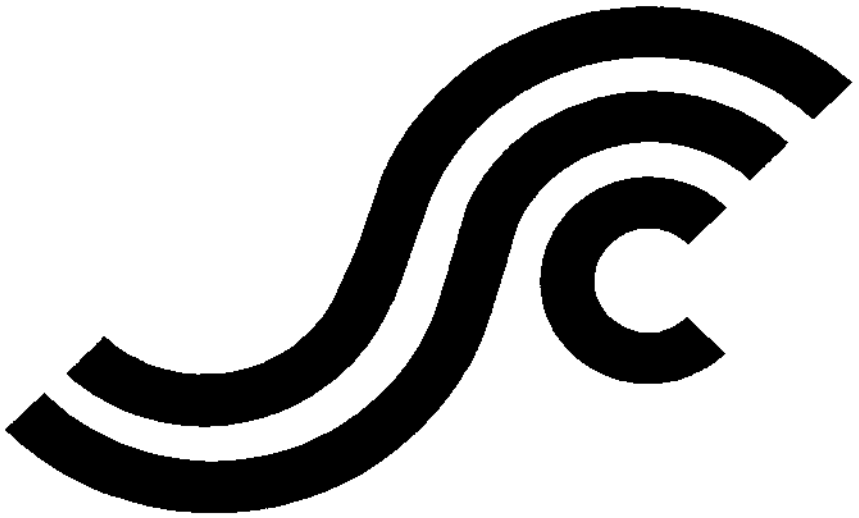

SHIP STRUCTURE COMMITTEE

1997

c|

SHIP STRUCTURE COMMITTEE

The SHIP STRUCTURE COMMITTEE is constituted to prosecute a research program to improve the hull structures of ships and other marine structures by an extension of knowledge pertaining to design, materials, and methods of construction.

RADM J. C. Card, USCG (Chairman)
Chief, Office of Marine Safety, Security
and Environmental Protection
U. S. Coast Guard

Mr. John Grinstead
Director, Policy and Legislation
Marine Regulatory Directorate
Transport Canada

Mr. Edwin B. Schimler
Associate Administrator for Ship-
building and Technology Development
Maritime Administration

Dr. Donald Liu
Senior Vice President
American Bureau of Shipping

Mr. Robert McCarthy
Director, Survivability and Structural
Integrity Group (SEA 03P)
Naval Sea Systems Command

Mr. Thomas Connors
Acting Director of Engineering (N7)
Military Sealift Command

Dr. Ross Grahm
Head, Hydronautics Section
Defence Research Establishment-Atlantic

EXECUTIVE DIRECTOR

CDR Stephen E. Sharpe, USCG
U. S. Coast Guard

CONTRACTING OFFICER TECHNICAL REPRESENTATIVE

Mr. William J. Siekierka
Naval Sea Systems Command

SHIP STRUCTURE SUBCOMMITTEE

The SHIP STRUCTURE SUBCOMMITTEE acts for the Ship Structure Committee on technical matters by providing technical coordination for determinating the goals and objectives of the program and by evaluating and interpreting the results in terms of structural design, construction, and operation.

MILITARY SEALIFT COMMAND

Mr. Robert E. Van Jones (Chairman)
Mr. Rickard A. Anderson
Mr. Michael W. Touma
Mr. Jeffrey E. Beach

MARITIME ADMINISTRATION

Mr. Frederick Seibold
Mr. Richard P. Voelker
Mr. Chao H. Lin
Dr. Walter M. Maclean

U. S. COAST GUARD

CAPT George Wright
Mr. Walter Lincoln
Mr. Rubin Sheinberg

AMERICAN BUREAU OF SHIPPING

Mr. Glenn Ashe
Mr. John F. Conlon
Mr. Phillip G. Rynn
Mr. William Hanzalek

NAVAL SEA SYSTEMS COMMAND

Mr. W. Thomas Packard
Mr. Charles L. Null
Mr. Edward Kadala
Mr. Allen H. Engle

TRANSPORT CANADA

Mr. Peter Timonin
Mr. Felix Connolly
Mr. Francois Lamanque

DEFENCE RESEARCH ESTABLISHMENT ATLANTIC

Dr. Neil Pegg
LCDR Stephen Gibson
Dr. Roger Hollingshead
Mr. John Porter

SHIP STRUCTURE SUBCOMMITTEE LIAISON MEMBERS

SOCIETY OF NAVAL ARCHITECTS AND MARINE ENGINEERS
Dr. William Sandberg

CANADA CENTRE FOR MINERALS AND ENERGY TECHNOLOGIES
Dr. William R. Tyson

U. S. NAVAL ACADEMY
Dr. Ramswar Bhattacharyya

U. S. MERCHANT MARINE ACADEMY
Dr. C. B. Kim

U. S. COAST GUARD ACADEMY
CDR Bruce R. Mustain

U. S. TECHNICAL ADIVSORY GROUP TO THE INTERNATIONAL STANDARDS ORGANIZATION
CAPT Charles Piersall

AMERICAN WELDING SOCIETY
Mr. Richard French

NATIONAL ACADEMY OF SCIENCES - MARINE BOARD
Dr. Robert Sielski

NATIONAL ACADEMY OF SCIENCES - COMMITTEE ON MARINE STRUCTURES
Dr. John Landes

WELDING RESEARCH COUNCIL
Dr. Martin Prager

AMERICAN IRON AND STEEL INSTITUTE
Mr. Alexander D. Wilson

OFFICE OF NAVAL RESEARCH
Dr. Yapa D. S. Rajapaske

MASSACHUSETTS INSTITUTE OF TECHNOLOGY
CAPT Alan J. Brown

STUDENT MEMBER
Mr. Jason Miller
Massachusetts Institute of Technology

c2

COMMITTEE ON MARINE STRUCTURES

Commission on Engineering and Technical Systems

National Academy of Sciences - National Research Council

The **COMMITTEE ON MARINE STRUCTURES** has technical cognizance over the interagency Ship Structure Committee's research program.

Dr. John Landes, *Chairman*, University of Tennessee, Knoxville, TN

Mr. Howard M. Bunch, University of Michigan, Ann Arbor, MI

Dr. Dale G. Karr, University of Michigan, Ann Arbor, MI

Mr. Andrew Kendrick, NKF Services, Montreal, Quebec

Dr. John Niedzwecki, Texas A & M University, College Station, TX

Dr. Alan Pense, NAE, Lehigh University, Bethlehem, PA

Dr. Barbara A. Shaw, Pennsylvania State University, University Park, PA

Dr. Robert Sielski, National Research Council, Washington, DC

CDR Stephen E. Sharpe, Ship Structure Committee, Washington, DC

DESIGN WORK GROUP

Dr. John Niedzwecki, *Chairman*, Texas A&M University, College Station, TX

Dr. Bilal Ayyub, University of Maryland, College Park, MD

Mr. Ovide J. Davis, Pascagoula, MS

Mr. Andy Davidson, NASSCO, San Diego, CA

Dr. Maria Celia Ximenes, Chevron Shipping Co., San Francisco, CA

Mr. Jeffrey Geiger, Bath Iron Works, Bath, ME

Mr. Hugh Rynn, Sea-Land Services, Elizabeth, NJ

MATERIALS WORK GROUP

Dr. Barbara A. Shaw, *Chairman*, Pennsylvania State University, University Park, PA

Dr. David P. Edmonds, Edison Welding Institute, Columbus, OH

Dr. John F. McIntyre, Advanced Polymer Sciences, Avon, OH

Dr. Harold S. Reemsnyder, Bethlehem Steel Corp., Bethlehem, PA

Dr. Bruce R. Somers, Lehigh University, Bethlehem, PA

RECENT SHIP STRUCTURE COMMITTEE PUBLICATIONS

Ship Structure Committee Publications - A Special Bibliography This bibliography of SSC reports may be downloaded from the internet at: "http://www.dot.gov/dotinfo/uscg/hq/nmc/nmc/ssc1/index.htm".

SSC-394 Strength Assessment of Pitted Plate Panels J. Daidola, J. Parente, I. Orisamolu, K-t. Ma 1997

SSC-393 Evaluation of Ductile Fracture Models R. Dexter, M. Gentilcore 1997

SSC-392 Probability Based Ship Design: Implementation of Design Guidelines A. Mansour, P. Wirsching, G. White, B. Ayyub 1996

SSC-391 Evaluation of Marine Structures Education in North America R. Yagle 1996

SSC-390 Corrosion Control of Inter-hull Structures M. Kikuta, M. Shimko, D Ciscom 1996

SSC-389 Inspection of Marine Structures L. Demsetz, R. Cario, R. Schulte-Strathaus, B. Bea 1996

SSC-388 Ship Structural Integrity Information System-Phase II M. Dry, R. Schulte-Strathaus, B. Bea 1996

SSC-387 Guideline for Evaluation of Finite Elements and Results R. I. Basu, K. J. Kirkhope, J. Srinivasan 1996

SSC-386 Ship's Maintenance Project R. Bea, E. Cramer, R. Schulte-Strauthaus, R. Mayoss, K. Gallion, K. Ma, R. Holzman, L. Demsetz 1995

SSC-385 Hydrodynamic Impact on Displacement Ship Hulls - An Assessment of the State of the Art J. Daidola, V. Mishkevich 1995

SSC-384 Post-Yield Strength of Icebreaking Ship Structural Members C. DesRochers, J. Crocker, R. Kumar, D. Brennan, B. Dick, S. Lantos 1995

SSC-383 Optimum Weld-Metal Strength for High Strength Steel Structures R. Dexter and M. Ferrell 1995

SSC-382 Reexamination of Design Criteria for Stiffened Plate Panels by D. Ghose and N. Nappi 1995

SSC-381 Residual Strength of Damaged Marine Structures by C. Wiernicki, D.

Member Agencies:

American Bureau of Shipping
Defence Research Establishment Atlantic
Maritime Administration
Military Sealift Command
Naval Sea Systems Command
Transport Canada
United States Coast Guard

Ship
Structure
Committee

An Interagency Advisory Committee

Address Correspondence to:

Executive Director
Ship Structure Committee
U.S. Coast Guard (G-MSE/SSC)
2100 Second Street, S.W.
Washington, D.C. 20593-0001
Ph: (202) 267-0003
Fax: (202) 267-4816

SSC-395
SR-1360
SR-1371

February 27, 1997

SHIP MAINTENANCE PROJECT
Phases II and III

This report presents the results of the second and third phases of the subject project of which phase one was first presented in our four volume set -- SSC-386. These studies investigated the development of engineering technology that could lead improvements in structural maintenance for new and existing tankers. These projects built further upon the work started in phase I specifically focusing on critical structural details and corrosion limits.

The report has been divided into five volumes, each of which may stand alone. Volume one opens with a summary of all three phases by Professor Robert G. Bea, the coordinating investigator for the program and follows with a report on corrosion limits for tankers. The second and fifth volumes look into evaluation of cracked critical structural details in tankers. The third volume presents theory and user instructions for software to manage repair of critical structural details. The fourth volume applies to fatigue classification of critical structural details. The software developed in the project will be available on the next Ship Structure Committee CD Rom release, which is anticipated to be released in the next year. The industry is encouraged to contact Professor Bea at the University of California, Berkeley to discuss further possibilities in application of the work undertaken here in the industry.

J. C. CARD
Rear Admiral, U.S. Coast Guard
Chairman, Ship Structure Committee

1
ZX

Technical Report Documentation Page

1. Report No.	2. Government Accession No.	3. Recipient's Catalog No.
SSC-395-4	PB97-142855	

4. Title and Subtitle	5. Report Date
Ship Maintenance Project Phases II and III Volume 4 Fatigue Classification of Critical Structural Details in Tankers	1997
	6. Performing Organization Code
	8. Performing Organization Report No.
7. Author(s) Robert Bea, Rolf Schulte-Strathaus	
9. Performing Agency Name and Address University of California at Berkeley Department of Naval Architecture and Ocean Engineering Berkeley, CA 94720	10. Work Unit No. (TRAIS)
	11. Contract or Grant No.
	13. Type of Report and Period Covered Final
12. Sponsoring Agency Name and Address Ship Structure Committee U. S. Coast Guard (G-MSE/SSC) 2100 Second St. S.W. Washington, DC 21\0593-0001	14. Sponsoring Agency Code G-M

15. Supplementary Notes
Sponsored by the Ship Structure Committee. Jointly funded by other organizations as a joint industry project. See inside the report for futher details on sponsors.

16. Abstract
This report presents the results of the second and third phases of the subject project of which phase one was first presented in our four volume set - SSC-386. These studies investigated the development of engineering technology that could lead to improvements in structural maintenance for new and existing tankers. These projects built further upon the work started in phase I specifically focusing on critical structural details and corrosion limits.

The report has been divided into five volumes, each of which may stand alone. Volume one opens with a summary of all three phases by Professor Robert G. Bea, the coordinating investigator for the program, and follows with a report on corrosion limits for tankers. The second and fifth volumes look into evaluation of cracked critical structural details in tankers. The third volume presents theory and user instructions for software to manage repair of critical structural details. The fourth volume applies to fatigue classification of critical structural details. The software developed in the project will be available on the next Ship Structure Committee CD Rom release which is anticipated to be released in the next year. The industry is encouraged to contact Professor Bea at the University of California, Berkeley to discuss further possibilities in application of the work undertaken here in the industry.

17. Key Words	18. Distribution Statement
fatigue, critical structural details, tanker structures, fatigue classification	Distribution unlimited, available from: National Technical Information Service U.S. Department of Commerce Springfield, VA 22151 (703)487-4690

19. Security Classif. (of this report)	20. SECURITY CLASSIF. (of this page)	21. No. of Pages	22. Price
Unclassified	Unclassified	184	$38.00

Form DOT F 1700.7 (8/72) Reproduction of form and completed page is authorized.

NIST United States Department of Commerce
Technology Administration
National Institute of Standards and Technology
Metric Program, Gaithersburg, MD 20899

METRIC CONVERSION CARD

Approximate Conversions to Metric Measures

Symbol	When You Know	Multiply by	To Find	Symbol
LENGTH				
in	inches	2.5	centimeters	cm
ft	feet	30	centimeters	cm
yd	yards	0.9	meters	m
mi	miles	1.6	kilometers	km
AREA				
in^2	square inches	6.5	square centimeters	cm^2
ft^2	square feet	0.09	square meters	m^2
yd^2	square yards	0.8	square meters	m^2
mi^2	square miles	2.6	square kilometers	km^2
	acres	0.4	hectares	ha
MASS (weight)				
oz	ounces	28	grams	g
lb	pounds	0.45	kilograms	kg
	short tons (2000 lb)	0.9	metric ton	t
VOLUME				
tsp	teaspoons	5	milliliters	mL
Tbsp	tablespoons	15	milliliters	mL
in^3	cubic inches	16	milliliters	mL
fl oz	fluid ounces	30	milliliters	mL
c	cups	0.24	liters	L
pt	pints	0.47	liters	L
qt	quarts	0.95	liters	L
gal	gallons	3.8	liters	L
ft^3	cubic feet	0.03	cubic meters	m^3
yd^3	cubic yards	0.76	cubic meters	m^3
TEMPERATURE (exact)				
°F	degrees Fahrenheit	subtract 32, multiply by 5/9	degrees Celsius	°C

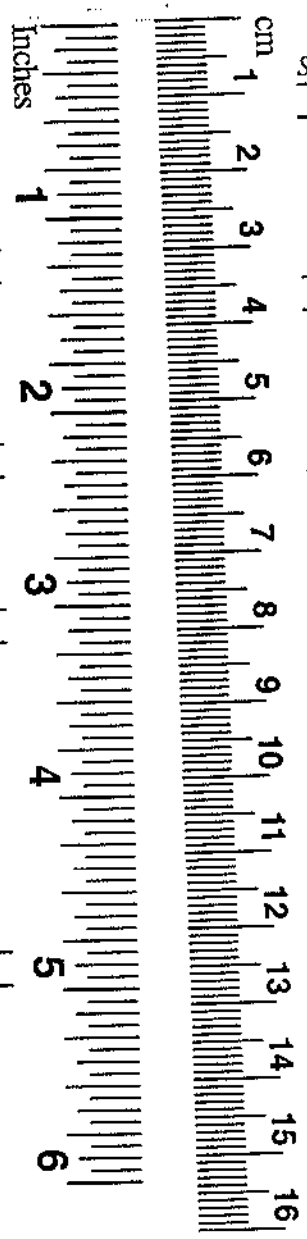

Approximate Conversions from Metric Measures

Symbol	When You Know	Multiply by	To Find	Symbol
LENGTH				
mm	millimeters	0.04	inches	in
cm	centimeters	0.4	inches	in
m	meters	3.3	feet	ft
m	meters	1.1	yards	yd
km	kilometers	0.6	miles	mi
AREA				
cm^2	square centimeters	0.16	square inches	in^2
m^2	square meters	1.2	square yards	yd^2
km^2	square kilometers	0.4	square miles	mi^2
ha	hectares (10,000 m^2)	2.5	acres	
MASS (weight)				
g	grams	0.035	ounces	oz
kg	kilograms	2.2	pounds	lb
t	metric ton (1,000 kg)	1.1	short tons	
VOLUME				
mL	milliliters	0.03	fluid ounces	fl oz
mL	milliliters	0.06	cubic inches	in^3
L	liters	2.1	pints	pt
L	liters	1.06	quarts	qt
L	liters	0.26	gallons	gal
m^3	cubic meters	35	cubic feet	ft^3
m^3	cubic meters	1.3	cubic yards	yd^3
TEMPERATURE (exact)				
°C	degrees Celsius	multiply by 9/5, add 32	degrees Fahrenheit	°F

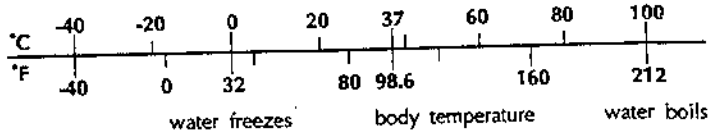

Ship Structural Maintenance Projects II and III
Cross Reference Listing

SSC Vol.	SMP #	Title	Authors	Date	NTIS Number
	II				
2	-1	Fatigue Analysis of CSD in a 150K DWT Double-Hull Tanker	Xu, Bea	10/93	PB97-142830
2	-2	Fatigue Analysis of CSD in a 190K DWT Double-Hull Tanker	Xu, Bea	10/93	PB97-142830
2	-3	CSD Library and Finite Element Stress Contours	Xu, Bea	10/93	PB97-142830
1	-4	Development of a Rational Basis for Defining Corrosion Limits in Tankers	Mayoss, Bea	12/93	PB97-142822
3	-4a	RMS for CSD in Ships - User Manual	Ma, Bea	9/93	PB97-142848
3	-4b	RMS for CSD in Ships - Theory	Ma, Bea	9/93	PB97-142848
4		Fatigue Classification of CSD in Tankers	Schulte-Strathaus, Bea	1/94	PB97-142855
	III				
3	-1-1	RMS for Fatigue Cracks in Ship CSDs	Ma, Bea	10/94	PB97-142848
5	-2-1	Fitness for Purpose Analysis Procedure of Cracked CSDs in Tankers	Xu, Bea	1/95	PB97-142863
5	-2-2	A Load Shedding Model of Fracture Mechanics Analysis of Cracked SCDs in Tankers	Xu, Bea	1/95	PB97-142863
5	-2-3	FRACTURE- A Computer Code for Fracture Mechanics Analysis of Crack Growth of Cracked CSD in Tankers	Xu, Bea	1/95	PB97-142863
5	-5	Pro-IMR: A Computer Code for Probability-Based Inspection Planning	Xu, Bea	10/94	PB97-142863

Fatigue Classification of Critical Structural Details in Tankers

Rolf Schulte-Strathaus
and
Professor Robert G. Bea

Department of Naval Architecture and Offshore Engineering
University of California, Berkeley

PREFACE

The one year Joint Industry Research Project "**Fatigue Classification of Critical Structural Details in Tankers (FACTS)**" was initiated in 1992 by the University of California at Berkeley Department of Naval Architecture and Offshore Engineering as a follow-up project of the "**Structural Maintenance for New and Existing Ships Project (SMP)**. The FACTS project will develop methods to obtain calibrated S-N curves for the use with finite element analysis results. In addition a selection system for S-N information will be developed.

This project was made possible by the following sponsoring organizations:

- **American Bureau of Shipping**
- **ARCO Marine Ltd.**
- **Newport News Shipbuilding & Dry Dock Co.**
- **Ship Structure Committee**

This report documents the development of calibrated S-N curves for the use in conjunction with hot-spot stresses obtained from finite element analyes. In addition the development of a *System for the Selection of S-N curves* is documented.

Contents

List of Tables

List of Figures

15
16X

Chapter 1

Introduction

In the following, the development of the calibrated S-N curves for the use with hot-spot stresses obtained from finite element analyses is presented. This development was one of the objectives of the FACTS project.

The FACTS project (FAtigue Classification of Critical Structural Details in TankerS) is a one-year joint industry project, which was initiated by the Department of Naval Architecture & Offshore Engineering at the University of California at Berkeley in September 1992. The project is a follow-up of the **Structural Maintenance Project for New and Existing Ships**, a two-year, international joint industry project, which was conducted in 1990 -1992.

The FACTS project focuses on two topics:

- **Fatigue Classification of Critical Structural Details (CSD)**
- **Management System for the Selection of S-N Curves**

1.1 Fatigue Classification of CSD

Although fatigue cracking in CSD in general does not result in ship casualties, it is one of the two main causes for repair and maintenance operations. The other major cause is corrosion.

The increase in the number of fatigue cracks in tankers fundamentally is the result of increases in stress levels in CSD. These durability problems are the product of attempts to facilitate construction, and extrapolations of rule based design methods to the current generation of tankers. To avoid such problems in the next generation of these ships and yet optimize structural weight, it is desirable to perform realistic fatigue analyses of CSD. It is also desirable to be able to perform realistic fatigue analyses of repairs to CSD in existing vessels. The accuracy of these analyses depends strongly on the representation of the long-term stress ranges and on the use of realistic S-N (Stress range - Number of cycles to failure) curves.

This project will develop a procedure to use the stresses at the *Hot Spots* (areas of high stress concentrations) of proposed CSD. These *Hot Spots* are identified based on the results from finite element analyses (FEA) of a CSD. This approach makes it necessary to define the way the hot spot stresses are obtained from FEA and to use S-N curves which are calibrated for this procedure.

17

This development will allow the definition of a consistent and realistic approach for fatigue analyses of CSD in tankers.

1.2 Management System for the Selection of S-N curves

At the present time S-N curves are selected by engineers mainly based on experience and the use of established rules. These rules can be as simple as the association of a certain S-N curve with a specific detail or as sophisticated as the choice of a S-N curve based on the type of weld and the direction of the principal stresses.

This project proposes to develop a computer based management system which will assist naval architects in choosing appropriate S-N curves for given CSD. The main focus of this project will be to develop the basic framework of this system. This will serve as a basis for future development of rules to assist engineers in the selection of S-N curves for fatigue analyses.

1.3 Overview

This report is divided into 6 chapters; In **Chapter 2** the theoretical background related to the S-N fatigue life evaluation and the development of S-N curves based on fatigue tests is briefly described. Also included is a description of the main sets of S-N curves that are currently used for the fatigue life evaluation of CSD, i.e. IIW curves and UK department of Energy curves.

Chapter 3 describes in detail the development of the size definition of the finite element mesh near the hot-spot. This definition is based on parametric analyses for simple geometries with known stress concentration factors (K_t).

Chapter 4 contains the results of the calibration analyses for the S-N test specimen. It describes the finite element models, the loads and the resulting stress concentration factors. The calculated stress concentration factors are then used to calibrate the original S-N curves. This calibration process is also documented.

Chapter 5 describes the implementation of the calibrated S-N curves into the SMP fatigue analysis software. Using the modified software the verification cases that have been analysed as part of the SMP project, see [1], are re-analysed. The results of these analyses are documented.

Chapter 6 documents the development of the *System for the Selection of S-N Curves* including a detailed description of the implemented S-N curve database.

Chapter 2

Fatigue Calculation

2.1 Introduction

It has been the main purpose of the SMP project to develop a system to calculate the fatigue damage for Critical Structural Details (CSD) in tankers. The procedure was intended for the use for the design and repair of CSD. In addition to the analysis of uncracked CSD a method for the residual life estimation of cracked CSD had to be developed.

In order to take account of the uncertainties inherent in the calculation process a reliability format has been used. This format is based on the standard Miner summation method and assumes all uncertainties to have a lognormal probability distribution.

The fatigue strength is represented in the form of stress range vs. number of cycles curves (S-N curves). For cracked CSD a method has been developed to calculate the S-N curve based on a given crack length. For uncracked CSD the S-N curve representation depends on the type of stress and the stress recovery procedure used for the determination of the long-term loads. In this chapter the necessary theory for the above mentioned components is documented. This includes

- the Palmgren-Miner cumulative damage model
- the linear-elastic fracture mechanics model
- the Wirsching fatigue reliability model
- a description of the different fatigue calculation methods
- the FM / S-N model to develop S-N curves for cracked CSD

2.2 Cumulative Damage

For a constant amplitude cyclic loading, the number of cycles to failure is in most cases determined through fatigue tests of small specimen. Based on the results of these tests curves that characterize the fatigue behaviour under constant amplitude loading are developed. These curve are in general of the form

$$NS^m = K \tag{2.1}$$

3. the local notch strain approach

4. the fracture mechanics approach

For the purpose of fatigue life evaluations of welded details in the design stage only the first two approaches are of interest. Both approaches require the definition of the fatigue strength of the welded detail in terms of a stress range - number of cycle curve (S-N curve).

In the following both the nominal stress and the hot-spot stress approach are described. Using the nominal stress approach including a geometric stress concentration factor is in principle identical to the hot-spot stress approach.

2.4.2 Nominal Stress Approach

The nominal stress is generally calculated using the simple formula

$$\sigma_x = \frac{F}{A} + \frac{M}{W} \qquad (2.4)$$

where

F = axial force
A = area of cross section
M = bending moment
W = section modulus

Global geometric effects cause stresses that exceed those calculated by elementary stress analysis. The stresses caused by global geometric effects must therefore be included in the nominal stress, if the nominal stress approach is to be used for fatigue life evaluation.

The fatigue strength is defined through S-N curves. The S-N curves used in combination with nominal stresses are determined by testing either small specimen or near full-scale beams. It is essential that the stress used to develop the S-N curves is the nominal stress. All local effects and all local notch effects are thus implicitly included in the denoted fatigue strength.

It is important that the stress analysis is performed to the same level as the laboratory tests. Thus, the nominal stress must include the global geometric effects.

The nominal stress approach forms the basis for most design rules for steel structures and is therefore widely used. In [6] it is stated that the nominal stress yields satisfactory results with minimum calculation effort under the following conditions:

- there is a well defined nominal stress, not complicated by global geometric effects
- the local geometry is comparable with one of those compiled in the design rules
- variable amplitude loading does not consist mainly of stress ranges below the constant amplitude endurance limit

2.4.3 Hot-Spot Stress Approach

A hot-spot is defined as critical point in a structure, usually at a weld toe, where a fatigue crack is supposed to initiate. The hot-spot stress is the value of the structural stress at the hot-spot. Although the hot-spot is located at a local notch, the peak stress caused by the local notch is excluded from the hot-spot stress.

The structural stress is defined in [6] as the sum of membrane and shell bending stresses in structures consisting of plate elements or curved shells. The structural stress can be calculated by any suitable method, e.g. theory of shells or the finite element method (FEM). The structural stress contains the effects of geometric discontinuities which can be caused e.g. by welded attachment or misalignments.

Fatigue strength for the use with the hot-spot approach is determined from test pieces of different forms. Structural strains are measured with strain gauges at several locations along the weld toe. The principal stress is then extrapolated to the hot-spot. Since the strain gauges are placed sufficiently far away from the weld toe to exclude the effects of the local notch from the measured strains, the hot-spot strain includes both global and local geometric effects but not the local notch effects.

It is important to note that the stress and strain analyses used in the fatigue analysis yield results comparable with the fatigue strength determination used for the development of the S-N curve. According to [6] there are three possible approaches to determine the hot-spot stress for a welded detail

1. the calculated nominal stress is multiplied by the stress concentration factor, K_s, valid for the local geometry
2. strain ranges are measured duing prototype or model tests at the hot-spot
3. stresses and strains are analysed by FEM using shell or solid elements

One advantage of the hot-spot approach is that one S-N curve can be used to predict the fatigue life of many types of joint configurations. Different S-N curves are only needed if the variations in the smoothness of the local notch or the material thickness effect are taken into account.

Based on the definition of the structural stress the peak stress is excluded from the hot-spot stress. For hot-spot stresses obtained from finite elemente analyses the situation is complicated by the fact that the stress cannot be unambiguously calculated since it depends both on the mesh size and the stress recovery procedure.

According to [6] the hot-spot approach is most suitable for welds transverse to the direction of the fluctuating stresses. Compared with the nominal stress approach, this approach is more suitable for use in the following cases

1. there is no clearly defined nominal stress due to complicated geometric effects
2. the local geometry is not comparable with any of those cases compiled in the design rules based on the nominal stress method
3. for the above mentined reasons, the finite element method is in use with shell or solid element modelling
4. field testing of prototype structures is performed using strain gauge measurements
5. the offset or angular misalignments exceed the fabrication tolerances, which are implicitly basic conditions for the use of the nominal stress approach

Since the location of the hot-spot is in general known, it is possible to automate the stress recovery procedure of a finite element analyses. For complex details it is not possible to determine the nominal stress in the same automated way. The possibility to automate the stress recovery is another advantage of the hot-spot stress approach.

2.4.4 Conclusions for Ship Critical Structural Details

To perform fatigue life evaluations of ship Critical Structural Details (CSD) in the design or repair stage only the nominal stress or the hot-spot stress approach are suitable. The nominal stress approach is widely used based on class requirements and recommended procedures.

However, for the purpose of developing an automated system to perform fatigue life evaluations this approach is not suitable. Typical ship CSD are complex welded details where global geometric effects cannot easily be analysed. The determination of the nominal stress generally requires a visual inspection of the analysis results.

The hot-spot stress approach allows it to develop automated stress recovery procedures based on finite element analyses of the CSD. One difficulty, which has significantly hindered the usage of the hot-spot stress approach, is the fact that the S-N curve used to represent the fatigue strength of the CSD at the hot-spot has to be based on the same stress recovery procedure.

The greatest difficulty in using the hot-spot stress approach is the definition of the appropriate S-N curve. The curve Most design S-N curves have been developed based on the nominal stress in the test specimen. These curves cannot be used for the hot-spot approach. Although many S-N tests have been performed using strain measurements and extrapolating to the hot-spot, the resulting S-N curves have to be used in conjunction with hot-spot stresses obtained by using a stress recovery procedure identical to the one used in the S-N tests.

A calibration procedure has been developed that allows it to transform design S-N curves into S-N curves that can be used in conjunction with hot-spot stresses obtained using a defined stress recovery procedure. The procedure and its application are documented in chapter 4.

Table 2.1: DoE: Details of Basic S-N curves - Air

	$N \leq 10^7$				$N > 10^7$	
Class	$\log a$	$\log s$	$\log \bar{a}$	m	$\log \bar{a}$	m
B	15.3697	0.1821	15.01	4.0	17.01	5.0
C	14.0342	0.2041	13.63	3.5	16.47	5.0
D	12.6007	0.2095	12.18	3.0	15.63	5.0
E	12.5169	0.2509	12.02	3.0	15.37	5.0
F	12.2370	0.2183	11.80	3.0	15.00	5.0
F2	12.0900	0.2279	11.63	3.0	14.72	5.0
G	11.7525	0.1793	11.39	3.0	14.32	5.0
W	11.5662	0.1846	11.20	3.0	14.00	5.0
T	12.6606	0.2484	12.16	3.0	15.62	5.0

The S-N curve is written as

$$\begin{aligned} \log(N) &= \log a - 2\log s - m\log \Delta\sigma \\ &= \log \bar{a} - m\log \Delta\sigma \end{aligned}$$

where:

N predicted number of cycles to failure for stress range $\Delta\sigma$
$\log a$ cut of the the $\log N$-axis by the mean S-N curve
$\log s$ standard deviation of $\log N$
m negative inverse slope of the S-N curve
$\log \bar{a}$ $\log a - 2\log s$

25

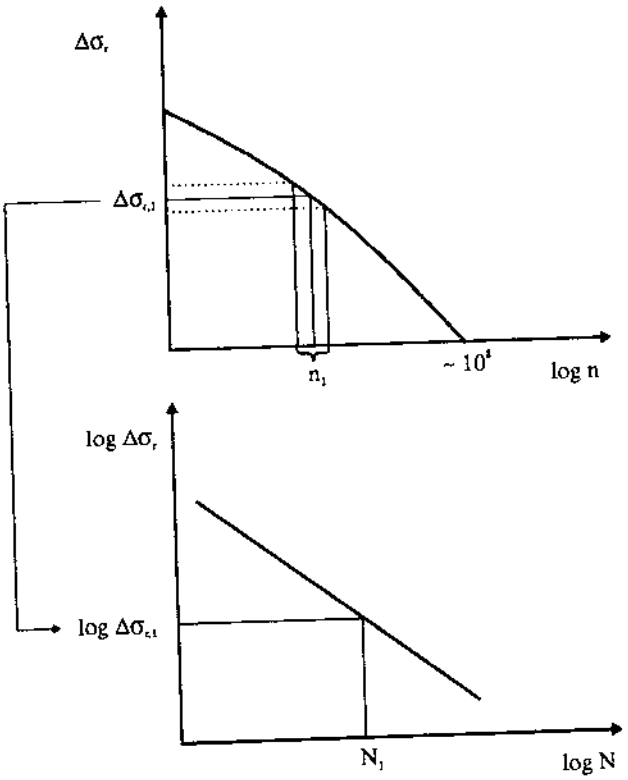

Figure 2.1: The Miner summation procedure for one stress block

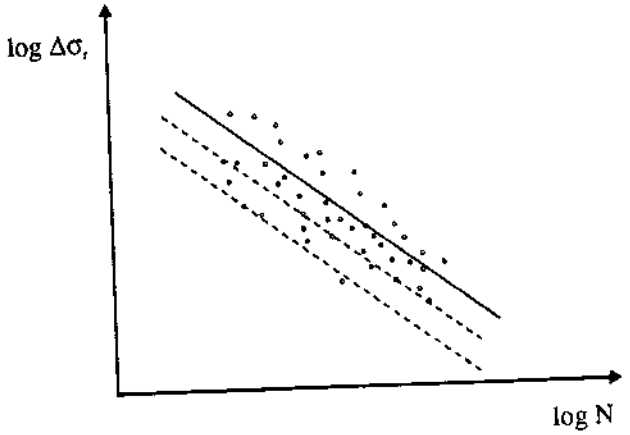

Figure 2.2: Schematic regression lines for fatigue life at different safety factors

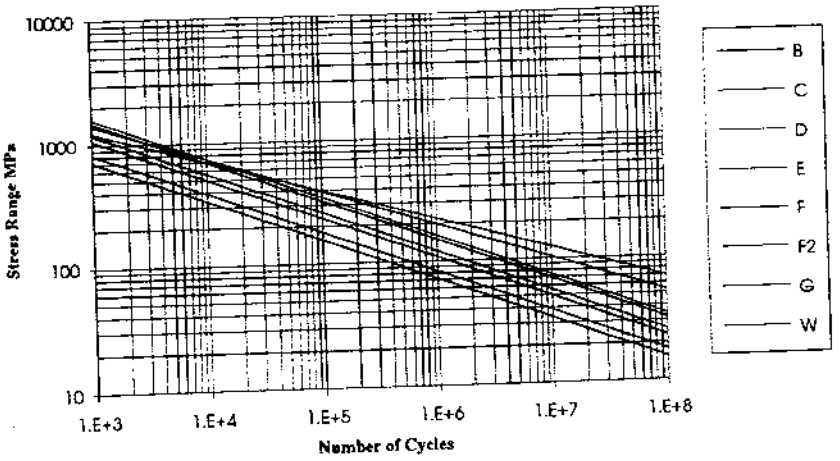

Figure 2.3: Fatigue design S-N curve for planar welded joints, DoE, NPD, DnV

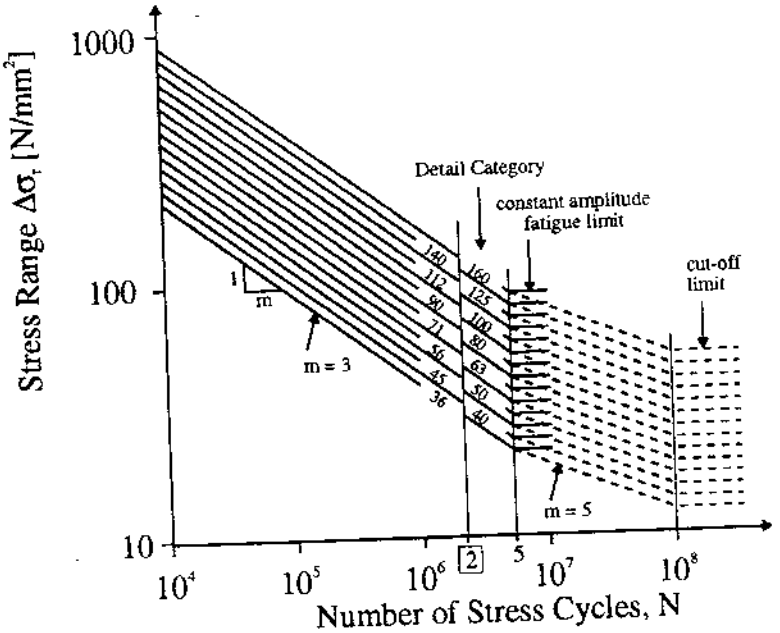

Figure 2.4: Fatigue design S-N curve for planar welded joints, IIW/ECCS

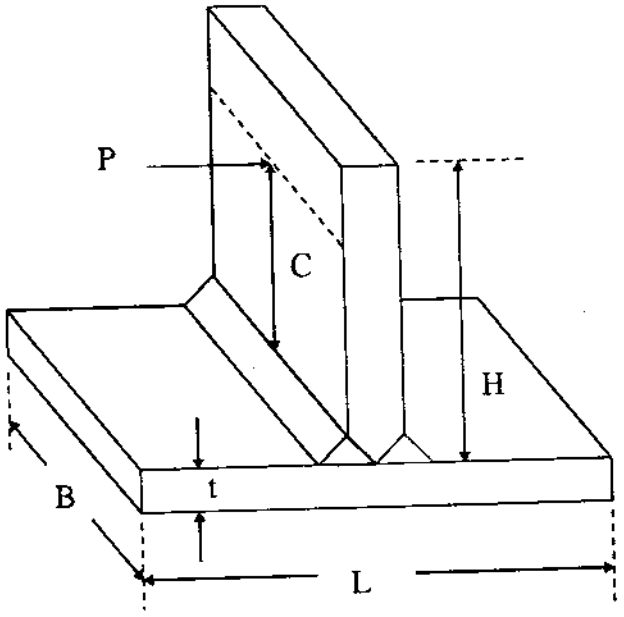

Figure 2.5: Geometry for HTS T-joint

with N = Number of cycles to failure
S = Stress range
m = Empirical constant
K = Empirical constant

The fatigue life of a structural detail can be calculated using the theory of cumulative damage. Cumulative damage is in general the fatigue damage under stochastic or random loading. The most well-known theory to calculate the cumulative damage is the *Palmgren-Miner summation model*, [2], [3].

The basic assumption in the Miner summation method is that the damage D for one load cycle is

$$D = \frac{1}{N} \tag{2.2}$$

Here N defines the number of constant amplitude cycles at a given stress range that cause failure.

For a long-term load on a structure consisting of i blocks of stress ranges $S_{r,i}$ each with a number of cycles n_i the total damage is

$$D = \sum_i \frac{n_i}{N_i} \tag{2.3}$$

Failure occurs for D = 1. N_i defines the number of cycles to failure for the stress range in block i.

Fig. (2.1) shows qualitatively the procedure. It will be shown that the Miner summation conforms with the integration of the Paris equation. This fact is of major importance for the development of the FM / S-N approach, which will be used to calculate the residual life of critical structural details.

2.3 Establishing of Design S-N Curves

Design S-N curves are based on constant amplitude fatigue tests of in general small scale specimen. A statistical analysis is performed to determine the mean regression line on a log-log scale. Confidence intervals based on the standard deviation of the test samples are calculated. The confidence interval defines the probability that similar S-N test results will be within the given limits.

Design curves for a given class of welds are defined by the mean line and the standard deviation for different safety levels, Fig. (2.2) shows schematically the mean fatigue life, mean minus one standard deviation (b) and minus two standard deviations (c). Most design curves use curve (c) to account for a confidence level of 94.5 %.

For the fatigue design of structural details several engineering guidelines have been established, primarily for tubular joints in the offshore industry and for welded structures like bridges. The fatigue strength in these guidelines is normally characterized by a set of empirical S-N curves for different welded details.

The building codes of many different organizations (American Welding Society, AWS, Det norske Veritas, DnV, National Petroleum Directorate, NPD) use the S-N curves established by the UK Department of Energy (UKDEn). These curves have been derived on the basis of statistical analyses of S-N data for each design class. This procedure has resulted in differences in the slope of the curves, the fatigue limit and the categorization of weld details between the curves for the design classes.

Table (2.1) documents the curve parameters for the different UKDEn S-N curves and Fig. (2.3) shows the S-N curves.

In the recommendations of the International Institute of Welding (IIW) the inverse procedure has been used. Here conveniently spaced S-N curves have been defined a priori, see Fig. (2.4), and the various weld details have been allocated to these curves by judgement based on statistical analysis of S-N data. For the purpose of fatigue design this set of S-N curves is more convenient to use.

2.3.1 Fatigue Properties of High Tensile Steel (HTS)

The use of HTS allows development of higher design stresses; thus, decreasing member thicknesses and helping reduce building costs. For this reason the use of HTS has rapidly increased in the last years. This fact has led to increased research activity especially with regard to the fatigue properties of HTS in order to determine the influences of the use of HTS on the overall strength of ships and on the fatigue behaviour of ship structural details built of HTS.

A study conducted by British Steel [4] has summarized the results of research regarding the fatigue behaviour of HTS . The tests were performed on 50 mm thick parent plate and welded T-joints of 25, 50 and 80 mm. The joints were both in air and in seawater. Fig. (2.5) shows the geometry of the T-joint. The variables for the tests were plate thickness, stress ratio and PWHT (Post Weld Heat Treatment).

The results of this test programs imply that the fatigue endurance of HTS in air and seawater is similar to that of a lower strength steel for a similar thickness of joint. It can therefore be concluded that the design rules for lower strength steel are applicable to HTS. This means that the same S-N curves can be used for both the lower strength steels and HTS. For this reason it can be benefical to use HTS especially in areas not sensitive to fatigue loading.

In a different publication [5] it is stated that the use of HTS has brought about better designing of structural details to avoid high stress concentration and better production quality control. The 'penalties of using HTS, which include lower relative fatigue strength and buckling by corrosion can be minimized by further research and technical development. Although this paper is therefore very optimistic about the use of HTS, it does not imply that HTS has to be treated differently for fatigue life calculations.

On the basis of this information, it has been concluded that the same S-N curves can be used for both mild steels and HTS.

2.4 Fatigue Analysis Approaches

2.4.1 Introduction

In [6] a good overview over the different approaches to fatigue life prediction is presented. In addition recommendations are given with respect to stress calculations for welded details.

The approaches differ in the extent of stress and strain analyses, i.e. the levels of stress raisers which are taken into account. Four basic approaches exist

1. the nominal stress approach
2. the hot-spot stress approach

Chapter 3

Definition of Mesh Size near Hot Spots

3.1 Introduction

In order to perform fatigue life analyses it is necessary to have precise knowledge about the stress level for a given loading in a CSD. Traditionally the *nominal* stress has been used to describe the fatigue loading, see section 2.4. The increase in the stress level at the hot-spot due to the geometry of the detail is taken into consideration through the choice of the S-N curve.

The finite element method makes it possible to directly obtain the *hot-spot* stress. Unfortunately, for certain geometries the accuracy of the finite element results depends directly on the element size for a given type of element. A finer mesh will in general improve the accuracy of the results, but will also increase the amount of time necessary for the analysis. The calculated hot-spot stress converges to the actual stress in the structure with decreasing element size.

For geometrically discontinuous details, e.g. sudden change in the cross section due to a bracket, the hot-spot stress does not converge, but will keep increasing.

In order to develop guidelines for the mesh size to be used for the calibration analyses it was necessary to perform parametric analyses for simple details with known stress concentration factors (K_t).

3.2 General Procedure

The database analyses that have been performed as part of the SMP project, [7], have shown that one type of CSD, the side shell longitudinal to webframe connection, experiences the majority of fatigue damages. This detail is shown in Fig. (3.1).

In order to perform fatigue analyses using an automated recovery of the hot spot stresses a finite number of hot spots have been defined. The hot spots in the cutout are shown in Fig. (3.2) and the hot spots at the connection of the longitudinal to the stiffening bracket are shown in Fig. (3.3).

It can be seen from these figures that the hot spots can be classified in two categories:

1. **Parent material with smooth change of geometry**, e.g. radius of the webframe cutout.
2. **Welded connections with sudden change of geometry**, e.g. connection of bracket to sideshell longitudinal.

For the first category the *exact* stress at the hot spot can be calculated with an acceptable accuracy by using a fine enough mesh near the hot spot. Parametric analyses have to be performed to determine the minimum fineness of the mesh.

For the second category the situation is more complicated. Due to the geometric singularity at the hot spot the theoretical stress will reach infinity, which results in the formation of a local plastic zone. A linear elastic finite element analysis can not represent this behaviour. A reduction of the element size near the hot spot will therefore result in an increased hot spot stress.

Several stress interpolation procedures are currently used to obtain a hot spot stress based on linear static finite element analysis that agrees well with measured hot spot stresses. Parametric analyses of simple geometries have to be performed to determine a stress recovery procedure in combination with a defined mesh size that will result in consistent hot spot stresses for different geometries.

The geometries for the parametric analyses are chosen to resemble hot spot locations found in ship CSD. In addition typical dimensions of ship CSD are used for these simple details. Fig. (3.4) shows the construction drawing of a typical sideshell longitudinal to webframe connection. The dimensions are in [mm].

All finite element analyses are performed using COSMOS/M [1] . This system contains a graphic, interactive pre- and post-processor, GEOSTAR, that has been used to develop the models and to view the calculated deformations and stresses. The linear elastic, static module SSTAR of COSMOS/M has been used to perform the analyses.

3.3 Mesh Size for Smooth Change of Geometry

3.3.1 Selected Geometry and Dimensions

As seen in Fig. (3.2) several of the hot spots in the cut-out of the webframe are located in the parent material and the observed stress concentration is caused by the smooth change of the geometry, e.g. the radius at the corner of the cut-out.

The closest geometry with a known stress concentration factor is the finite width plate with a transverse hole under axial loading. The stress concentration factors for this case for different ratios of hole diameter to plate width are found in [8].

Fig. (3.5) shows the geometry for this case and the curve, which relates the stress concentration factor K_t to the ratio a/w, where a is the hole diameter and w is the plate width. K_t is based on the net section.

For the test case the following ratio a/w has been chosen:

$$a/w = 0.20$$

The resulting stress concentration factor is:

$$K_t = 2.53$$

[1] COSMOS/M Finite Element Analysis System, Structural Research & Analysis Corporation, Santa Monica, CA

The actual dimensions of the simple model have been chosen to be similar to the dimensions of the sideshell longitudinal detail shown in Fig. (3.4). The chosen dimensions are shown in Fig. (3.6).

The area where the highest stress concentration due to axial loading occurs, i.e. the location of K_t , is also indicated in Fig. (3.6).

An axial force of 400 kN on both sides of the plate will result in a *nominal* stress of $100 N/mm^2$. This facilitates the determination of K_t . This axial force will be uniformly distributed over the width of the plate.

In order to assure a uniform stress distribution over the width of the plate near the hole, a large length to width ratio has been selected for the plate.

3.3.2 Finite Element Model

Due to the symmetry of the plate only one quarter of the plate has been modelled. Ship CSD are in general modelled using thin shell elements to account for the out-of plane loads. Since this simple model is used for parametric analyses to determine the best mesh size to be used for ship CSD, four-node quadrilateral thin shell elements are used to model the plate.

A second model has been prepared using 8-node solid elements. The plate thickness is modelled by one element. The plate model has been prepared to compare the accuracy of the results and to compare the performance characteristics, i.e. the number of equations to be solved for otherwise identical meshes. Solid models have the advantage the out-of-plane behaviour can be easily analysed, which allows it to evaluate the stress concentrations due to out-of-plane bending in lap-joints.

The solid models are generated by extruding the two-dimensional shell models in the thickness direction and thus creating volume elements. This procedure assures that the elements for the shell and the solid model have the same shape.

In order to account for the large stress gradient near the location of K_t the element size is small compared to other areas of the model. The number of elements and the node spacing have been chosen to assure aspect ratios close to unity near the hot spot.

The axial force has been applied as a pressure acting on the surface. This assures that the resulting fixed-end moments are applied automatically. Fig. (3.7) shows the first very coarse mesh (8 elements along the quarter circle) including displacement and force boundary conditions.

Truss elements with minimal stiffness are placed along the quarter circle to obtain the stresses around the hole. This method facilitates the stress recovery.

A parametric input method has been used that allows it to vary the mesh size easily. The number of elements along the quarter circle has been used as an indicator of the relative fineness of the mesh. All other mesh geometries have been varied accordingly to assure reasonable aspect ratios throughout the mesh, especially near the hot spot.

Eleven different models have been prepared and analysed. The number of elements for the quarter circle has been varied between 6 and 44 elements. Fig. (3.8) shows an intermediate mesh with 12 elements for the quarter circle. Fig. (3.9) shows the finest mesh, where 44 elements are used to model the quarter circle.

3.3.3 Analysis and Interpretation

A linear static finite element analysis has been performed for each of the eleven **shell** models and the eleven **solid** models. The purpose of these analyses was to compare the calculated hot spot stress concentration factor K_t against the theoretical value obtained from [8]. Based on this comparison the minimum mesh for an acceptable error margin of the hot spot stress K_t can be selected.

Figs. (3.10, 3.11, 3.12) show the axial stresses in x-direction for meshes with 8, 12 and 44 elements for the quarter circle, respectively. It can be seen that for the very coarse mesh (8 elements for the quarter circle) the location of the stress concentration is not very accurately defined and the interpolated stress distribution is very ragged.

For the medium mesh (12 elements for the quarter circle) both the location of the stress concentration and the interpolated stress distribution are much more reasonable.

The stress plot for the very fine mesh (44 elements for the quarter circle) does not show a significant improvement in the location of the stress concentration or the interpolated stress distribution.

Table (3.1) summarizes the performed analyses. For both the **shell** element and the **solid** element models the number of equations and the total solution time is listed for the 11 different meshes.

It can be seen that the **shell** element meshes require less analysis time, which was expected. The performance penalty for **solid** elements is smaller than expected due to the fact that only one layer of elements is used to model the thickness of the plate.

The main purpose of the parametric analyses is to determine the mesh size that will result in an accurate hot spot stress. For both the **shell** and the **solid** element meshes the hot spot stress is plotted over the ratio of *element* length to *radius* (t/a).

This non-dimensionalized representation of the element length is necessary to develop guidelines for the appropriate mesh size around a hole (e.g. cutout).

Fig. (3.13) shows the stress concentration factor K_t for the plate with a transverse hole for both the **shell** and the **solid** element models. The target value for K_t that has been obtained from [8] is also shown. It can be seen for a ratio of t/a greater than 0.4 the resulting errors for K_t exceed 10%. In order to reduce the error to less than 1% the ratio a/t has to be smaller than 0.1.

Especially for smaller element sizes both **shell** and **solid** elements produce approximately identical stress results.

3.3.4 Mesh Size and Stress Recovery Recommendations

Based on the stress results shown in Fig. (3.13) a ratio of $\boxed{a/t = 0.1}$ will be used to determine the element size around holes and cutouts. This element size has been selected to ensure that the stresses are obtained with sufficient accuracy. It is advised, however, to perform test calculations to verify that the desired accuracy is achieved with this defined mesh size.

In order to obtain the actual edge stresses truss elements with a minimum thickness are placed along the edge and are used to determine the hot-spot stress.

3.4 Mesh Size near Geometric Discontinuities

As seen in Figs. (3.3) the hot spots at the connection of the sideshell longitudinal to toe of the bracket and the heel of the bracket are the result of the sudden change of geometry. Linear elastic analysis will predict an infinite stress at the hot spot. For steel commonly used for ship CSD this stress will be redistributed locally due to plastic stress redistribution effects. An actual *hot spot stress* cannot be determined by a linear elastic analysis.

In order to define an appropriate mesh size and compare different stress interpolation methods to obtain reliable reference stress close to the hot spot two different parameter studies are performed:

1. **FE model of flat bar with a shoulder fillet**: The model consists of a flat bar with a change in height. The change from height 1 (D_1) to height 2 (D_2) is accomplished through a small fillet of radius r.

   For the two load cases *axial force* and *bending moment* the stress concentration factor K_t is obtained from [8]. Due to the shoulder fillet, which provides a smooth transition between the two different plate width, no geometric singularity occurs.

2. **FE model of flat bar without shoulder fillet**: The model consists of a flat bar with a sudden change in height. No shoulder fillet is used. Since no stress concentration factor can be obtained from literature, the parametric analyses are used to compare the results for the different mesh sizes only.

3.4.1 Model *with* Shoulder Fillet

3.4.1.1 Selected Geometry and Dimensions

In [8] the stress concentration factor K_t for a flat bar with shoulder fillet is given for different ratios D/d and r/d.

Fig. (3.14) shows the geometry of the flat bar and the resulting curves for different ratios D/d that relate the stress concentration factors K_t to the ratio r/d for the case of an *axial force* P.

Fig. (3.15) shows the geometry of the flat bar and the resulting curves for different ratios D/d that relate the stress concentration factors K_t to the ratio r/d for the case of an *bending moment* M.

In order to use the same finite element model for the two load cases the same ratios of D/d and r/d have been chosen:

$$r/d = 0.06$$

$$D/d = 2.0$$

The resulting stress concentration factor is:

Axial Force:	$K_t = 2.71$
Bending Moment:	$K_t = 2.20$

The actual dimensions of the flat bar have been chosen to be similar to the dimensions of the sideshell longitudinal detail shown in Fig. (3.4). The chosen

dimensions are shown in Fig. (3.16) for the axial force and in Fig. (3.17) for the bending moment.

An axial force of 250 kN on both sides of the plate will result in a *nominal* stress of $100N/mm^2$. This facilitates the determination of K_t . This axial force will be uniformly distributed over the width of the plate.

A bending moment of 10.416 kNm is used to produce a *nominal* stress at the plate edge of $100N/mm^2$. This moment will be represented by a linearly distributed axial force.

3.4.1.2 Finite Element Model

Due to the symmetry of the plate only one half of the plate has been modelled. Ship CSD are in general modelled using thin shell elements to account for the out-of plane loads. Since this simple model is used for parametric analyses to determine the best mesh size to be used for ship CSD, four-node quadrilateral thin shell elements are used to model the plate.

In order to account for the large stress gradient near the location of K_t the element size is small compared to other areas of the model. The number of elements and the node spacing have been chosen to assure aspect ratios close to unity near the hot spot.

For a length of 200 mm from the end of the radius a uniform element spacing has been used. The number of elements in this section has been methodically increased and has been used as a measure for the mesh size, i.e. number of elements / 200 mm.

For the *axial force* load case symmetric displacement boundary conditions are used on the centerline of the model. For the *bending moment* load case anti-symmetric boundary conditions are used on the centerline of the model.

The axial force has been applied as a uniform pressure acting on the surface. The bending moment has been applied as a linearly varying pressure, which is zero on the centerline. Fig. (3.18) shows the first very coarse mesh including displacement and force boundary conditions.

Truss elements with minimal stiffness are placed along the edge of the model to obtain the stresses near the hot spot. This method facilitates the stress recovery.

A parametric input method has been used that allows it to vary the mesh size easily. The number of elements in the 200 mm distance from the hot spot has been used as an indicator of the relative fineness of the mesh. All other mesh geometries have been varied accordingly to assure reasonable aspect ratios throughout the mesh.

Fourteen different models have been prepared and analysed. The number of elements for the 200 mm distance has been varied between 4 and 30 elements. Fig. (3.19) shows an intermediate mesh with 18 elements for the 200 mm distance. Fig. (3.20) shows the finest mesh, where 30 elements are used to model the 200 mm distance.

For the models with very fine mesh spacing (more than 20 elements for 200 mm) only the number of elements along the 200 mm distance away from the radius has been methodically increased. All other mesh characteristics have been kept identical. This procedure has kept the model sizes within reasonable bounds.

3.4.1.3 Analysis and Interpretation

The parametric analyses are aimed to define the appropriate mesh size and a stress recovery procedure that will result in consistent stress results for the analysis of ship CSD.

A linear static finite element analysis has been performed for each of the fourteen models. For the *bending moment* load case the displacement boundary conditions have been modified for each of the fourteen models and a linear static finite element analysis has been performed for these models. The purpose of these analyses was to compare the calculated hot spot stress concentration factor K_t against the theoretical value obtained from [8], to compare the effects of the mesh size on the results of different stress interpolation procedures and find a stress recovery procedure that will result in a stress value that is independent of the mesh size.

Based on this comparison the minimum mesh for an acceptable error margin of the hot spot stress K_t can be selected and the best stress recovery procedure can be selected.

Table (3.2) summarizes the performed analyses for the axial load case. For all 14 meshes the number of elements for the 200 mm distance away from the radius, number of equations and the total solution time are listed.

Figs. (3.21, 3.22, 3.23) show the axial stresses in x-direction for meshes with 4, 18 and 30 elements for the 200 mm distance away from the radius for the axial load case.

It can be seen that for the very coarse mesh (4 elements for the 200 mm distance) the location of the stress concentration is not very accurately defined and the interpolated stress distribution is very ragged. For this mesh the radius of the fillet has been modelled by two elements only.

For the medium mesh (18 elements for the 200 mm distance away from the radius) both the location of the stress concentration and the interpolated stress distribution are much more reasonable.

The stress plot for the very fine mesh (30 elements for the 200 mm distance away from the radius) does not show a significant improvement in the location of the stress concentration or the interpolated stress distribution.

It can be seen in the three stress plots (3.21, 3.22, 3.23) that the location of the maximum stress lies on the plate edge slightly away from the beginning of the radius.

For the bending moment load case similar results have been obtained.

For the purposes of obtaining a thorough understanding of the factors influencing the value of the stress concentration at the hot spot the actual element dimensions are used to document the results. It is anticipated that the final recommendations for the stress recovery procedure and mesh size will use a non-dimensional form to represent the element size.

The maximum value of the stress concentration factor K_t has been plotted over the element length for all meshes for both the axial load and the bending moment. This plot is shown in Fig. (3.24) together with the measured values obtained from [8].

For both cases the computed values of K_t are higher than the measured value. For the *axial* load case the calculated value of K_t converges to 2.96 and the measured value is 2.71, as shown in Fig. (3.14). For the *bending* load case the calculated value of K_t converges to 2.26 and the measured value is 2.20, as shown in Fig. (3.15).

No explanation for this behaviour has been found. [8] does not contain specific

information with respect to the location of the hot spot or the exact methods used to obtain K_t . Since the main objective for this test case is to define the appropriate mesh size and stress recovery procedure at the beginning of the radius no additional calculations have been performed to investigate the discrepancies between calculated and measured stress concentration factors.

Several extrapolation methods and stress recovery procedures are currently used by classification societies in order to estimate the hot spot stress near a geometric discontinuity. The most common procedure uses the center stresses in the last two elements before the hot spot ($a/2$ and $3a/2$ with a = element length) and extrapolates linearly to the hot spot. As an alternative the center stresses in the second and third elements ($3a/2$ and $5a/2$) are used for the extrapolation.

In order to judge the effects of the mesh size on different extrapolation procedures the stress at the beginning of the radius has been calculated for each mesh size using two different procedures:

- The stresses at the center of the last two truss elements have been linearly extrapolated to the beginning of the radius
- The stresses at the center of the second and third truss elements away from the beginning of the radius have been linearly extrapolated to the beginning of the radius.

Fig. (3.25) shows schematically the two different extrapolation methods used to obtain K_t for the plate with a shoulder fillet. The stresses are extrapolated to the beginning of the fillet radius.

Figs. (3.26, 3.27) show the resulting K_t values for the different mesh sizes for both extrapolation methods for the axial and the bending moment load case, respectively. It can be seen that for both load cases the resulting K_t value is very sensitive to the mesh size for both extrapolation methods. The resulting stress concentration factor K_t depends strongly on the chosen mesh size.

In order to get a better understanding of the effect of the mesh size the stress distribution along the plate edge up to the beginning of the radius has been plotted. Fig. (3.28) shows the different stress distributions for the axial load case. It can be seen that for all but the very coarse meshes the calculated stress distributions are almost identical.

Based on this observation the stress distributions along the plate edge are plotted for all meshes that result in an *acceptable* stress distribution near the beginning of the fillet radius. Fig. (3.29) shows this plot. This figure indicates that the same stress value can be obtained from all *acceptable* meshes at a given distance away from the hot spot. This distance has to be larger than 1/2 the element length of the coarsest *acceptable* mesh.

Fig. (3.30) shows the different stress distributions for the bending moment case. It can be seen that for all but the very coarse meshes the calculated stress distributions are almost identical.

As in the axial force load case the stress distributions along the plate edge are plotted for all meshes that result in an *acceptable* stress distribution near the beginning of the fillet radius. Fig. (3.31) shows this plot. This figure indicates that the same stress value can be obtained from all *acceptable* meshes at a given distance away from the hot spot. This distance has to be larger than 1/2 the element length of the coarsest *acceptable* mesh.

For the plate with shoulder fillet the choice of a non-dimensionalization of the element size is less intuitive than for the model of the plate with a transverse hole. The choice of the fillet radius as the non-dimensionalization constant is not practical since the resulting mesh definitions are intended for geometries without a defined radius.

3.4.2 Model *without* Shoulder Fillet

In order to investigate the different stress recovery procedures and to compare and validate the results obtained for the plate *with* a shoulder fillet a model without a shoulder fillet has been analysed. For this model no measured stress concentration factor is available.

3.4.2.1 Selected Geometry and Dimensions

Fig. (3.32) shows the geometry and the dimensions for the plate without shoulder fillet for the axial force load case. An axial force of 250 kN on both sides of the plate will result in a *nominal* stress of $100N/mm^2$. This facilitates the determination of K_t . This axial force will be uniformly distributed over the width of the plate.

Fig. (3.33) shows the geometry and the dimensions for the plate without shoulder fillet for the bending moment load case. A bending moment of 10.416 kNm is used to produce a *nominal* stress at the plate edge of $100N/mm^2$. This moment will be represented by a linearly distributed axial force.

3.4.2.2 Finite Element Model

Due to the symmetry of the plate only one half of the plate has been modelled. Ship CSD are in general modelled using thin shell elements to account for the out-of plane loads. Since this simple model is used for parametric analyses to determine the best mesh size to be used for ship CSD, four-node quadrilateral thin shell elements are used to model the plate.

In order to account for the large stress gradient near the location of K_t the element size is small compared to other areas of the model. The number of elements and the node spacing have been chosen to assure aspect ratios close to unity near the hot spot.

For a length of 200 mm from hot spot a uniform element spacing has been used. The number of elements in this section has been methodically increased and has been used as a measure for the mesh size, i.e. number of elements / 200 mm.

For the *axial force* load case symmetric displacement boundary conditions are used on the centerline of the model. For the *bending moment* load case anti-symmetric boundary conditions are used on the centerline of the model.

The axial force has been applied as a uniform pressure acting on the surface. The bending moment has been applied as a linearly varying pressure, which is zero on the centerline. Fig. (3.34) shows the first very coarse mesh including displacement and force boundary conditions.

Truss elements with minimal stiffness are placed along the edge of the model to obtain the stresses near the hot spot. This method facilitates the stress recovery.

A parametric input method has been used that allows it to vary the mesh size easily. The number of elements in the 200 mm distance from the hot spot has been used as an indicator of the relative fineness of the mesh. All other mesh geometries

have been varied accordingly to assure reasonable aspect ratios throughout the mesh.

Fourteen different models have been prepared and analysed. The number of elements for the 200 mm distance has been varied between 4 and 30 elements. Fig. (3.35) shows an intermediate mesh with 18 elements for the 200 mm distance. Fig. (3.36) shows the finest mesh, where 30 elements are used to model the 200 mm distance.

For the models with very fine mesh spacing (more than 20 elements for 200 mm) only the number of elements along the 200 mm distance away from the hot spot has been methodically increased. All other mesh characteristics have been kept identical. This procedure has kept the model sizes within reasonable bounds.

3.4.2.3 Analysis and Interpretation

The parametric analyses are aimed to define the appropriate mesh size and a stress recovery procedure that will result in consistent stress results for the analysis of ship CSD.

A linear static finite element analysis has been performed for each of the fourteen models. For the *bending moment* load case the displacement boundary conditions have been modified for each of the fourteen models and a linear static finite element analysis has been performed for these models. The purpose of these analyses was to compare the effects of the mesh size on the results of different stress interpolation procedures and find a stress recovery procedure that will result in a stress value that is independent of the mesh size.

Based on this comparison the minimum mesh for an acceptable error margin of the hot spot stress K_t can be selected and the best stress recovery procedure can be selected.

Table (3.3) summarizes the performed analyses for the axial load case. For all 14 meshes the number of elements for the 200 mm distance away from the hot spot, number of equations and the total solution time are listed.

Figs. (3.37, 3.38, 3.39) show the axial stresses in x-direction for meshes with 4, 18 and 30 elements for the 200 mm distance away from the hot spot for the axial load case.

It can be seen that for the very coarse mesh (4 elements for the 200 mm distance) the location of the stress concentration is not very accurately defined and the interpolated stress distribution is very ragged.

For the medium mesh (18 elements for the 200 mm distance away from the hot spot) both the location of the stress concentration and the interpolated stress distribution are much more reasonable.

The stress plot for the very fine mesh (30 elements for the 200 mm distance away from the hot spot) does not show a significant improvement in the location of the stress concentration or the interpolated stress distribution.

For the bending moment load case similar results have been obtained.

For the purposes of obtaining a thorough understanding of the factors influencing the value of the stress concentration at the hot spot the actual element dimensions are used to document the results. It is anticipated that the final recommendations for the stress recovery procedure and mesh size will use a non-dimensional form to represent the element size.

In order to judge the effects of the mesh size on different extrapolation procedures the stress at the beginning of the radius has been calculated for each mesh

size using two different procedures:

- The stresses at the center of the last two truss elements have been linearly extrapolated to the beginning of the radius
- The stresses at the center of the second and third truss elements away from the beginning of the radius have been linearly extrapolated to the beginning of the radius.

Fig. (3.40) shows schematically the two different extrapolation methods used to obtain K_t for the plate with a shoulder fillet. The stresses are extrapolated to the beginning of the fillet radius.

Figs. (3.41, 3.42) show the resulting K_t values for the different mesh sizes for both extrapolation methods for the axial and the bending moment load case, respectively. It can be seen that for both load cases the resulting K_t value is very sensitive to the mesh size for both extrapolation methods. The resulting stress concentration factor K_t depends strongly on the chosen mesh size.

In order to get a better understanding of the effect of the mesh size the stress distribution along the plate edge up to the beginning of the radius has been plotted. Fig. (3.43) shows the different stress distributions for the axial load case. It can be seen that for all but the very coarse meshes the calculated stress distributions are almost identical.

Based on this observation the stress distributions along the plate edge are plotted for all meshes that result in an *acceptable* stress distribution near the beginning of the fillet radius. Fig. (3.44) shows this plot. This figure indicates that the same stress value can be obtained from all *acceptable* meshes at a given distance away from the hot spot. This distance has to be larger than 1/2 the element length of the coarsest *acceptable* mesh.

Fig. (3.45) shows the different stress distributions for the bending moment case. It can be seen that for all but the very coarse meshes the calculated stress distributions are almost identical.

As in the axial force load case the stress distributions along the plate edge are plotted for all meshes that result in an *acceptable* stress distribution near the beginning of the fillet radius. Fig. (3.46) shows this plot. This figure indicates that the same stress value can be obtained from all *acceptable* meshes at a given distance away from the hot spot. This distance has to be larger than 1/2 the element length of the coarsest *acceptable* mesh.

3.4.3 Summary

For both test cases, plate with a shoulder fillet and plate without a shoulder fillet, parametric studies have been performed to determine a minimum acceptable mesh size and to find a stress recovery procedure that will result in hot spot stresses that are independent of the mesh size.

It has been found that hot spot stresses based on extrapolation methods that use the element stresses near the hot spot are very sensitive to the mesh size.

It has been concluded from plots of the stress distribution along the plate edge that for a certain *acceptable* mesh size the stresses at a given distance from the hot spot are identical for all meshes that are finer than the minimum *acceptable* mesh.

By defining the location for the stress recovery and the minimum *acceptable* mesh size the resulting hot spot stress will be independent of the mesh size.

3.4.4 Mesh Size and Stress Recovery Recommendations

Parametric analyses of a plate with and without a shoulder fillet have been performed with the aim to determine a method to obtain the hot spot stress concentration factor K_t that is independent of the chosen mesh size.

It has been found that extrapolation methods based on the element stresses in the last elements near the hot spot are very sensitive to the mesh size.

Alternatively, for a specified minimum mesh size the stress at a given distance away from the hot spot can be calculated using meshes that are finer than the minimum mesh size. The resulting stresses for all meshes will be almost identical. The magnitude of the calculated stress concentration factor K_t depends on the chosen distance from the hot spot.

For the purpose of defining a stress recovery procedure for hot spot stresses to be used in conjunction with fatigue life evaluations the absolute magnitude of K_t is unimportant. The S-N curve used in the fatigue life analysis has to be calibrated based on the same stress recovery procedure as the K_t value used for the analysis.

3.4.4.1 Minimum Mesh Size

From Figs. (3.29, 3.31, 3.44, 3.46) it can be seen that a minimum mesh size of 14 mm results in an acceptable stress distribution near the hot spot. In order to develop general recommendations for the minimum mesh size the plate thickness of the FE models (10 mm) is used.

The element length (height and width) of the elements near the hot spot has to be smaller or equal to the plate thickness.

3.4.4.2 Stress Recovery Location and Procedure

The comparison of the stress distributions towards the hot-spot has indicated that for a specified location near the hot-spot all meshes that are fine enough will result in approximately the same stress value.

The derivation of the calibrated S-N curve for the use in conjunction with hot-spot stresses obtained through finite element analyses requires a clear definition of the hot-spot stress. This includes the stress location and the extrapolation procedure used.

The resulting calibrated S-N curve is only valid for hot-spot stresses obtained using the defined procedure and location. A different extrapolation procedure will result in a different S-N curve. As long as the actual hot-spot stress used for a fatigue life analysis is calculated using the same extrapolation procedure and hot-spot definition as used for the derivation of the calibrated S-N curve, the resulting fatigue life will be identical for different extrapolation procedures.

Contrary to several published stress extrapolation recommendations, the presence of a weld is neglected for the extrapolation. The hot-spot is located at the intersection of the two plates. This decision has been based on the following arguments:

- In a linear finite element analysis using shell elements to represent the structure, the weld cannot be modelled. A different sized weld does therefore not change the results of the analysis. It is the purpose of the extrapolation to obtain the geometric stress concentration factor. The stress concentration due to the weld is included in the S-N curve.

- To allow for different sized welds complicates the stress recovery procedure. To ignore the weld simplifies both the finite element modelling and the stress recovery.
- In practical applications the actual weld size is often not known.

A linear extrapolation routine based on two stress values near the hot-spot will be used to calculate the hot-spot stress. The two stress recovery points are located at 1/2 plate thickness and 3/2 plate thickness away from the hot-spot. Fig. (3.47) shows the extrapolation method and the stress recovery locations. The stresses are extrapolated to the hot-spot ignoring the presence of the weld.

The decision to use the plate thickness to define the stress recovery locations has been made in order to be compatible with existing stress recovery procedures used by classification societies and other regulatory agencies. However, these organizations generally require the extrapolation to be carried out to the weld toe.

It has to be stated again that a particular choice of stress recovery procedure does not effect the validity of the resulting calibrated S-N curve as long as the same stress recovery procedure is used to obtain the hot-spot stress used in the actual fatigue life calculation.

Table 3.1: Plate with Transverse Hole: FE-Analysis Details

Elements / $\frac{1}{4}$ radius	Number of Equations		Total Solution Time [sec]	
	Shell	Solid	Shell	Solid
3	230	294	29	47
4	366	461	37	70
6	787	976	62	142
8	1289	1586	98	236
10	2010	2461	164	383
12	3015	3680	261	704
14	3505	4266	451	894
16	4487	5452	591	1373
18	5768	6999	872	1781
20	7209	8738	1164	2436
22	8367	10132	1556	3153

Table 3.2: Plate with Shoulder Fillet (Axial Force): FE-Analysis Details

El. / 200 mm	Number of Equations	Total Solution Time [sec]
4	423	38
6	942	68
8	1716	129
10	2427	185
12	3331	280
14	4298	465
16	5474	617
18	6586	831
20	7798	1026
22	8002	1041
24	8206	1059
26	8410	1075
28	8614	1090
30	8818	1105

Table 3.3: Plate without Shoulder Fillet (Axial Force): FE-Analysis Details

El. / 200 mm	Number of Equations	Total Solution Time [sec]
4	757	57
6	791	59
8	969	70
10	1503	102
12	1741	126
14	1999	143
16	2713	198
18	3031	232
20	3369	255
22	4263	340
24	4661	383
26	5695	571
28	6153	627
30	6631	680

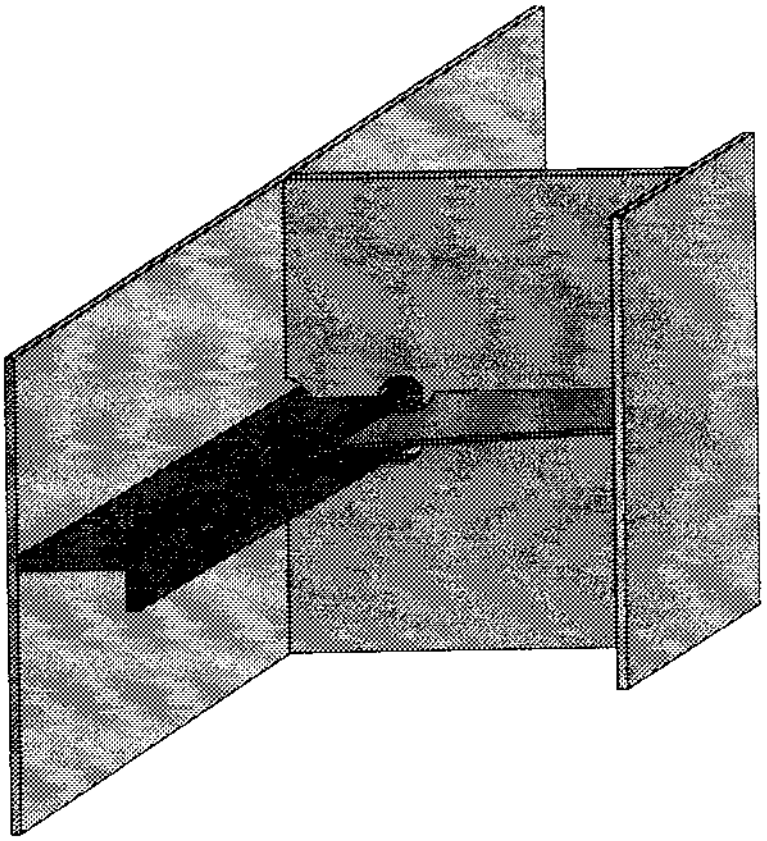

Figure 3.1: Sideshell Longitudinal to Webframe Connection

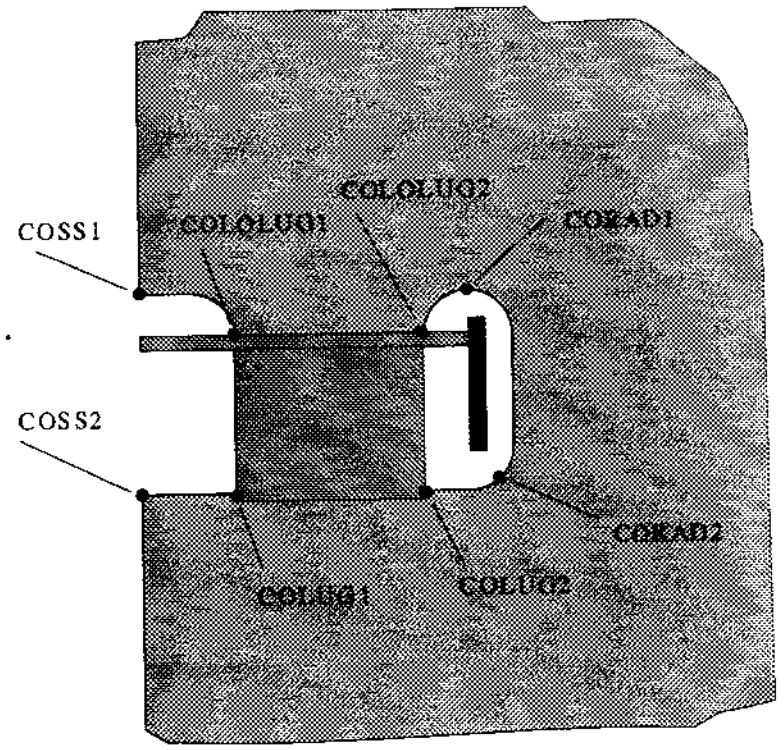

Figure 3.2: Hot Spots in Webframe Cutout

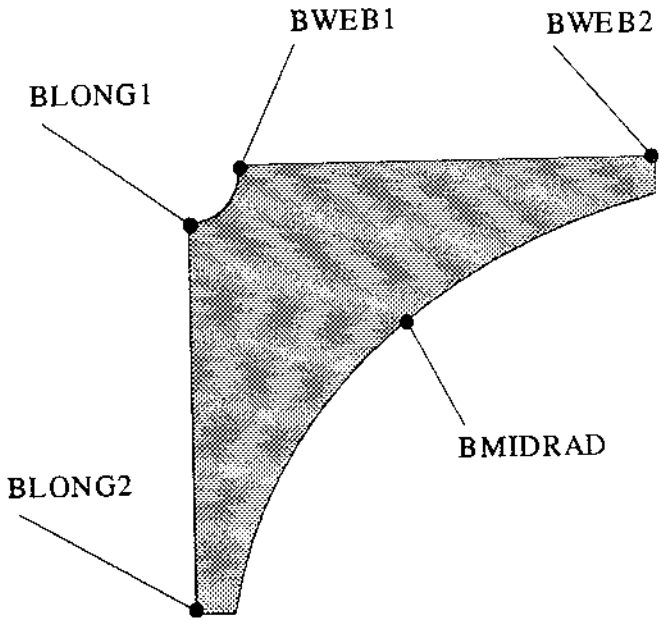

Figure 3.3: Hot Spots in Longitudinal to Bracket Connection

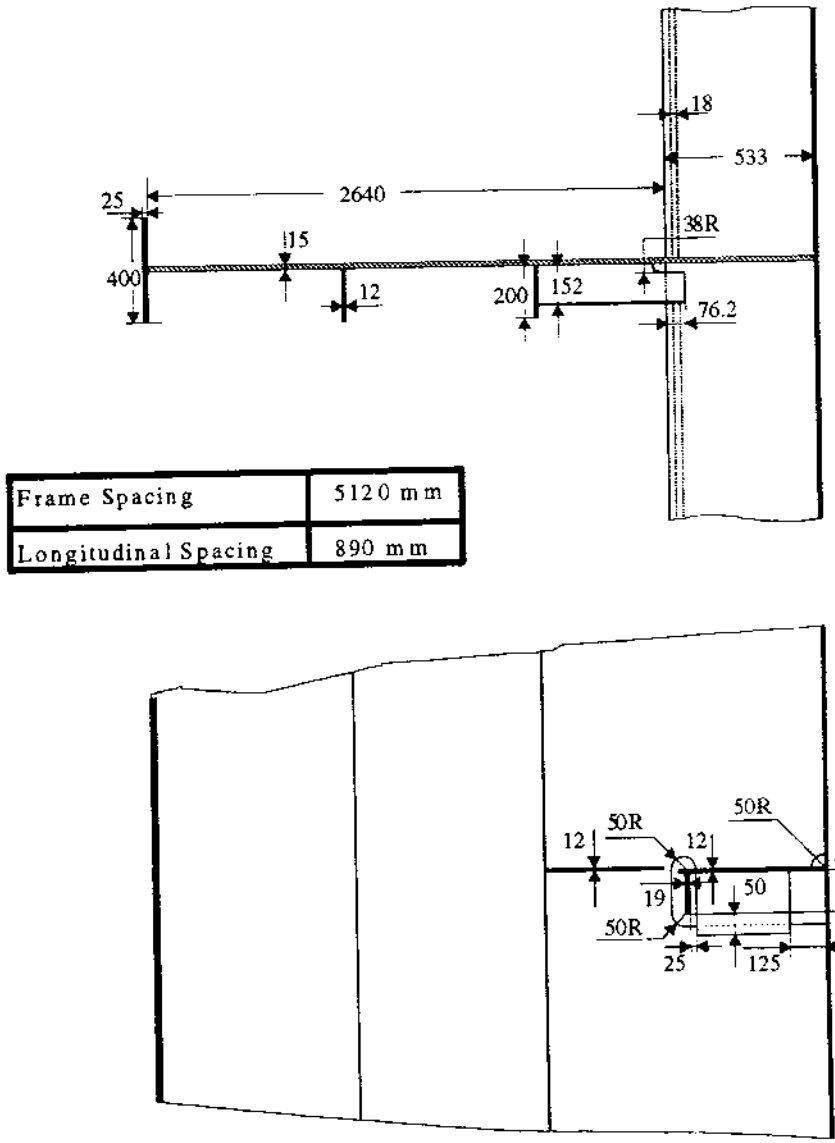

Figure 3.4: Construction Drawing of Sideshell Longitudinal Detail

Stress Concentration Factor K_t for Axial Loading Case of a Finite-Width Plate with a Transverse Hole

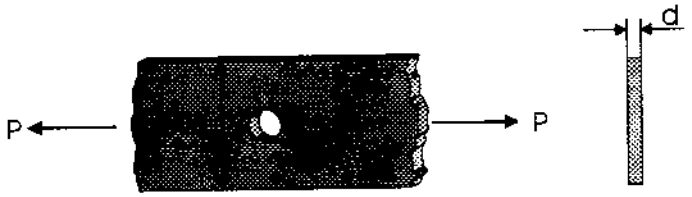

$$K_t = \frac{\sigma_{max}}{\sigma_{nom}} \qquad \text{Based on Net Section}$$

$$\sigma_{nom} = \frac{P}{(w-a)h}$$

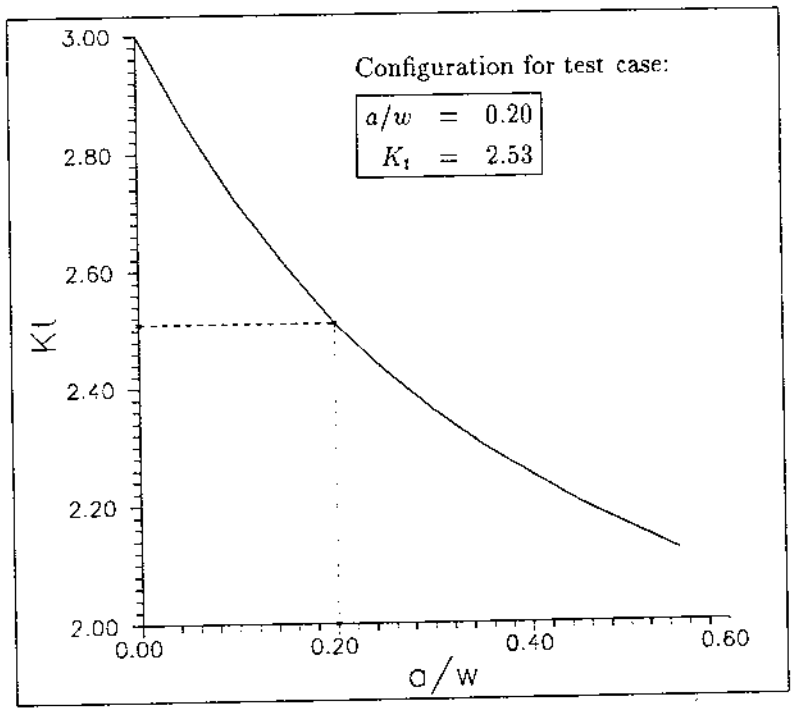

Figure 3.5: K_t for Transverse Hole in Finite-Width Plate

Test Case: Finite - Width Plate with a Transverse Hole

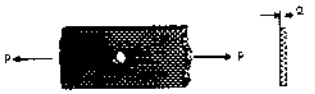

Configuration for test case:

a/w	=	0.20
K_t	=	2.53

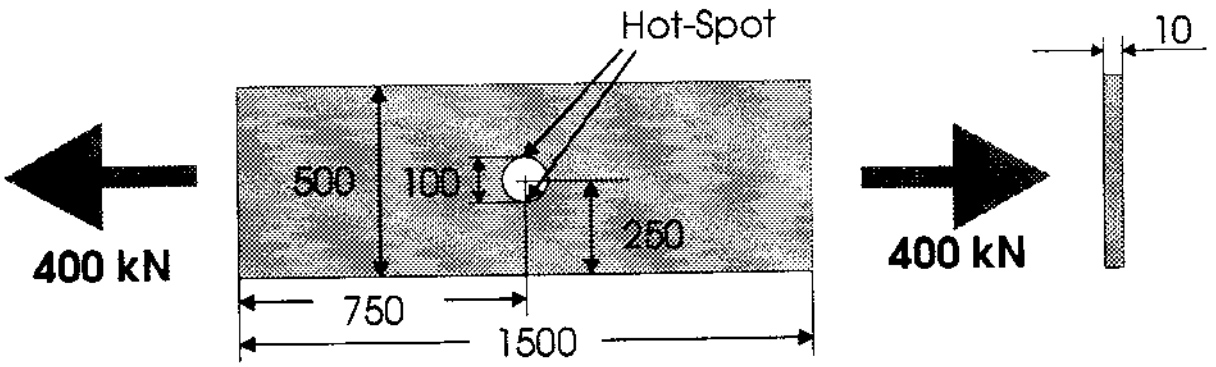

Figure 3.6: Geometry and Dimensions for Plate with Transverse Hole

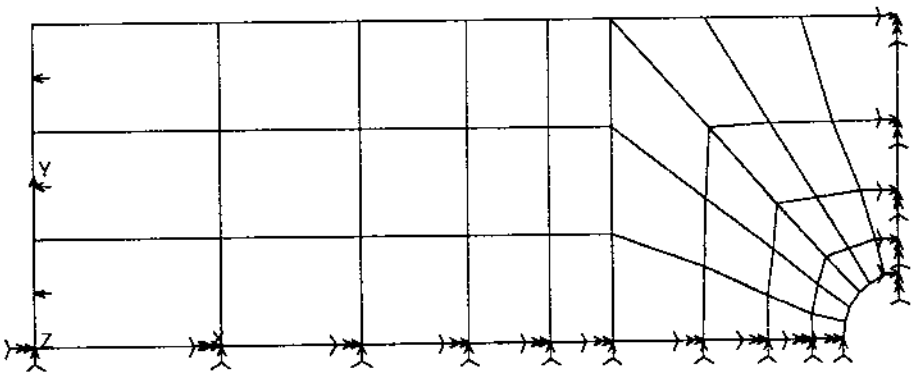

Figure 3.7: Mesh: 8 El. per 1/4 circle

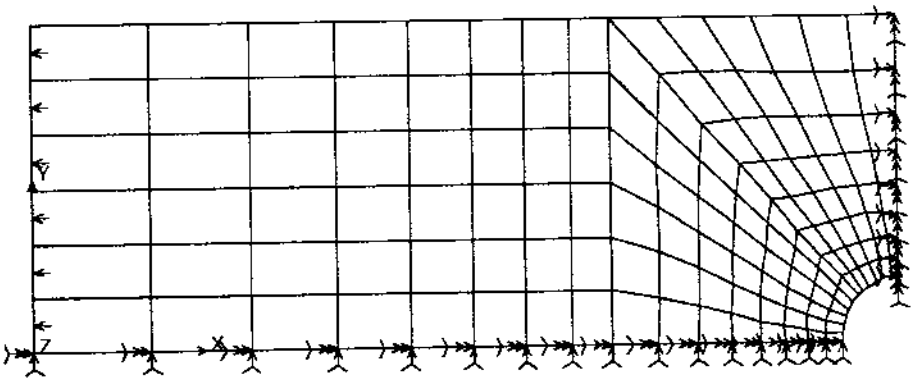

Figure 3.8: Mesh: 12 El. per 1/4 circle

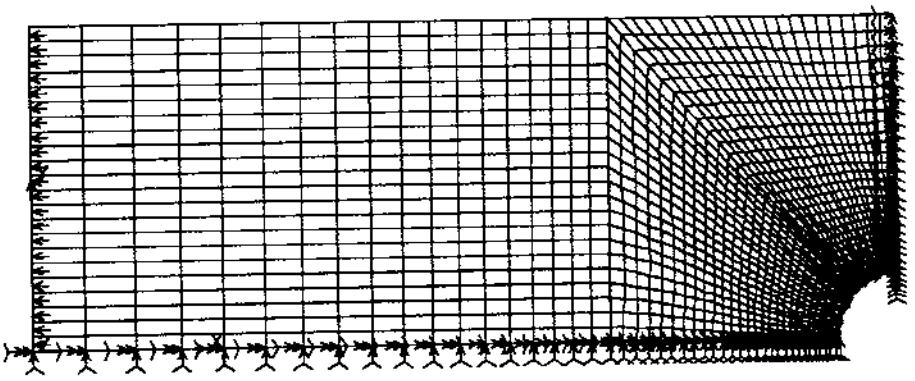

Figure 3.9: Mesh: 44 El. per 1/4 circle

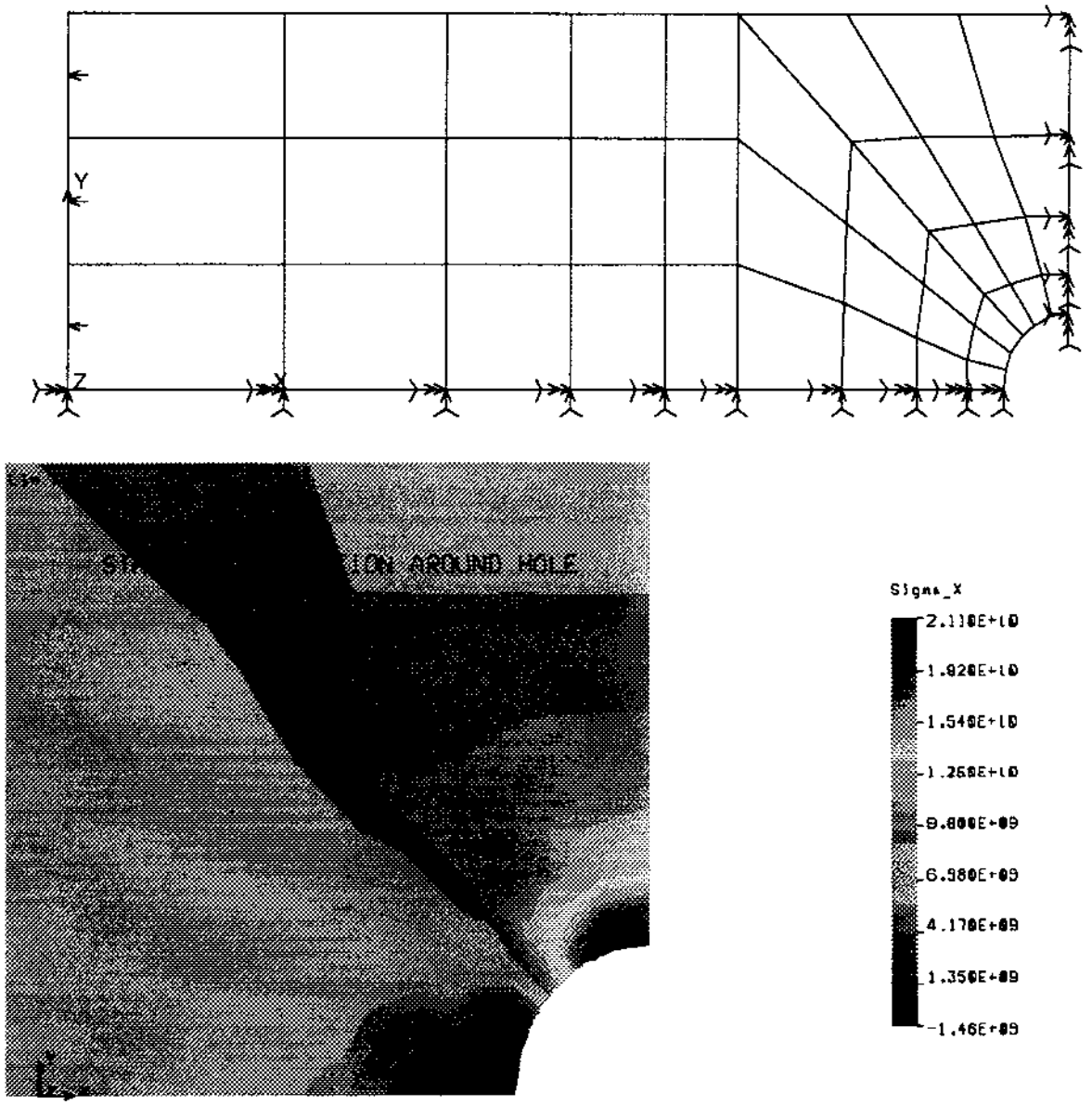

Figure 3.10: Mesh and Stress Distribution: 12 El. per 1/4 circle

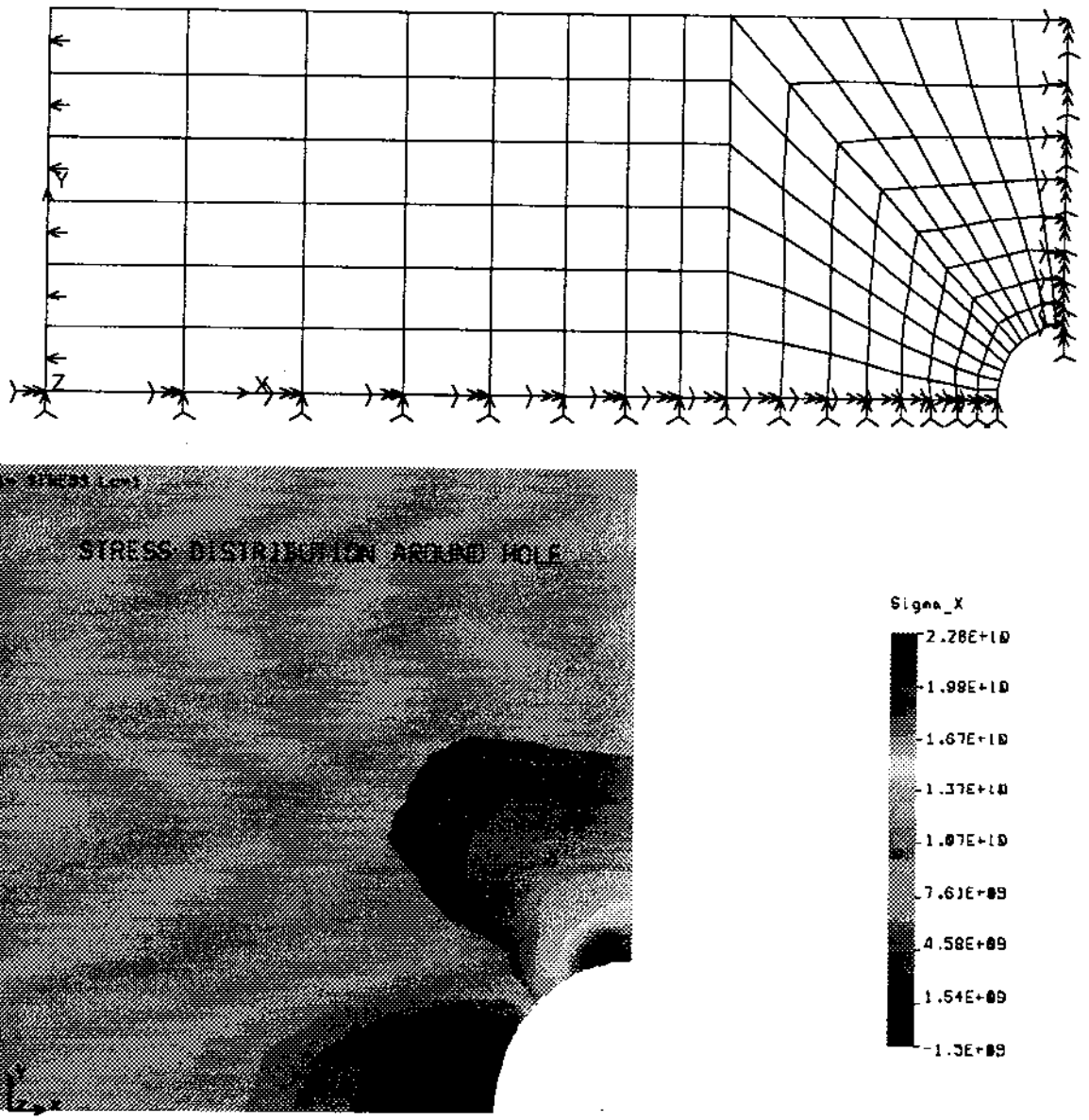

Figure 3.11: Mesh and Stress Distribution: 12 El. per 1/4 circle

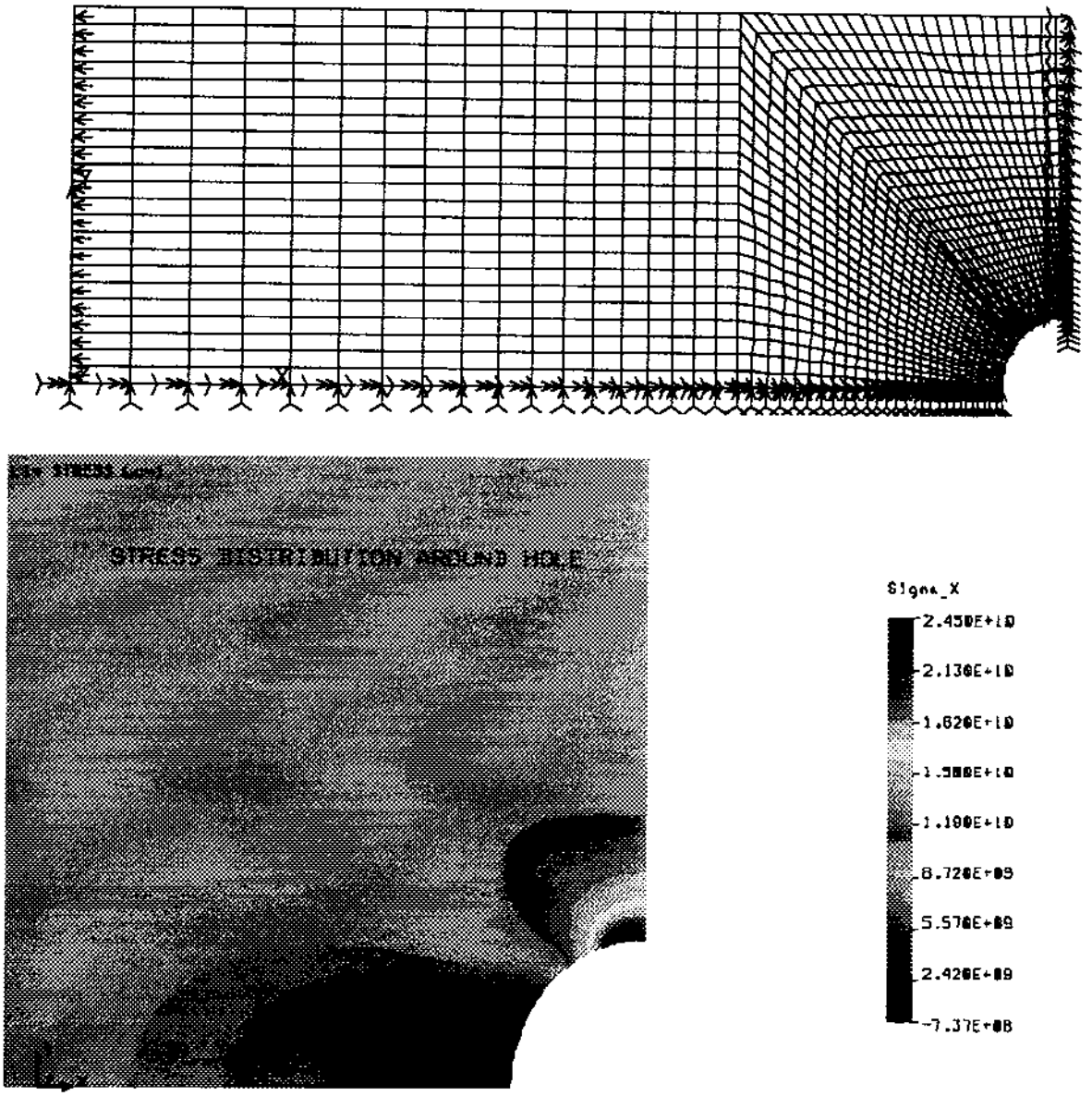

Figure 3.12: Mesh and Stress Distribution: 44 El. per 1/4 circle

Test Case: Finite - Width Plate with a Transverse Hole

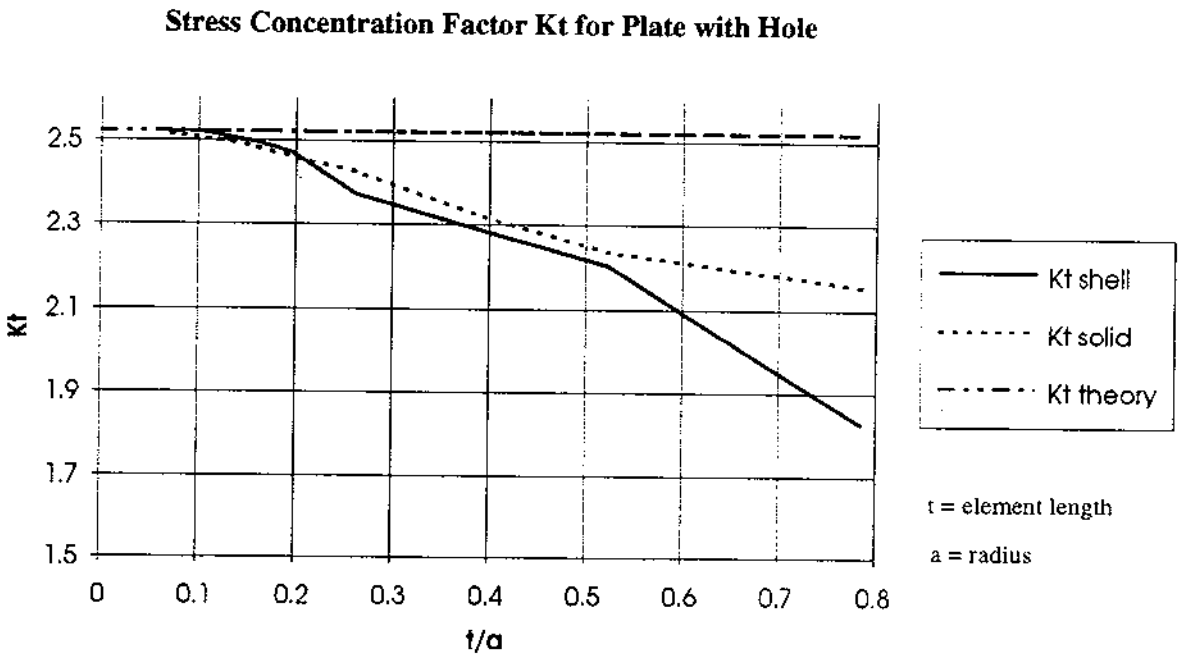

Figure 3.13: Stress Concentration Factor K_t for different Element Sizes

Stress Concentration Factor K_t for the Tension Case of a Flat Bar with a Shoulder Fillet

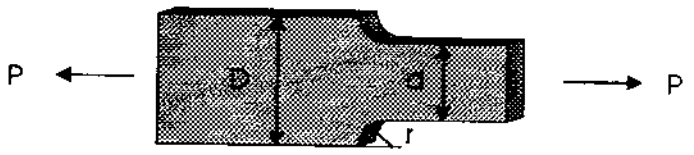

Configuration for test case:

D/d	=	2.00
r/d	=	0.06
K_t	=	2.71

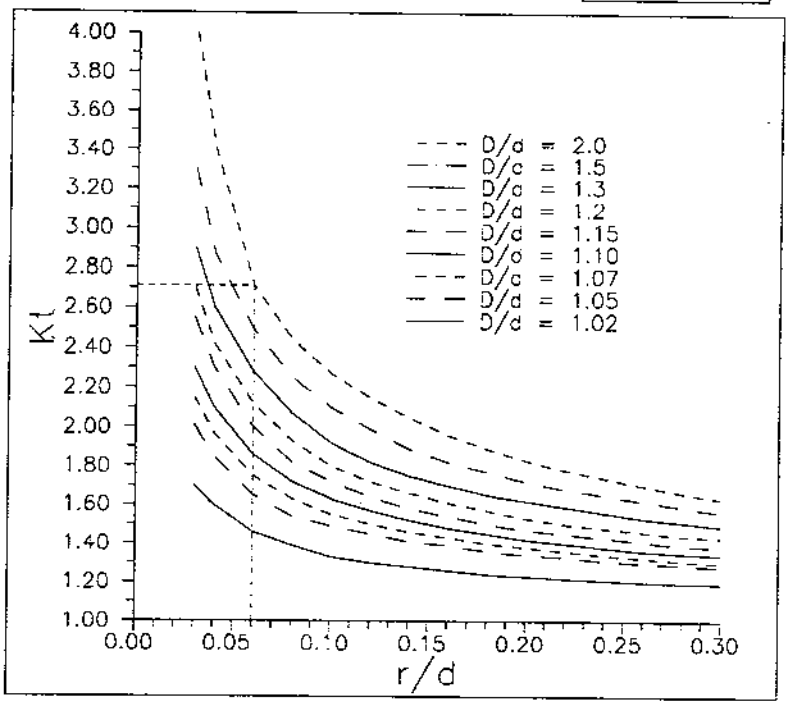

Figure 3.14: K_t for Plate *with* Shoulder Fillet (Axial Force)

Stress Concentration Factor K_t for the Tension Case of a Flat Bar with a Shoulder Fillet

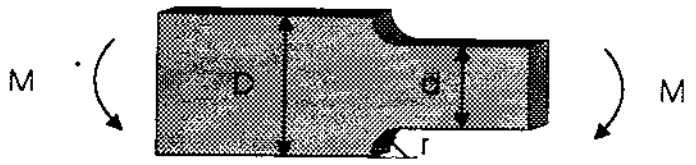

Configuration for test case:

D/d	=	2.00
r/d	=	0.06
K_t	=	2.20

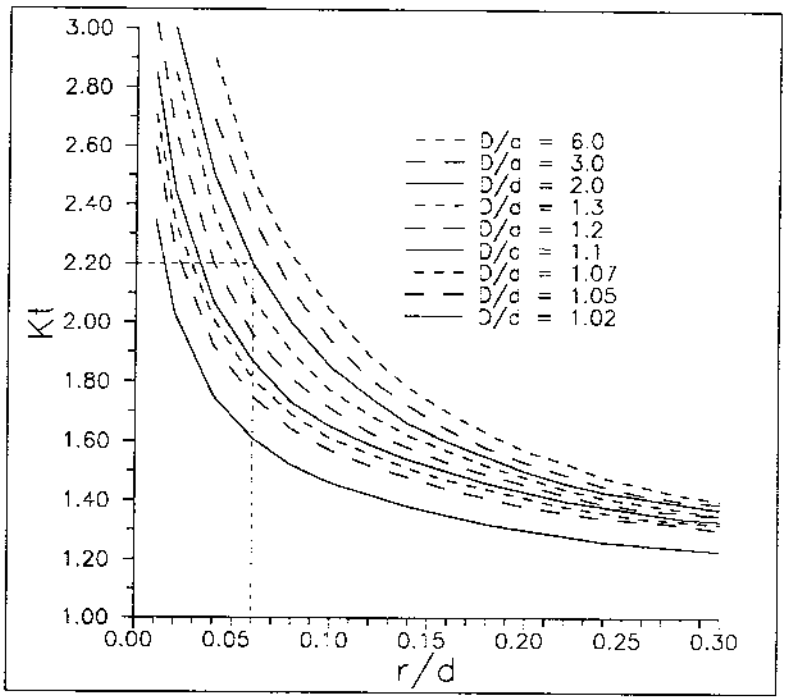

Figure 3.15: K_t for Plate *with* Shoulder Fillet (Bending Moment)

Test Case: Flat Bar *with* a Shoulder Fillet (Tension Case)

Configuration for test case:

D/d	=	2.00
r/d	=	0.06
K_t	=	2.71

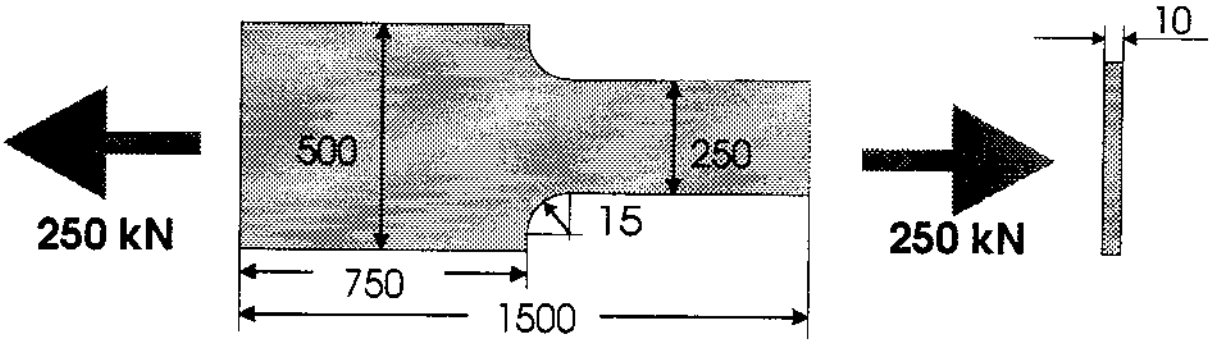

Figure 3.16: Geometry and Dimensions for Plate *with* Shoulder Fillet (Axial Force)

Test Case: Flat Bar *with* a Shoulder Fillet (Bending Case)

Configuration for test case:

D/d	=	2.00
r/d	=	0.06
K_t	=	2.20

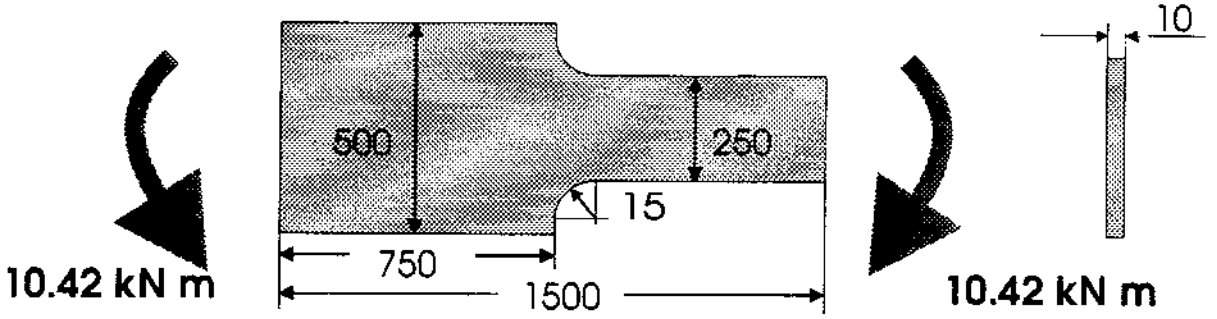

Figure 3.17: Geometry and Dimensions for Plate *with* Shoulder Fillet (Bending Moment)

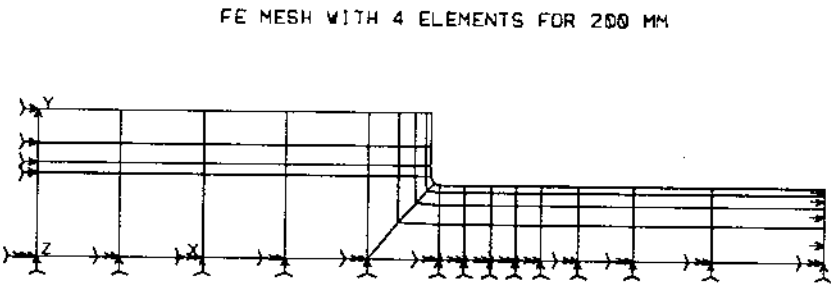

Figure 3.18: Mesh with 4 Elements per 200 mm (Axial)

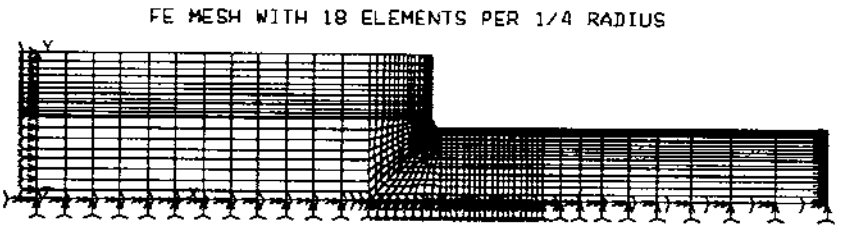

Figure 3.19: Mesh with 18 Elements per 200 mm (Axial)

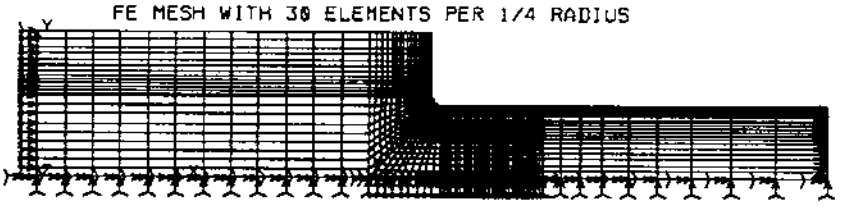

Figure 3.20: Mesh with 30 Elements per 200 mm (Axial)

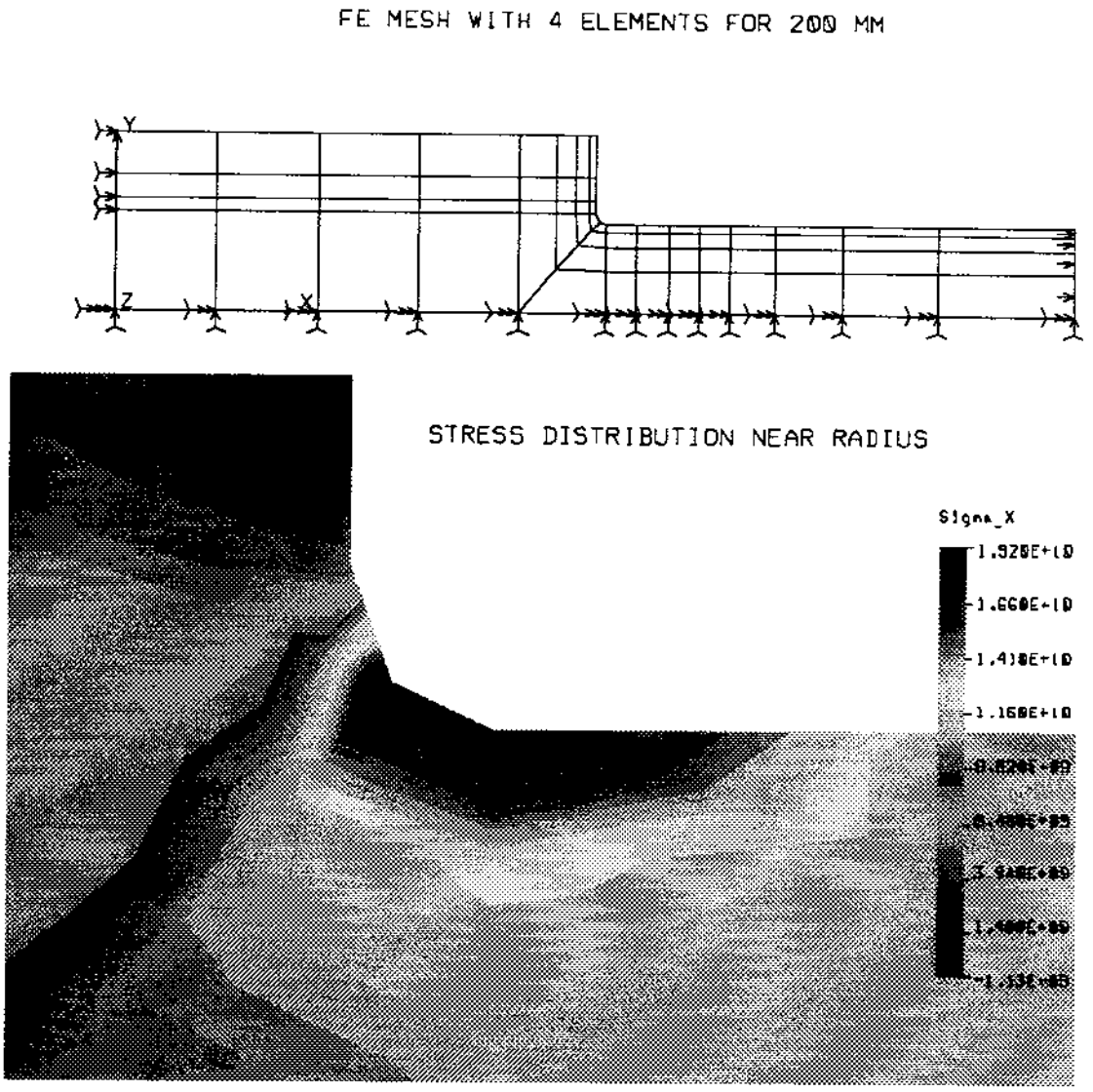

Figure 3.21: Mesh and Stress Distribution: Coarse FE Mesh

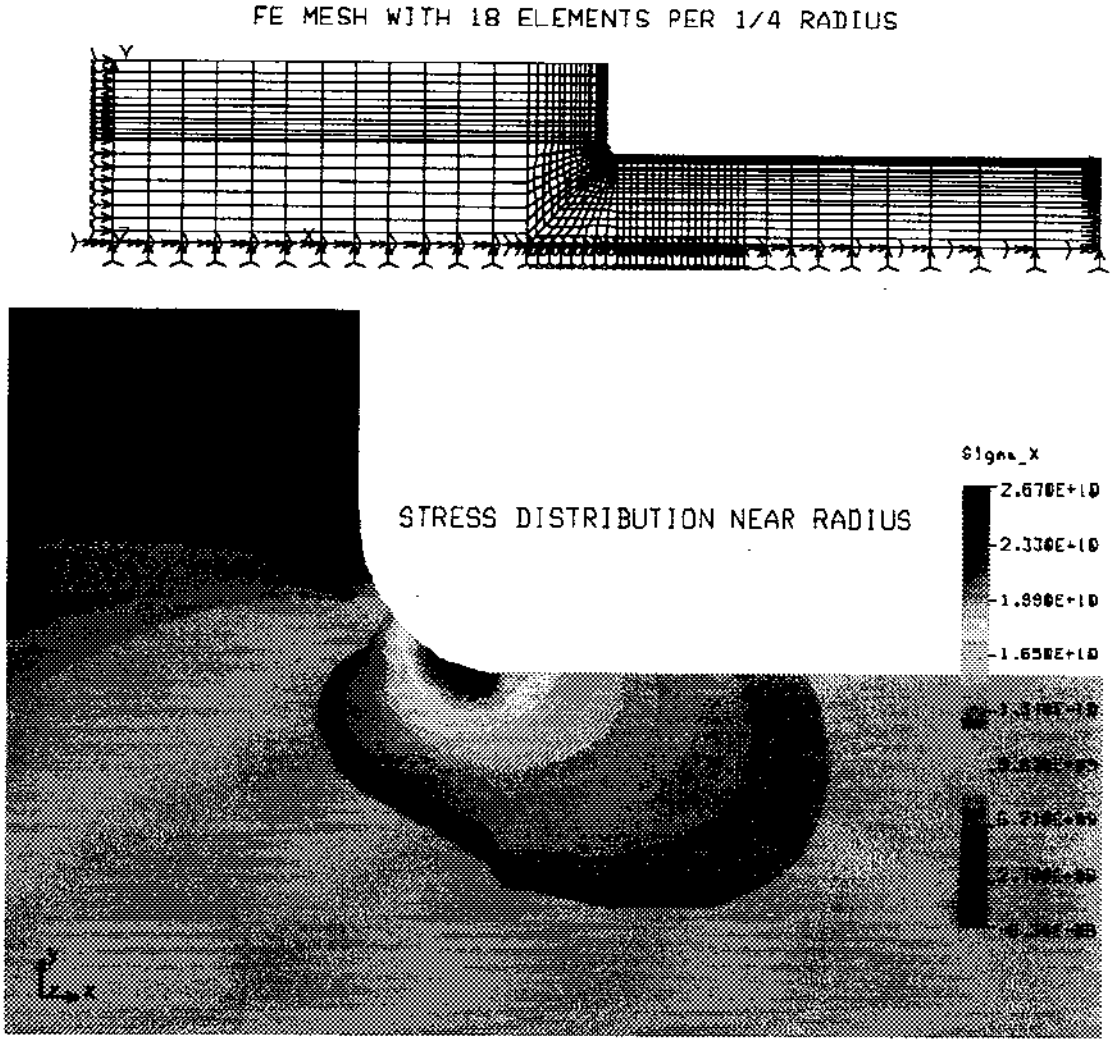

Figure 3.22: Mesh and Stress Distribution: 18 El. per 200mm

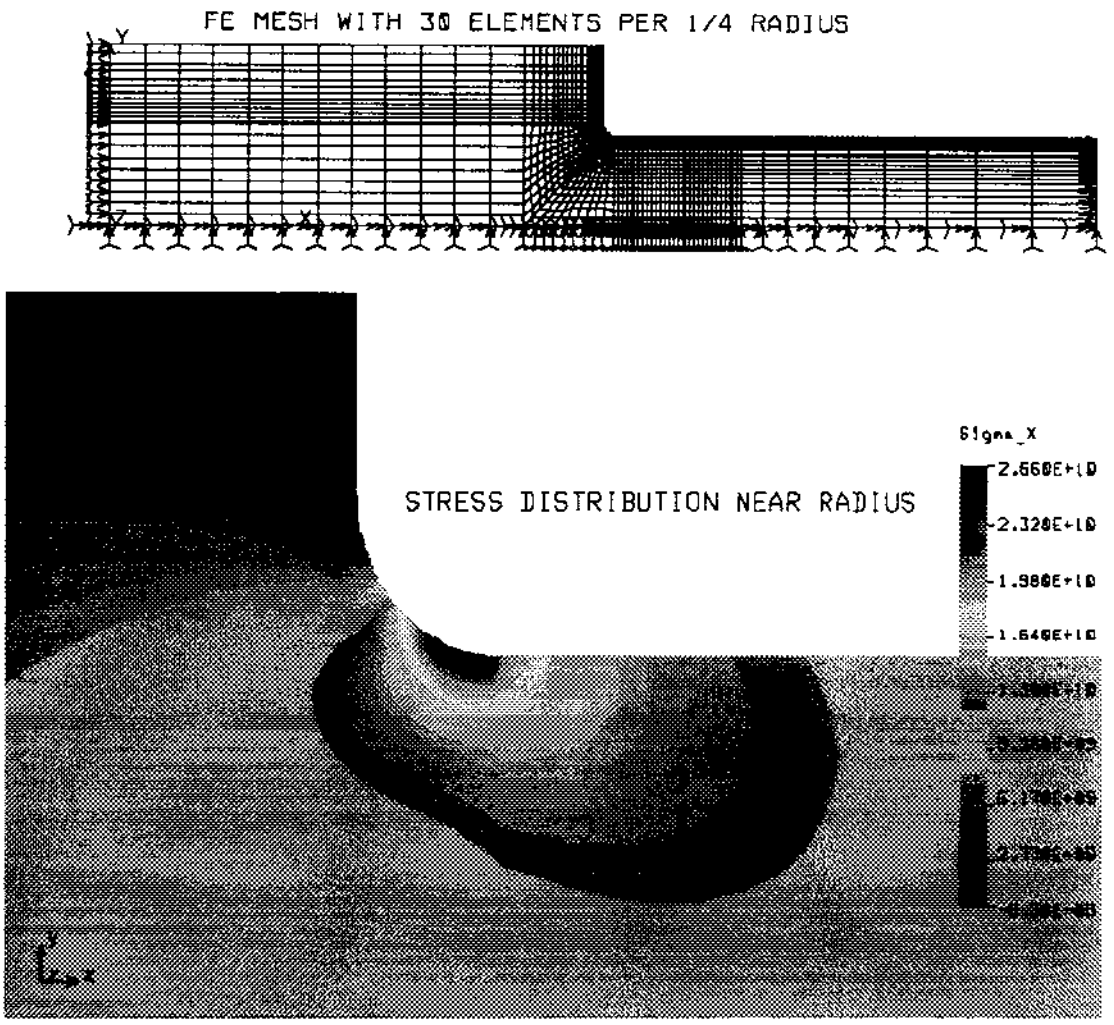

Figure 3.23: Mesh and Stress Distribution: 30 El. per $200mm$

Test Case: Flat Bar with a Shoulder Fillet

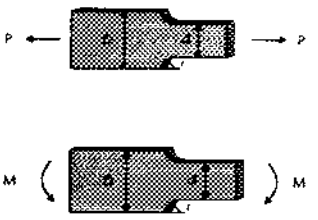

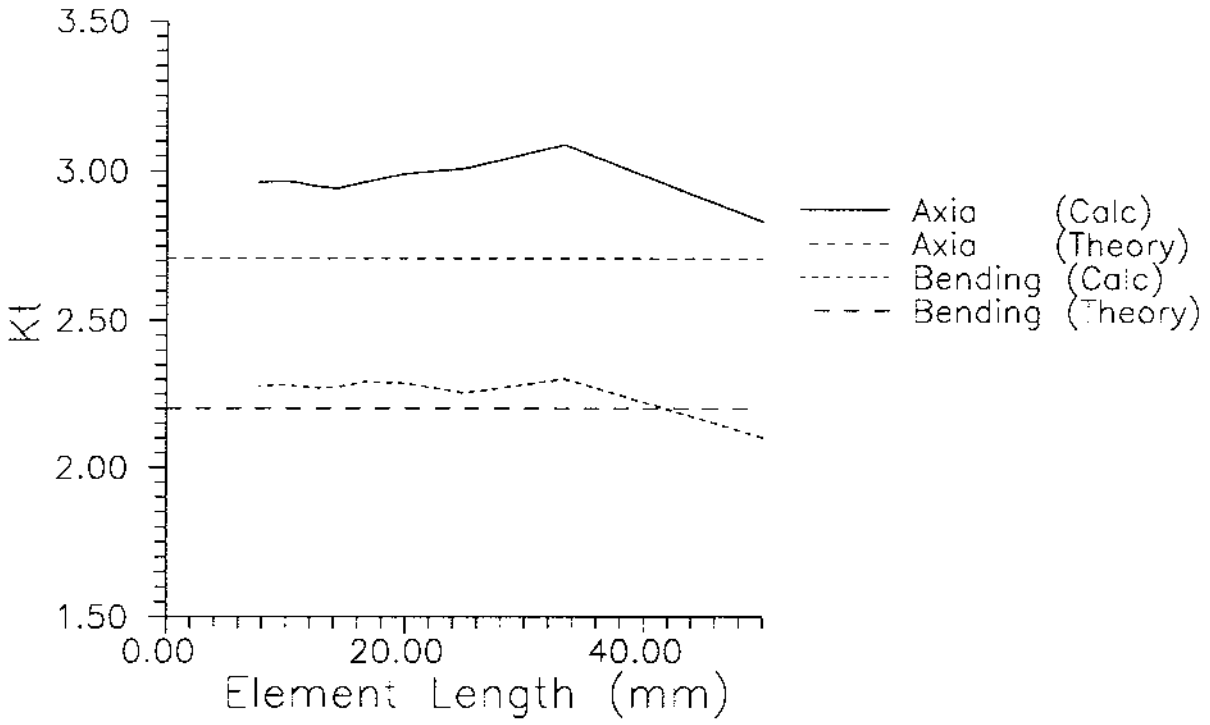

Figure 3.24: Hot Spot Stress Concentration Factor K_t

Test Case: Flat Bar *with* a Shoulder Fillet

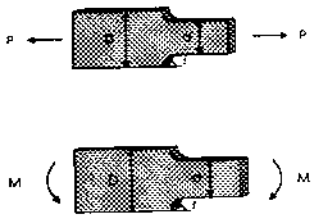

Different Extrapolation Methods (Plate with Shoulder Fillet)

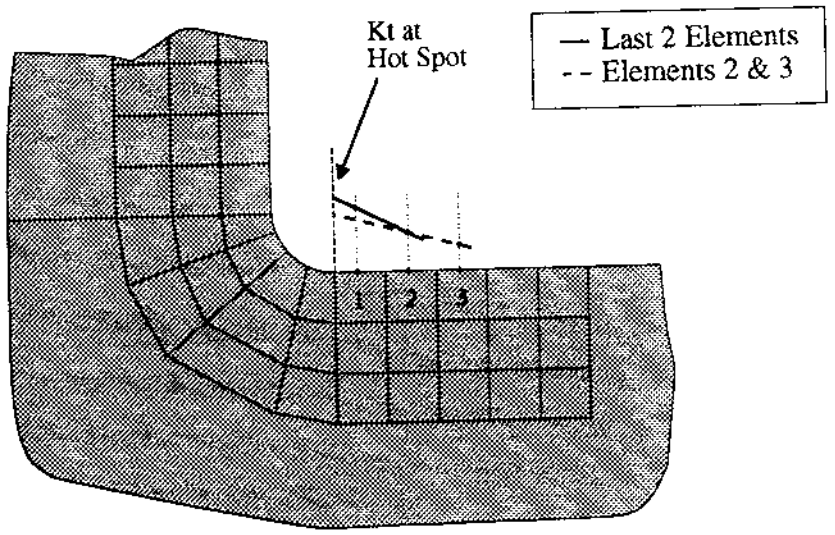

Figure 3.25: Extrapolation Methods used for Plate *with* Shoulder Fillet

Test Case: Flat Bar *with* a Shoulder Fillet

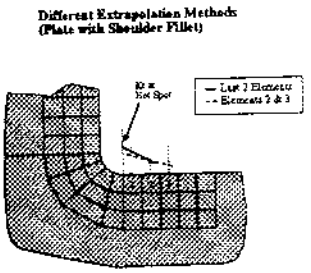

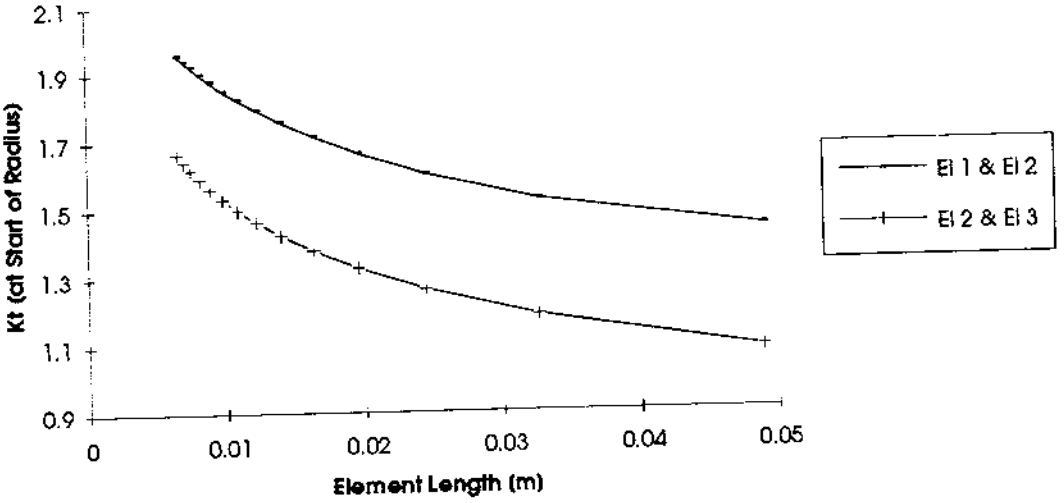

Figure 3.26: Stress Concentration Factor K_t for different Extrapolations

Test Case: Flat Bar *with* a Shoulder Fillet

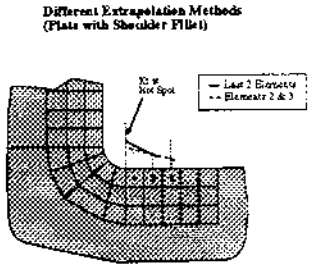

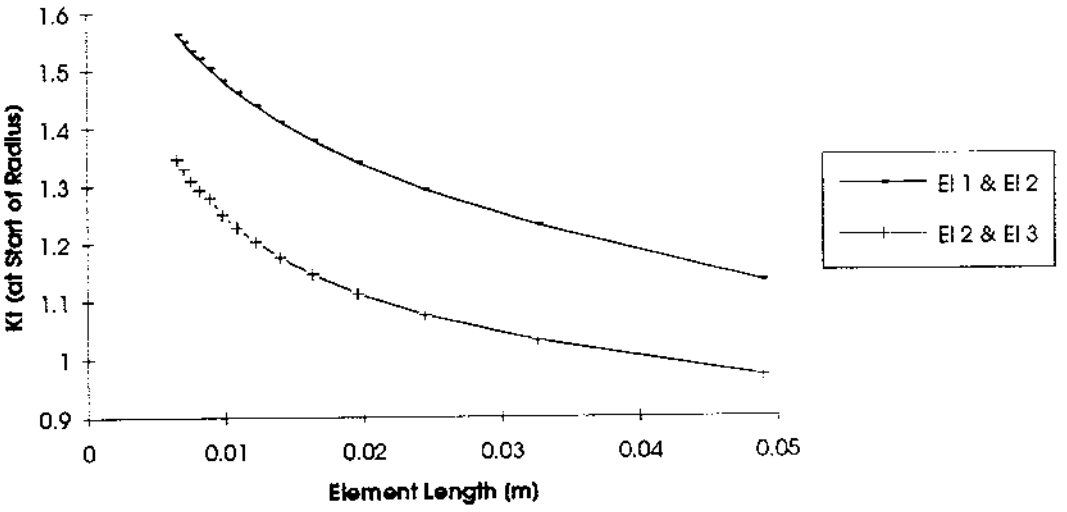

Figure 3.27: Stress Concentration Factor K_t for different Extrapolations

Stress Distribution along Plate Edge (Axial Load):
All Meshes

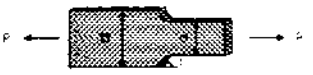

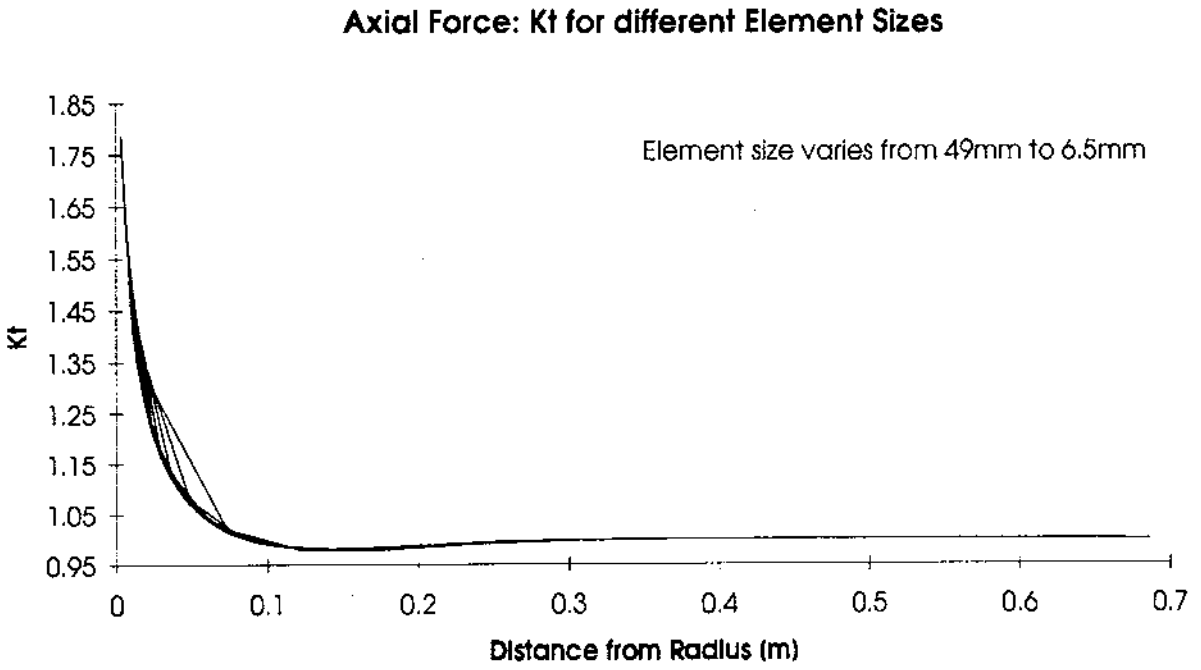

Figure 3.28: Stress Distribution along edge of plate (All Meshes)

Stress Distribution along Plate Edge (Axial Load):
Acceptable Meshes only

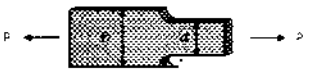

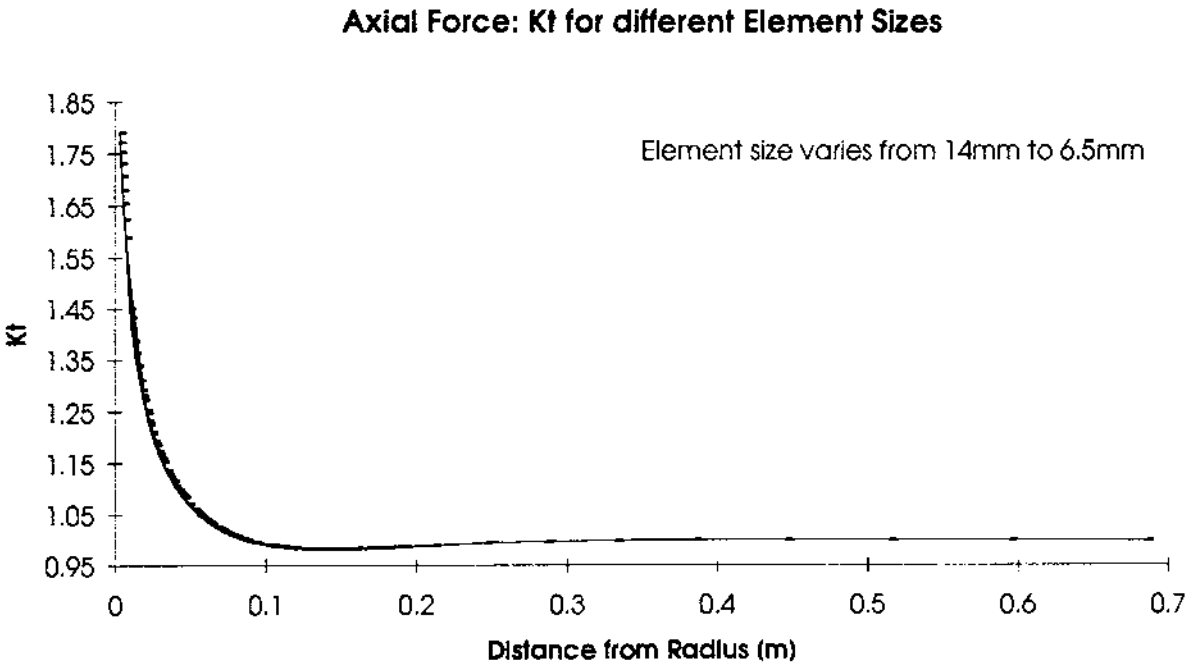

Figure 3.29: Stress Distribution along edge of plate (Acceptable Meshes)

Stress Distribution along Plate Edge (Bending Moment):
All Meshes

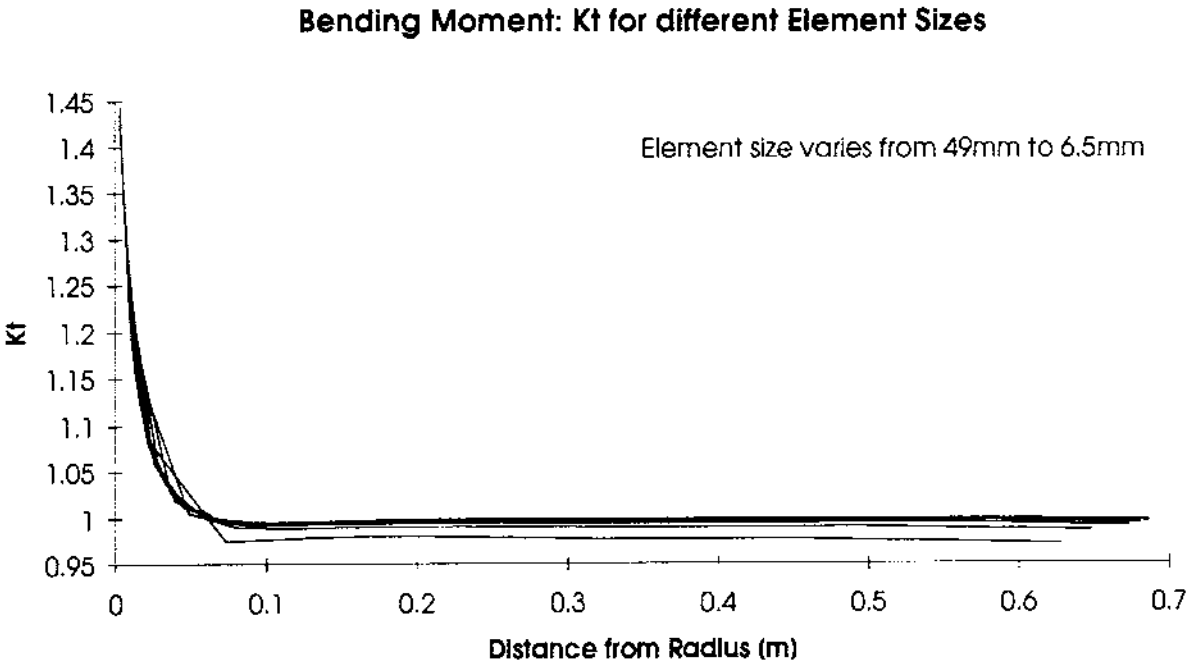

Figure 3.30: Stress Distribution along edge of plate (All Meshes)

Stress Distribution along Plate Edge (Bending Moment):
Acceptable Meshes only

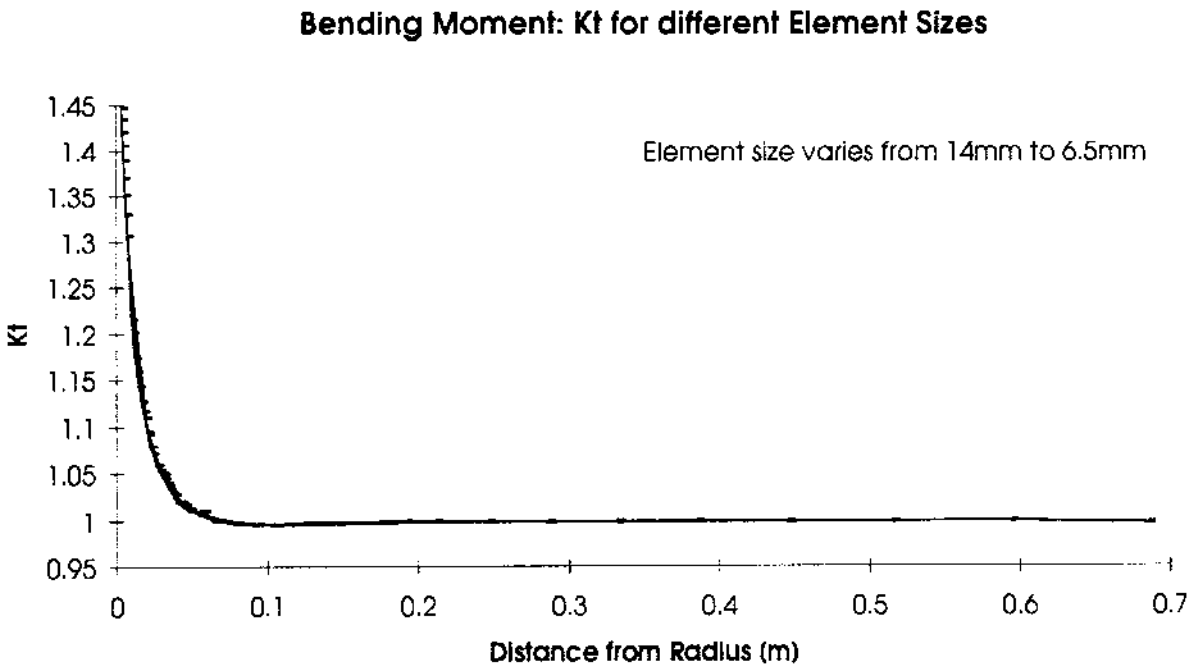

Figure 3.31: Stress Distribution along edge of plate (Acceptable Meshes)

Test Case: Flat Bar *without* a Shoulder Fillet (Tension Case)

Configuration for test case:

D/d	=	2.00
r/d	=	0.06
K_t	=	n/a

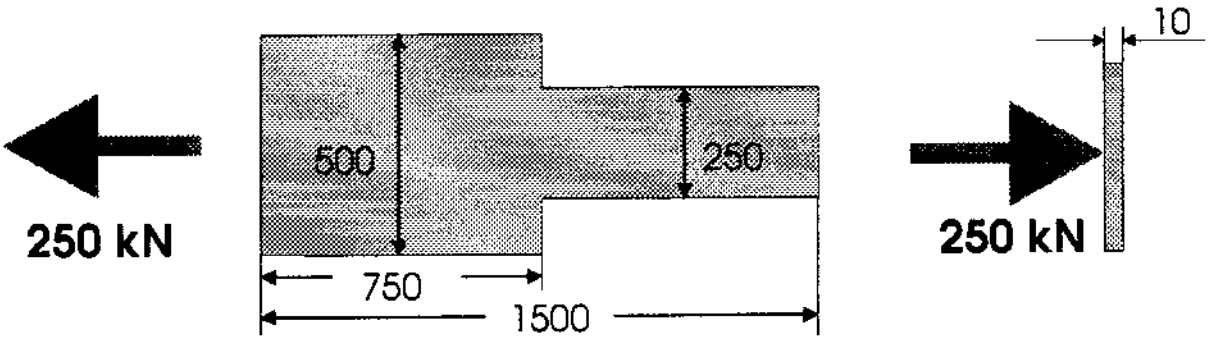

Figure 3.32: Geometry and Dimensions for Plate *without* Shoulder Fillet (Axial Force)

21

Test Case: Flat Bar **without** a Shoulder Fillet (Bending Case)

Configuration for test case:

D/d	=	2.00
r/d	=	0.06
K_t	=	n/a

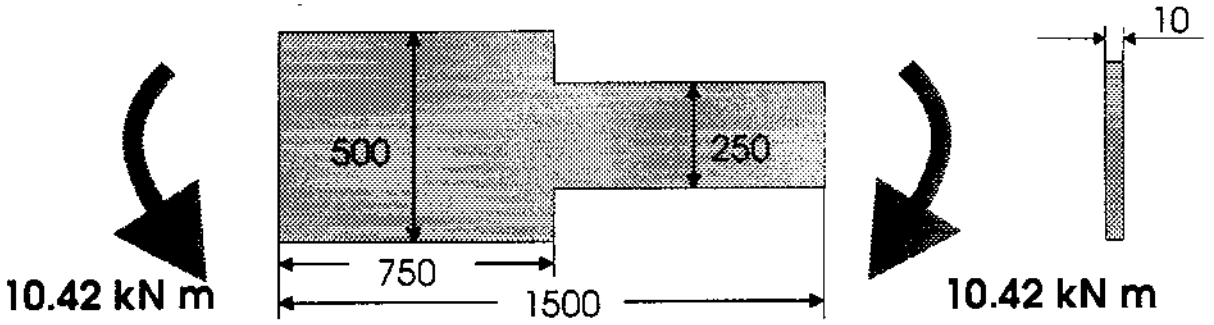

Figure 3.33: Geometry and Dimensions for Plate *without* Shoulder Fillet (Bending Moment)

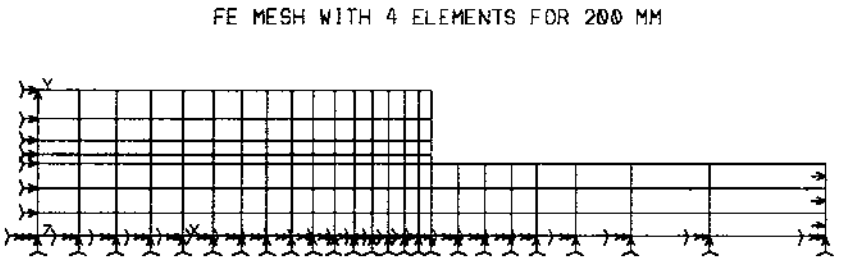

Figure 3.34: Mesh with 4 Elements per 200 mm (Axial)

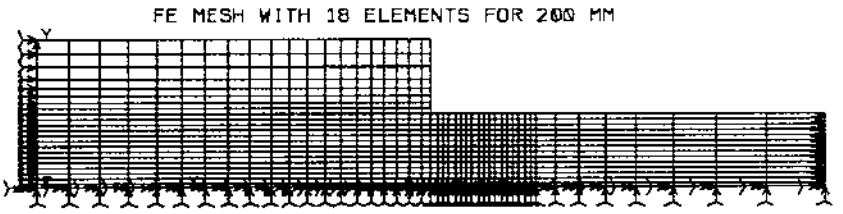

Figure 3.35: Mesh with 18 Elements per 200 mm (Axial)

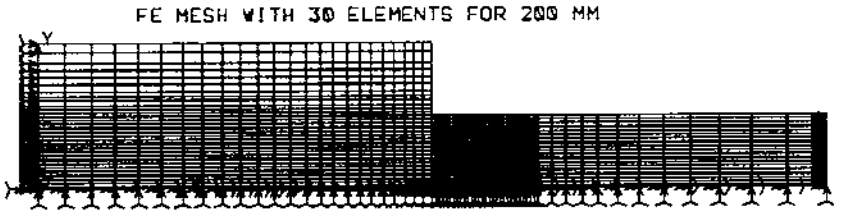

Figure 3.36: Mesh with 30 Elements per 200 mm (Axial)

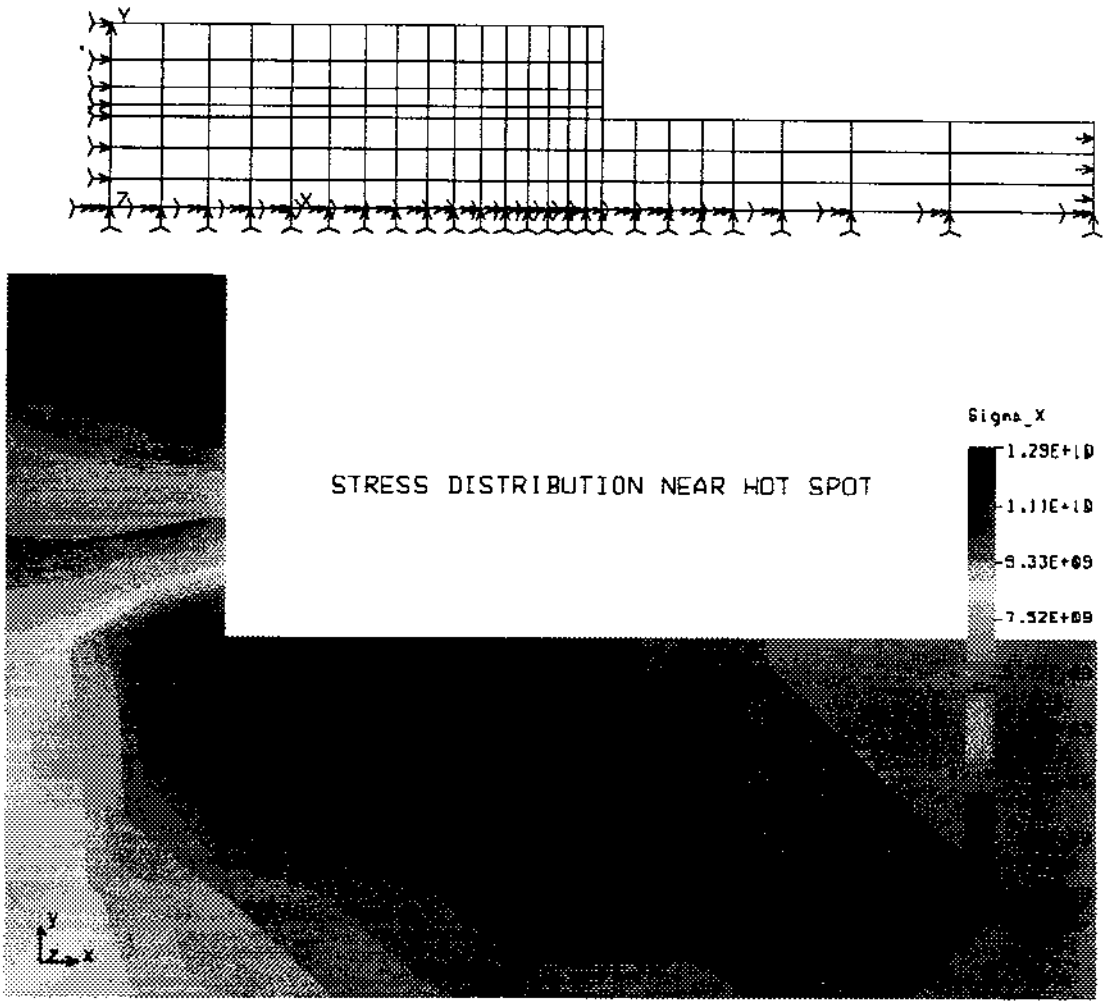

Figure 3.37: Mesh and Stress Distribution: Coarse FE Mesh

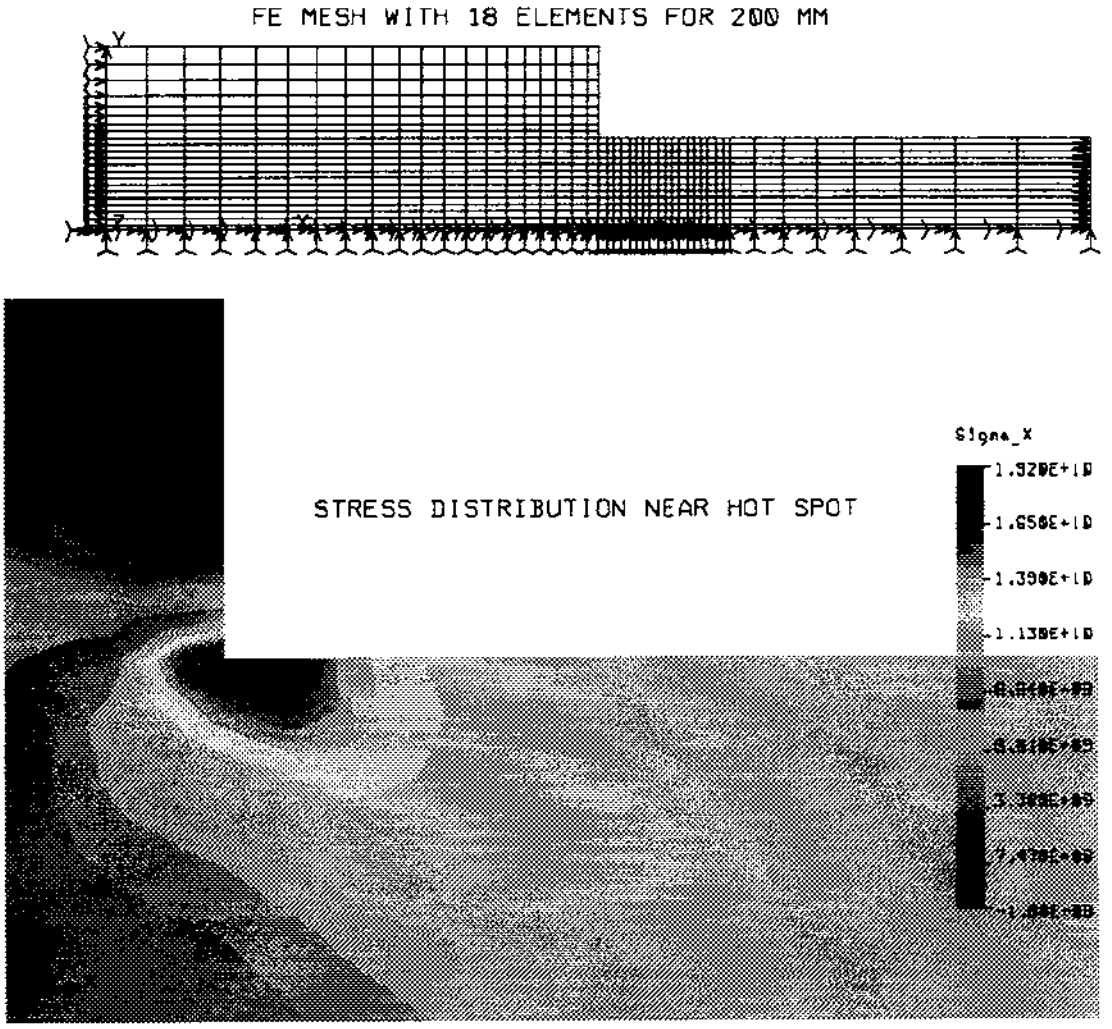

Figure 3.38: Mesh and Stress Distribution: 18 El. per $200mm$

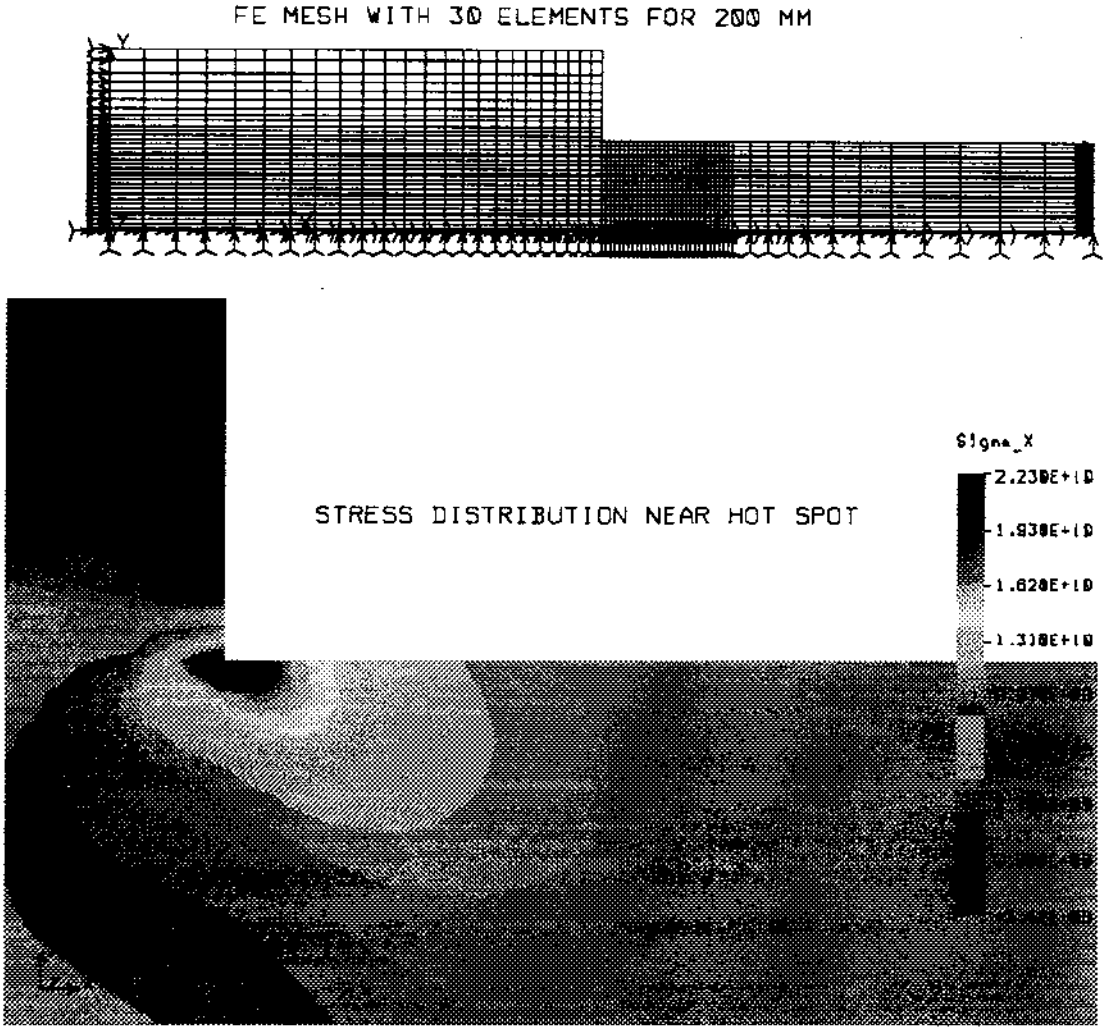

Figure 3.39: Mesh and Stress Distribution: 30 El. per $200mm$

Test Case: Flat Bar *without* a Shoulder Fillet

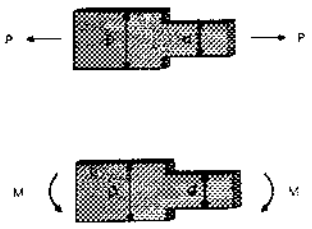

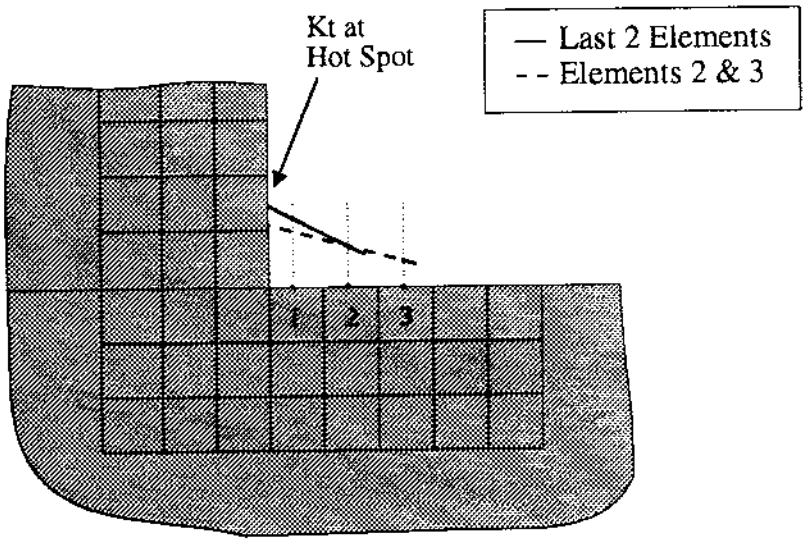

Figure 3.40: Extrapolation Methods used for Plate *without* Shoulder Fillet

77

Test Case: Flat Bar *without* a Shoulder Fillet

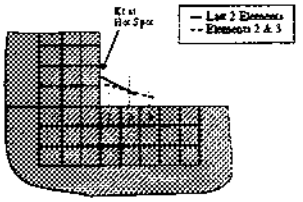

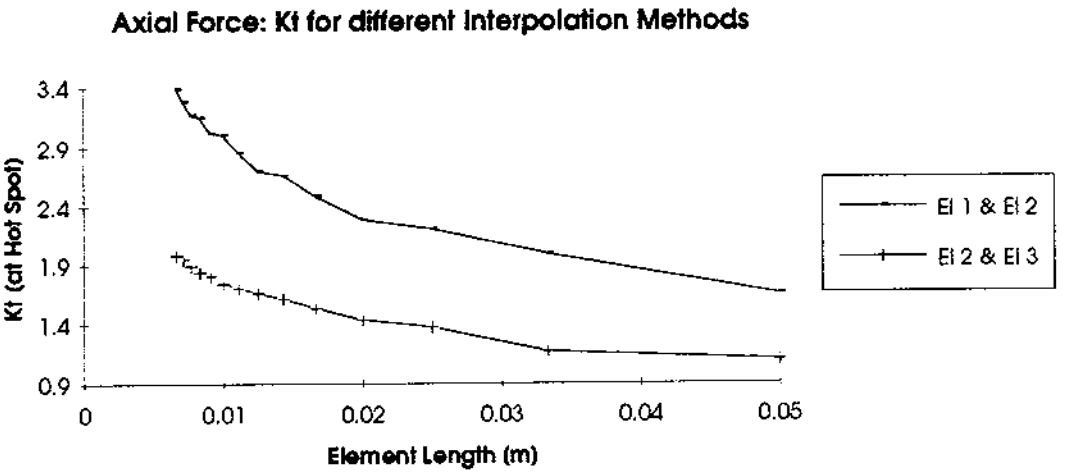

Figure 3.41: K_t for different Extrapolations: Axial Force

18

Test Case: Flat Bar *without* a Shoulder Fillet

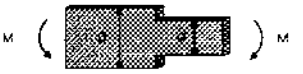

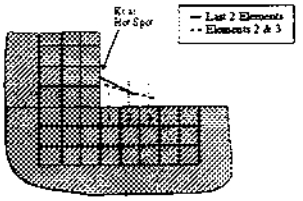

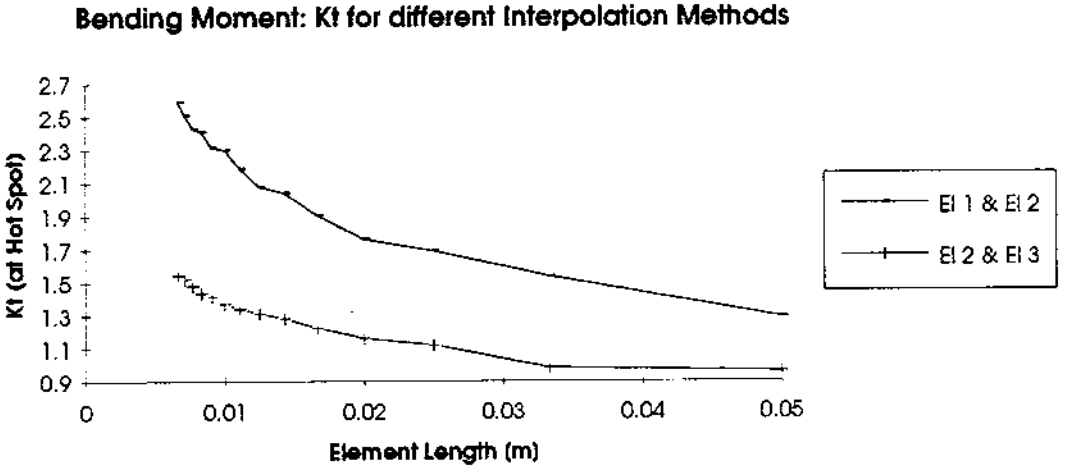

Figure 3.42: K_t for different Extrapolations: Bending Moment

Stress Distribution along Plate Edge (Axial Load):
All Meshes

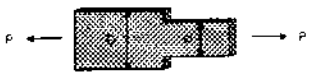

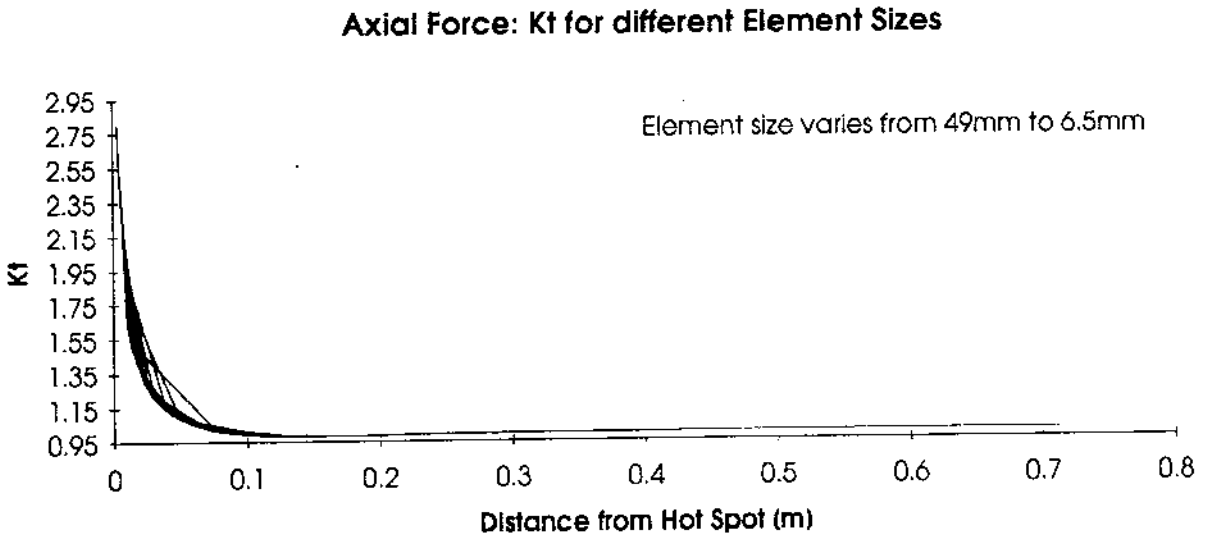

Figure 3.43: Stress Distribution along edge of plate (All Meshes)

Stress Distribution along Plate Edge (Axial Load):
Acceptable Meshes only

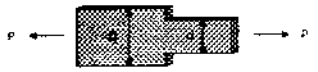

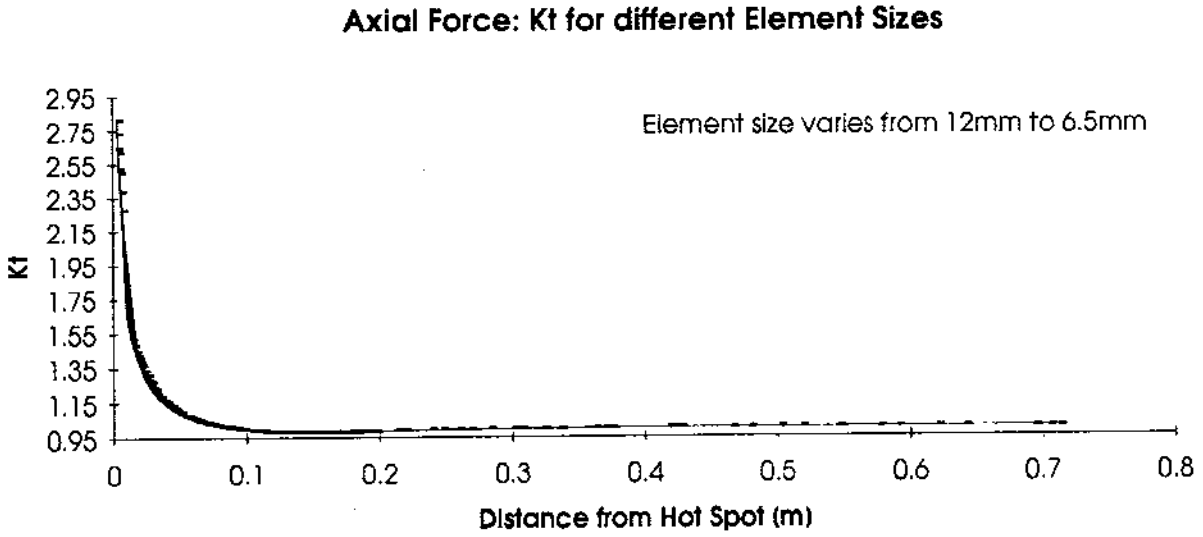

Figure 3.44: Stress Distribution along edge of plate (Acceptable Meshes)

Stress Distribution along Plate Edge (Bending Moment):
All Meshes

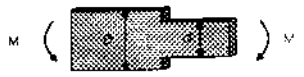

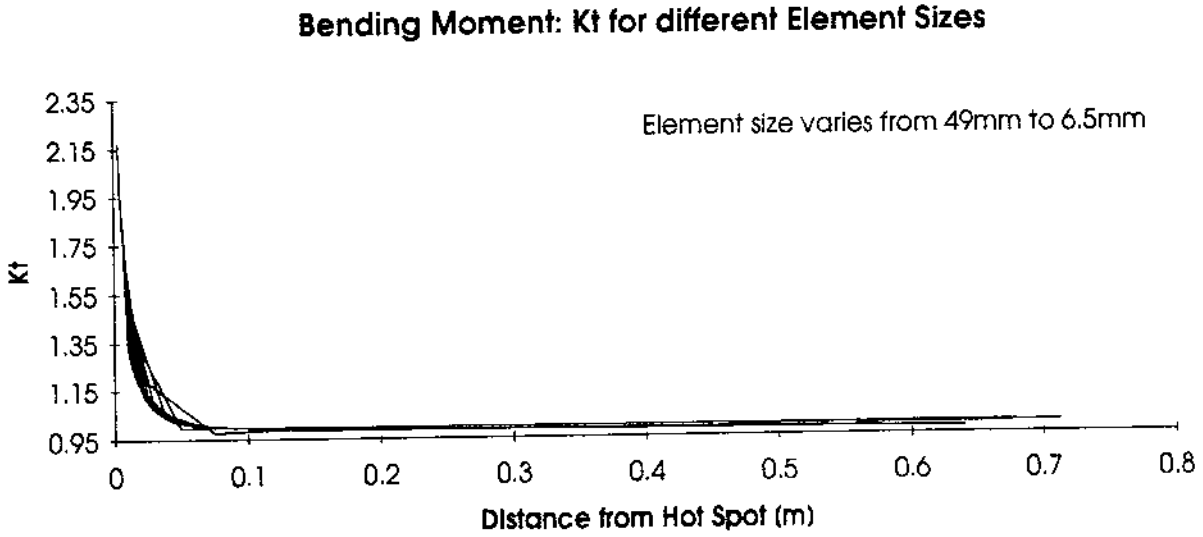

Figure 3.45: Stress Distribution along edge of plate (All Meshes)

Stress Distribution along Plate Edge (Bending Moment):
Acceptable Meshes only

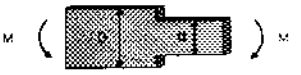

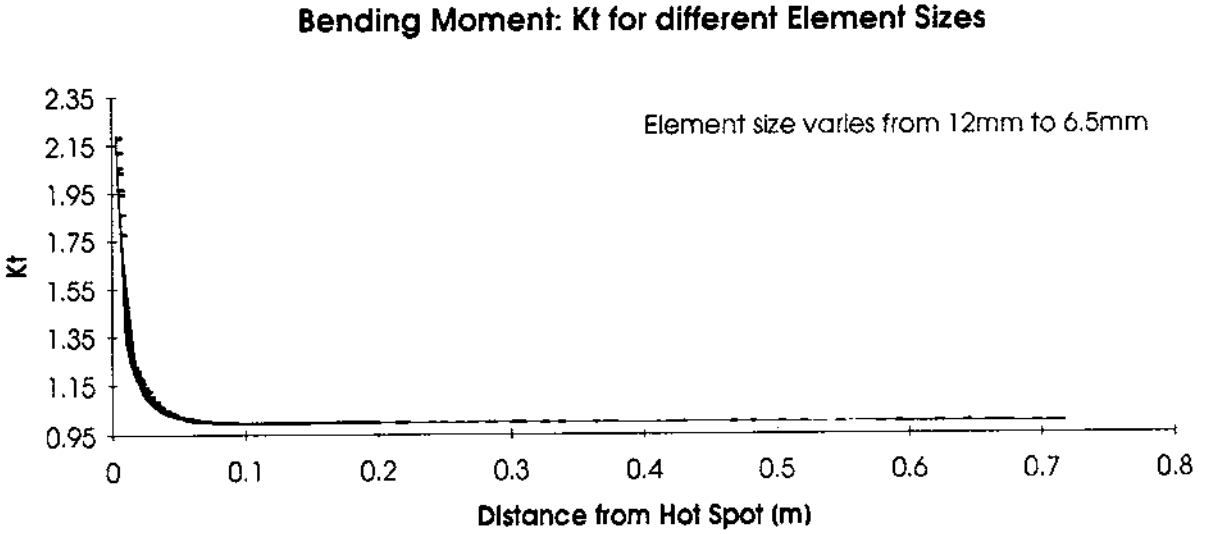

Figure 3.46: Stress Distribution along edge of plate (Acceptable Meshes)

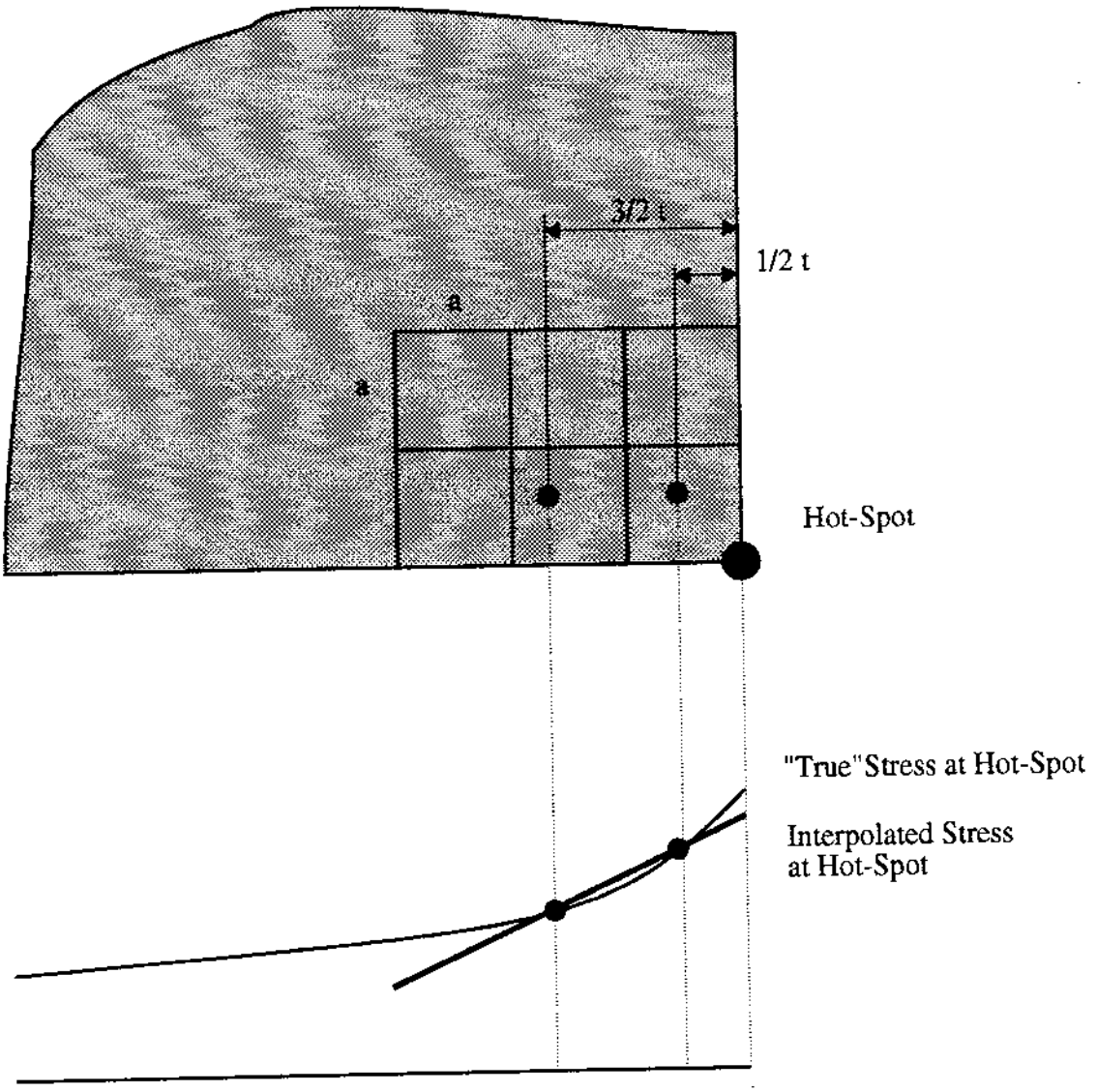

Figure 3.47: Extrapolation Method and Stress Locations

Chapter 4

Calibration of S-N Curves

4.1 Introduction

The procedure for the evaluation of fatigue damage for engineering applications is typically based on the use of S-N curves in combination with the Palmgren-Miner summation rule. Chapter 2 describes the theoretical background and also the different approaches to calculate fatigue life.

The use of S-N curves for fatigue life evaluations requires that the stresses used in the analysis are compatible with the stresses used for the derivation of the S-N curves. In the case of the S-N curves derived from tests of tubular joints the curves are based on the measured hot-spot stress. This requires that for the fatigue life analysis of a tubular joint the hot-spot stress has to be determined either through analysis or based on parametric formulae.

S-N data for most of the small-scale welded test specimen is represented based on the *nominal* stress, F/A for axial loading and M/W for bending (F = axial force, A = cross section, M = bending moment, W = section modulus). In order to use these curves for the fatigue life evaluation of complex details the *nominal* stress in the detail has to be determined.

If the *nominal* stress is used for fatigue life analysis, the influence of the local geometry on the hot-spot stress has to be accounted for through the choice of the S-N curve. For complex ship details the *nominal* stress can not be easily evaluated whereas the hot-spot stress can be obtained from finite element analysis in a straightforward manner. It is therefore desirable to develop calibrated S-N curves that are suitable for the use with *hot-spot* stresses obtained from finite element analyses.

In the following the calibration method is described. The calibration method is applied to several published S-N tests resulting in S-N curves that are suitable for the use with hot-spot stresses obtained from finite element analyses. The hot-spot stresses are obtained following the procedure developed in chapter 3.

Several organizations have developed fatigue design procedures that use a different extrapolation method to obtain hot-spot stresses from finite element analyses. In order to allow a future comparison of the different fatigue design procedures and the S-N curves used in the process, the calibration process has been repeated using hot-spot stresses obtained using a different extrapolation method. The extrapolation method and the resulting S-N curves are documented in section 4.4.

4.2 Development of Calibration Model

4.2.1 Overview

Two methods are available to obtain S-N curves that are that are suitable for the use with hot-spot stresses obtained from finite element analyses.

- Perform S-N tests for welded specimen that are similar to the structural details that are to be analysed and measure the principal stress at a defined distance from the hot-spot. From the finite element analysis of the structural detail the principal stress at the same distance from the hot-spot can be calculated. This procedure ensures that the stress used for the definition of the S-N curve and the stress obtained from the calculation are compatible.

  This procedure is very expensive since extensive S-N tests have to be performed of specimen that are comparable to the structural details to be analyzed. Nevertheless this procedure provides the largest degree of compatibility between S-N curve and analysis results.

- Calibrate existing S-N curves for the use with hot-spot stresses. This calibration requires that the calculated fatigue damage based on the original curve and the *nominal* stress is equal to the fatigue damage based on the calibrated curve in combination with the *hot-spot* stress.

4.2.2 Theoretical Calibration Model

The calibration model is developed based on the assumption that the S-N curve resulting from a series of S-N tests are represented in terms of the *nominal* stress σ_{nom}. The *nominal* stress is defined as

$$\sigma_{nom} = F/A \qquad \boxed{\text{uniaxial tensile loading}}$$

$$\sigma_{nom} = M/W \qquad \boxed{\text{bending moment}}$$

where:

F	axial force
A	area of cross-section
M	bending moment
W	section modulus

The general form of this type of S-N curve is thus given by

$$N = C(\Delta\sigma_{nom})^{-m} \tag{4.1}$$

where:

$\Delta\sigma_{nom}$	stress range based on nominal stress
m	negative inverse slope of S-N curve
$\log C$	intercept with $\log N$ axis

The parameters C and m are based on the curve fitting procedure that has been used to define the S-N curve. m represents the negative, inverse slope of the S-N curve in a log-log scale. For configurations where the contribution of the crack initiation period is insignificant e.g. welded structures this parameter can be

obtained from fracture mechanics. Most design S-N curves for welded geometries therefore have a slope parameter $m = 3.0$.

In order to calibrate existing S-N curves the parameter m is held constant. Fig. (4.1) shows a schematic view of the stress distribution in a test specimen. The nominal stress σ_{nom} is based on F/A or M/W. Due to the presence of the welded attachment this stress is increased with a maximum value of $K_t\sigma_{nom}$ at the beginning of the attachment. Here K_t represents the stress concentration factor and is defined as:

$$K_t = \frac{\sigma_{max}}{\sigma_{nom}} \tag{4.2}$$

In order to use the hot spot stress $K_t\sigma_{nom}$ for the calculation of the fatigue damage the S-N curve has to be modified. The number of cycles to failure at a given stress range for a particular test specimen is based on constant amplitude tests. The modified S-N curve therefore has to result in the same number of cycles to failure for a given hot spot stress $K_t\sigma_{nom}$. Fig. (4.2) shows the relation between the modified and the original S-N curve. The two curves have the same slope but the parameter C has been replaced by $\tilde{C}$. The following equation has been used to derive $\tilde{C}$:

$$N = C(\Delta\sigma_{nom})^{-m} = \tilde{C}(K_t\Delta\sigma_{nom})^{-m} \tag{4.3}$$

The curve parameter $\tilde{C}$ of the modified S-N curve can therefore be expressed as

$$\tilde{C} = CK_t^m \tag{4.4}$$

The modified S-N curve is depends on the method for obtaining the hot spot stress. The curve has to be used in combination with hot spot stresses that are obtained in the same way as the hot spot stress used for the determination of $\tilde{C}$.

If the hot spot stresses are compatible the calibration method used ensures that the use of the modified S-N curve in combination with the hot spot stress ($K_t\sigma_{nom}$) will result in the same fatigue life as would be obtained with the original S-N curve in combination with the nominal stress (σ_{nom}).

In chapter 3 guidelines have been developed for the mesh size and the stress recovery procedures to obtain the hot spot stress. These guidelines try to ensure that the calculated hot spot stresses are compatible independent of mesh size and model geometry. The procedure represents a compromise between generality and accuracy.

4.3 Calibration Examples

4.3.1 Introduction

Based on the calibration procedure developed in chapter 4.2 and the guidelines for mesh size and stress recovery procedure outlined in chapter def:hotspot S-N curves modified for the use with hot spot stresses are developed for three published S-N curves. For each test specimen the hot spot stress is obtained through a finite element analysis. Using equation 4.4 the modified curve parameter $\tilde{C}$ is found.

The choice of the calibration example has been governed by the availability of test data. The documentation of S-N test results has to include both the geometry of the test specimen and the curve parameters of the resulting S-N curve.

For each calibration example two finite element models are generated. The first model has the minimum mesh size near the cutout that has been specified in chapter 3.4.4 (element size = plate thickness). The second model has a very fine mesh near the hot spot (element size = 1/2 plate thickness).

The results of the analysis of the fine model make it possible to judge the accuracy of the standard model. It is planned to use the results of the standard model for the calibration. If the comparison of the results show that the standard mesh does not produce accurate results the stress concentration factor K_t is calculated using the results of the fine mesh.

4.3.2 Calibration I

4.3.2.1 Description of S-N Test Specimen

The test specimen used for Calibration I has been one of the specimen used to derive the UK Deptartment of Energy S-N curve of the F class. This fact makes the use of this specimen especially important as a calibration example. The test specimen have also been used for a series of tests under random variable amplitude loading. The specimen geometry and test results are documented in [9] and are summarized in [10].
The UKDEn S-N curve of the F class has the following parameters:

$$\begin{aligned} C &= 1.723 \times 10^{12} \\ m &= 3.0 \end{aligned}$$

The test specimen consists of a plate with a longitudinal attachment fillet welded on the center of the plate. The height of the attachment is smaller than for the detail of 2. The stiffening effect of the attachment is therefore less severe and a smaller stress concentration factor can be expected.

The model is subjected to a pulsating tension load. The specimen dimensions and the applied tension load are shown in Fig. (4.3). The magnitude of the axial force has been chosen in order to produce a *nominal* stress of $100N/mm^2$.

4.3.2.2 Finite Element Analysis

Based on the dimensions shown in Fig. (4.3) two finite element models of the test specimen have been generated. The first model has the minimum mesh size near the cutout that has been specified in chapter 3.4.4. The second model has a very fine mesh near the hot spot. The results of the analysis with the fine mesh are used to judge the accuracy of the standard mesh. Fig. (4.4) shows the two models. Both models consist of 4-node shell elements.

Both models have been subjected to the same axial force. The resulting stress distributions are shown in Fig. (4.5). For both models the stress distribution along the centerline towards the hot spot has been plotted, see Fig. (4.6). This plot indicates that the standard model does not calculate the stress distribution near the hot spot with sufficient accuracy. The determination of the stress concentration factor K_t has therefore been based on the stresses obtained from the fine model.

The stress concentration factor K_t has been obtained using the stresses at 1/2 and 3/2 plate thickness from the hot spot and linearly extrapolating to the hot spot. Since the stresses at 1/2 and 3/2 plate thickness are not directly available

(no Gauss points at these locations), they have been interpolated using the stresses at the center points of the two adjacent elements.
The following stress concentration factor K_t has been calculated:

$$K_t = 1.643$$

4.3.2.3 Calibration

Based on the calibration procedure described in chapter 4.2.2 using the S-N curve parameters listed above the calibrated S-N curve with the following curve parameters has been obtained:

$$\begin{aligned} m &= 3.0 \\ \tilde{C} &= 7.65 \times 10^{12} \\ \log \tilde{C} &= 12.884 \end{aligned}$$

4.3.3 Calibration II

4.3.3.1 Description of S-N Test Specimen

The test specimen used for Calibration II has been one of the specimen used to derive the UK Deptartment of Energy S-N curve of the F2 class. This fact makes the use of this specimen especially important as a calibration example. The S-N tests including specimen geometry and results are documented in [11].
The UKDEn S-N curve of the F2 class has the following parameters:

$$\begin{aligned} C &= 1.23 \times 10^{12} \\ m &= 3.0 \end{aligned}$$

The test specimen consists of a plate with a longitudinal attachment fillet welded on the center of the plate. The model is subjected to a pulsating tension load. The specimen dimensions and the applied tension load are shown in Fig. (4.7). The magnitude of the axial force has been chosen in order to produce a *nominal* stress of $100 N/mm^2$.

4.3.3.2 Finite Element Analysis

Based on the dimensions shown in Fig. (4.7) two finite element models of the test specimen have been generated. The first model has the minimum mesh size near the cutout that has been specified in chapter 3.4.4. The second model has a very fine mesh near the hot spot. The results of the analysis with the fine mesh are used to judge the accuracy of the standard mesh. Fig. (4.8) shows the two models. Both models consist of 4-node shell elements.

Both models have been subjected to the same axial force. The resulting stress distributions are shown in Fig. (4.9). For both models the stress distribution along the centerline towards the hot spot has been plotted, see Fig. (4.10). This plot indicates that the standard model does not calculate the stress distribution near the hot spot with sufficient accuracy. The determination of the stress concentration factor K_t has therefore been based on the stresses obtained from the fine model.

The stress concentration factor K_t has been obtained using the stresses at 1/2 and 3/2 plate thickness from the hot spot and linearly extrapolating to the hot

spot. Since the stresses at 1/2 and 3/2 plate thickness are not directly available (no Gauss points at these locations), they have been interpolated using the stresses at the center points of the two adjacent elements.
The following stress concentration factor K_t has been calculated:

$$K_t = 1.791$$

4.3.3.3 Calibration

Based on the calibration procedure described in chapter 4.2.2 using the S-N curve parameters listed above the calibrated S-N curve with the following curve parameters has been obtained:

$$\begin{aligned} m &= 3.0 \\ \tilde{C} &= 7.07 \times 10^{12} \\ \log \tilde{C} &= 12.849 \end{aligned}$$

4.3.4 Calibration III

4.3.4.1 Description of S-N Test Specimen

The test specimen used for Calibration III has been used for a series of S-N tests performed by the Welding Institute. The tests are documented in [12], [13].

The S-N curve that has been determined based on the tests under pulsating tension loading of constant amplitude at $R = 0$ has the following parameters:

$$\begin{aligned} C &= 0.568 \times 10^{12} \\ m &= 3.0 \end{aligned}$$

This S-N curve is very close to the Dept. of Energy S-N curve of the G class ($m = 3$, $C = 0.566 \times 10^{12}$).

The test specimen consists of a plate with a longitudinal attachment fillet welded to each edge. The specimen dimensions and the applied tension load are shown in Fig. (4.11). The magnitude of the axial force has been chosen in order to produce a *nominal* stress of $100 N/mm^2$.

4.3.4.2 Finite Element Analysis

Based on the dimensions shown in Fig. (4.11) two finite element models of the test specimen have been generated. The results of the analysis with the fine mesh are used to judge the accuracy of the standard mesh. Fig. (4.12) shows the two models. Both models consist of 4-node shell elements. Truss elements have been placed along the edge of the plate to facilitate the stress recovery.

Both models have been subjected to the same axial force. The resulting stress distributions are shown in Fig. (4.13). For both models the stress distribution along the centerline towards the hot spot has been plotted, see Fig. (4.14). This plot indicates that the standard model does not calculate the stress distribution near the hot spot with sufficient accuracy. The determination of the stress concentration factor K_t has therefore been based on the stresses obtained from the fine model.

The stress concentration factor K_t has been obtained using the stresses at 1/2 and 3/2 plate thickness from the hot spot and linearly extrapolating to the hot

spot. Since the stresses at 1/2 and 3/2 plate thickness are not directly available (no Gauss points at these locations), they have been interpolated using the stresses at the center points of the two adjacent elements.
The following stress concentration factor K_t has been calculated:

$$K_t = 2.339$$

4.3.4.3 Calibration

Based on the calibration procedure described in chapter 4.2.2 using the S-N curve parameters listed above the calibrated S-N curve with the following curve parameters has been obtained:

$$\begin{aligned} m &= 3.0 \\ \tilde{C} &= 7.32 \times 10^{12} \\ \log \tilde{C} &= 12.859 \end{aligned}$$

4.3.5 Calibration IV

4.3.5.1 Description of S-N Test Specimen

The test specimen used for Calibration IV has been investigated as part of a research project to develop thickness effect criteria for the fatigue strength evaluation of welded steel structures. This project is documented in [14]. The effects of weld improvements on the thickness effect were investigated. Overall profiling and toe-grinding were compared.

Nonload-carriying fillet-welded cruciform joints and T-joints were investigated. For Calibration IV a cruciform joint under tension load has been selected. Weld profiling has been used for this specimen.

Based on the test results for 7 specimen a S-N curve has been determined. This curve has the following parameters:

$$\begin{aligned} C &= 6.31 \times 10^{14} \\ m &= 4.05 \end{aligned}$$

The specimen dimensions and the applied tension load are shown in Fig. (4.15). The magnitude of the axial force has been chosen in order to produce a *nominal* stress of $100 N/mm^2$.

4.3.5.2 Finite Element Analysis

Based on the dimensions shown in Fig. (4.15) two finite element models of the test specimen have been generated. The first model has the minimum mesh size near the cutout that has been specified in chapter 3.4.4. The second model has a very fine mesh near the hot spot. A comparison of the stress concentration factors K_t obtained by the two meshes allows it to verify that mesh size has only an insignificant influence on the K_t values.

The results of the analysis with the fine mesh are used to judge the accuracy of the standard mesh. Fig. (4.16) shows the two models. Both models consist of 4-node shell elements. The actual stress distribution at the connection of the two

detail by using the main detail dimensions. A detailed study that investigates the factors that govern the required plate thickness in the different class rules would be very beneficial for this purpose.

It has to be stated again that the calibrated S-N curve with the parameters $\tilde{C}_0 = 7.32 \times 10^{12}$ and $m = 3.0$ can only be used in conjunction with the mesh size and the stress recovery procedure defined in section 3.4.4.

The hot-spot location for this stress recovery procedure ignores the presence of a weld. The calibrated S-N curve can therefore not be used for hot-spot stresses that have been obtained by extrapolation to the weld toe.

Table 4.1: Summary of Alternative Calibration Analyses

	Calibration I F-curve	Calibration II F2-curve	Calibration III G-curve
m	3	3	3
C	1.73E+12	1.23E+12	5.66E+11
$\log C$	12.237	12.09	11.7525
K_t	1.3578	1.45968	1.66048
$\tilde{C}$	4.33E+12	3.83E+12	2.59E+12
$\log \tilde{C}$	12.6365	12.5827	12.4135

Table 4.2: Summary of Calibration Analyses

	Calibration I F-curve	Calibration II F2-curve	Calibration III G-curve	Calibration IV
m	3	3	3	4.05
C	1.73E+12	1.23E+12	5.66E+11	6.31E+14
$\log C$	12.237	12.09	11.7525	14.80003
K_t	1.642593	1.791043	2.338553	1.002533
$\tilde{C}$	7.65E+12	7.07E+12	7.23E+12	6.37E+14
$\log \tilde{C}$	12.88359	12.84932	12.85934	14.80448

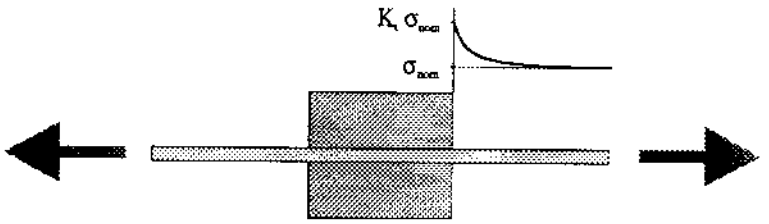

Figure 4.1: Stress distribution for S-N test specimen

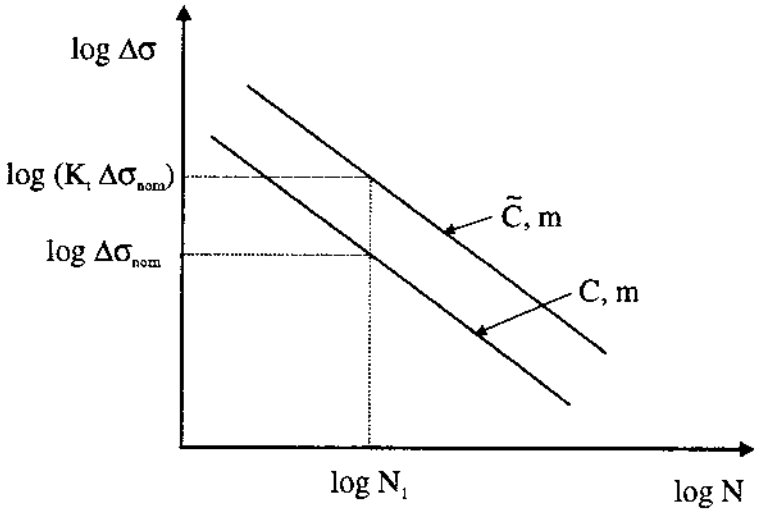

Figure 4.2: Relationship between original and modified S-N Curve

Standard Mesh

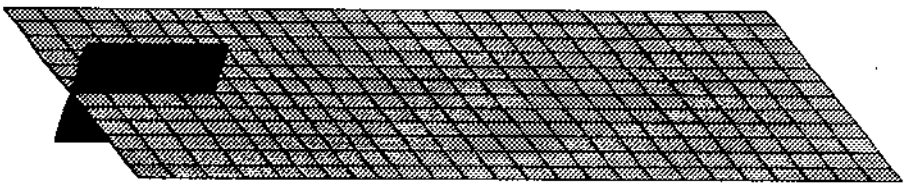

Fine Mesh

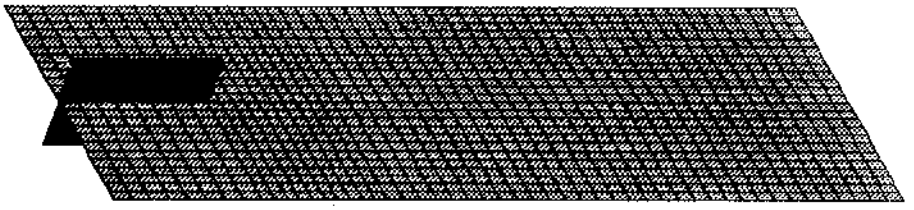

Figure 4.4: Finite Element Models for Calibration I

Standard Mesh

Fine Mesh

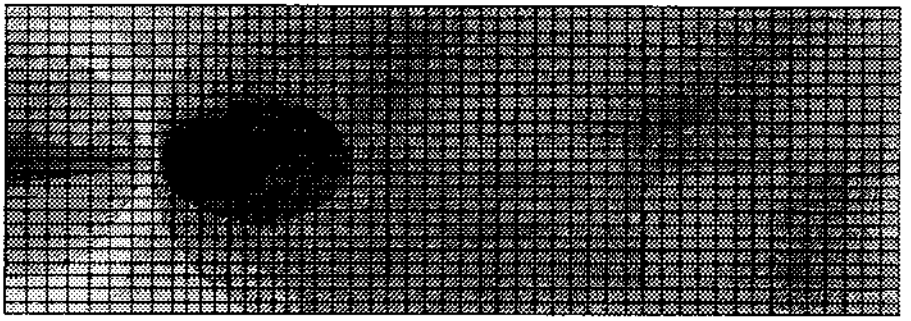

Figure 4.5: Stress Distributions for Calibration I

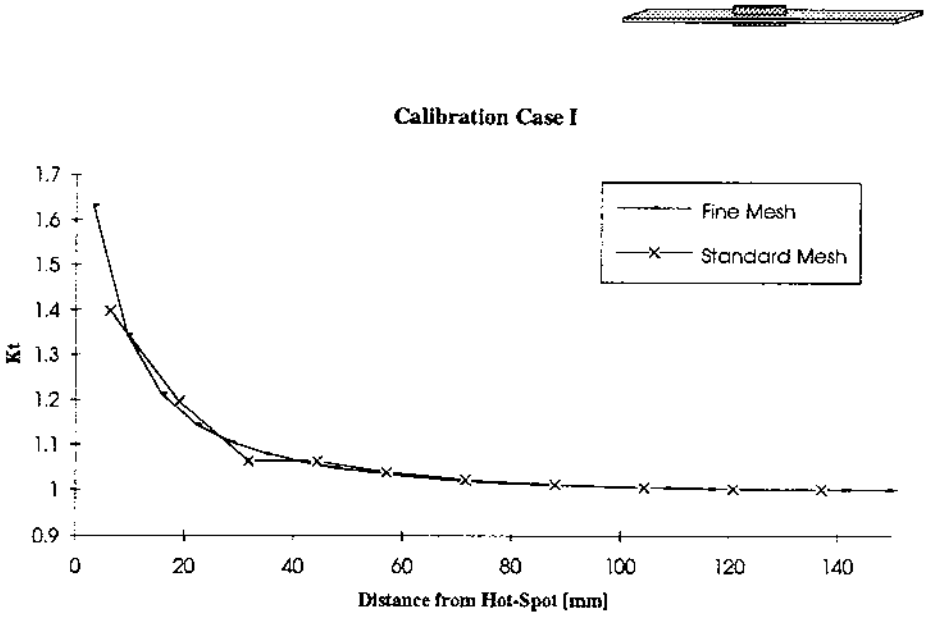

Figure 4.6: Distribution of Extrapolation Stresses for Calibration I

Calibration II

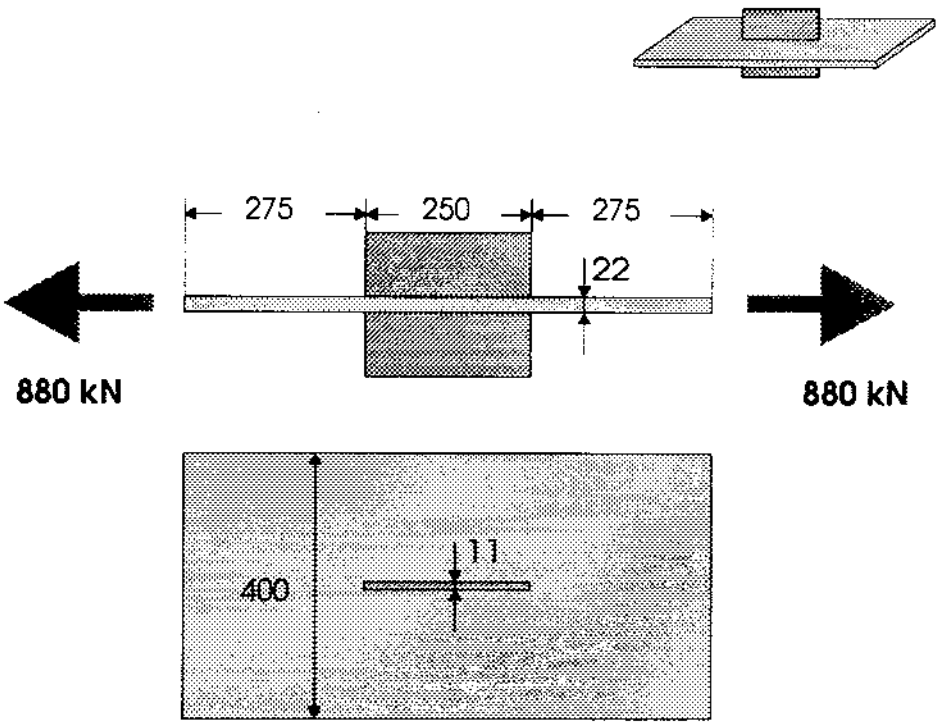

Figure 4.7: Geometry and Dimensions for Calibration II

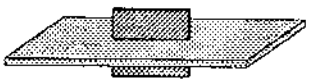

Standard Mesh

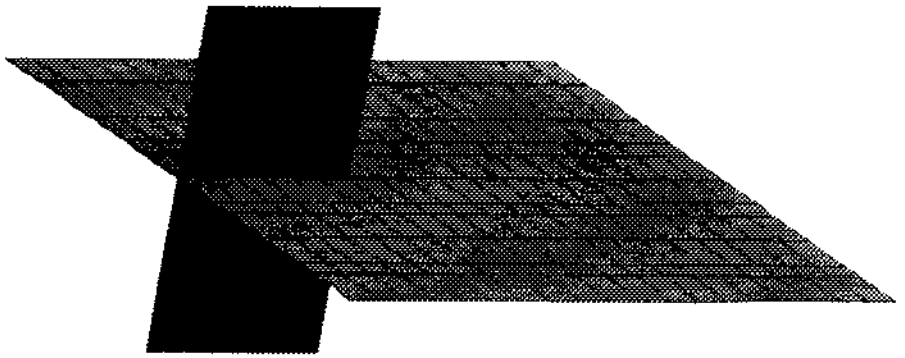

Fine Mesh

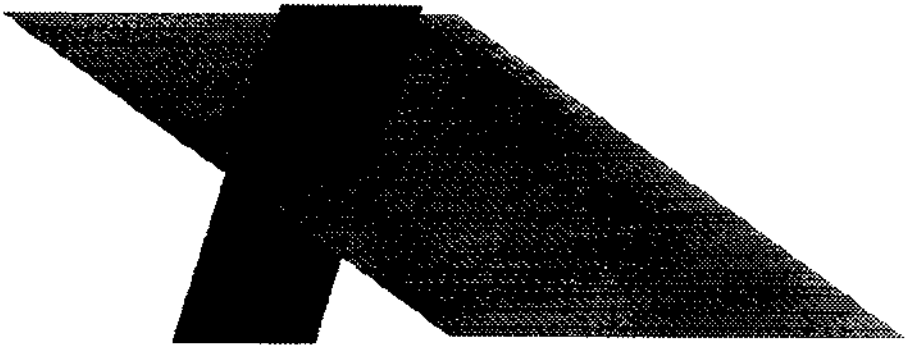

Figure 4.8: Finite Element Models for Calibration II

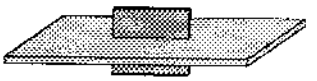

Standard Mesh

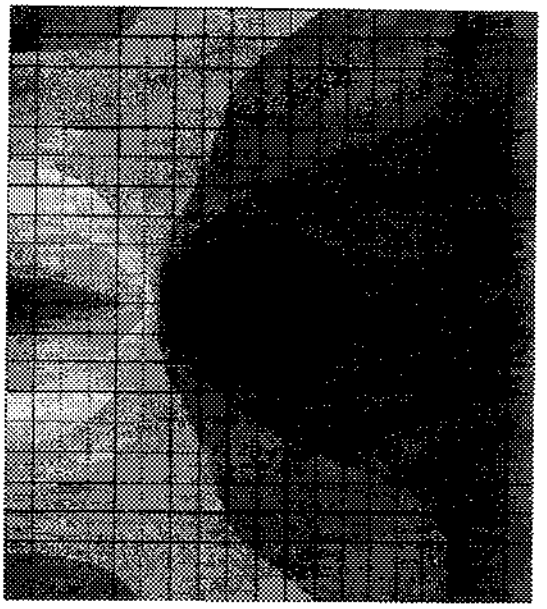

Fine Mesh

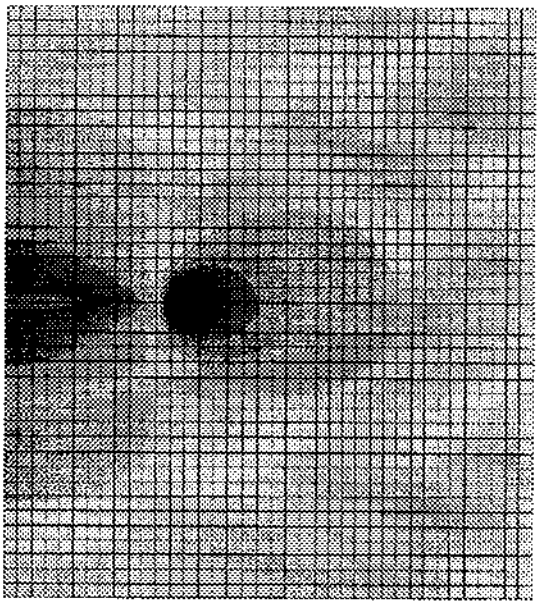

Figure 4.9: Stress Distributions for Calibration II

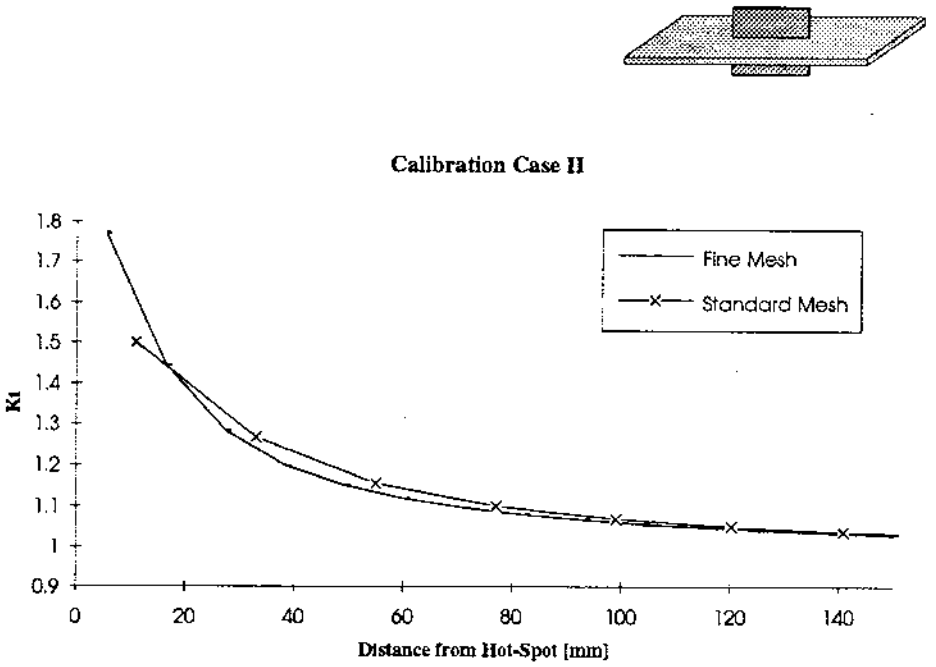

Figure 4.10: Distribution of Extrapolation Stresses for Calibration II

Calibration III

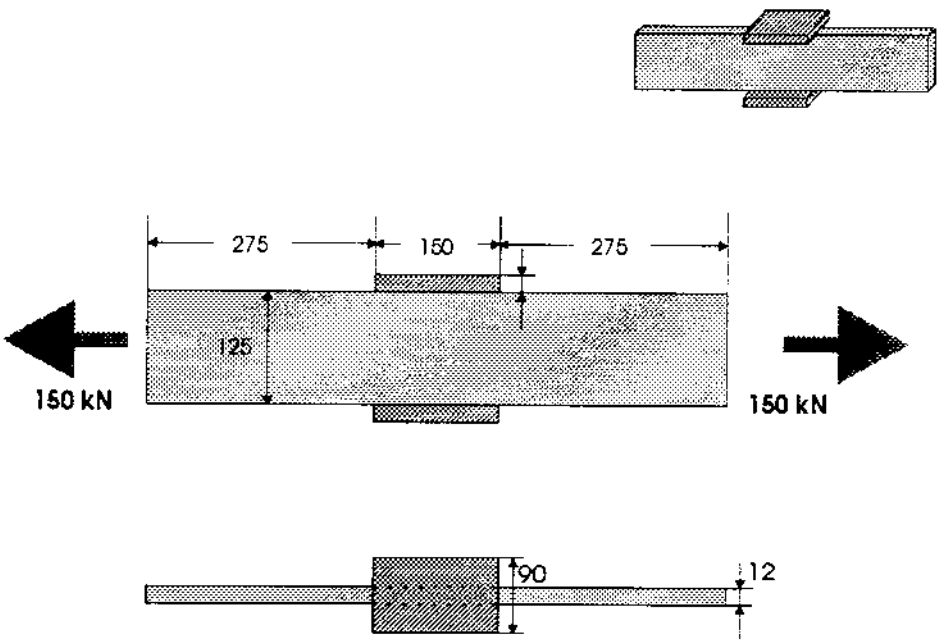

Figure 4.11: Geometry and Dimensions for Calibration III

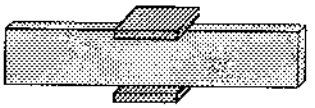

Standard Mesh

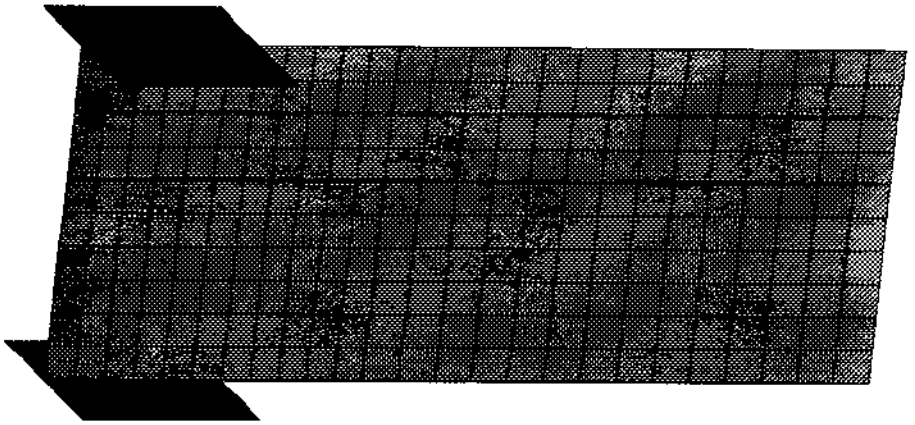

Fine Mesh

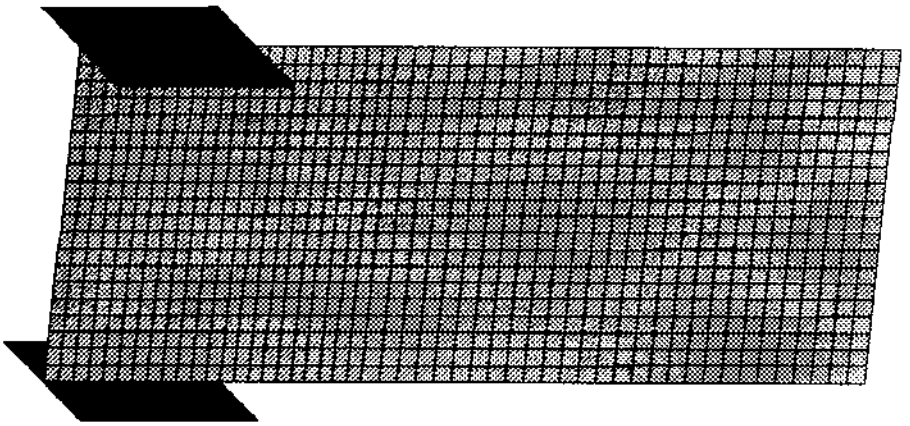

Figure 4.12: Finite Element Models for Calibration III

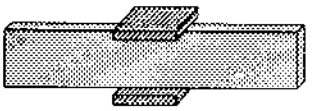

Standard Mesh

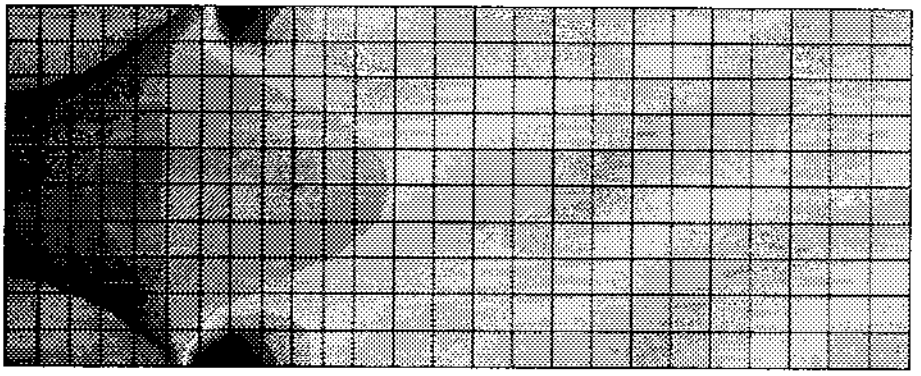

Fine Mesh

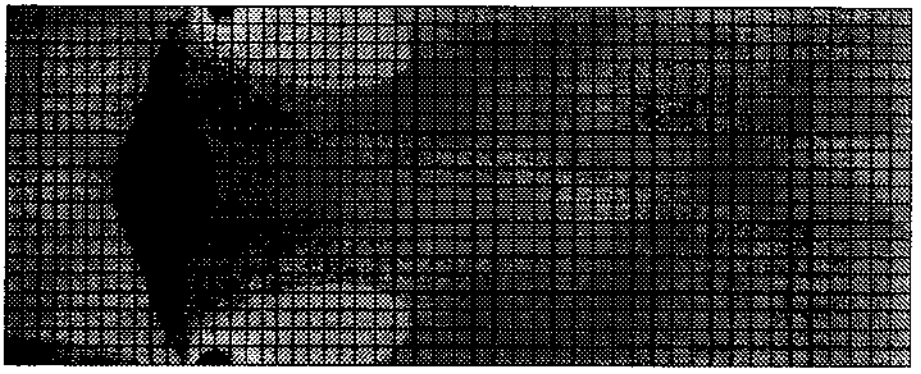

Figure 4.13: Stress Distributions for Calibration III

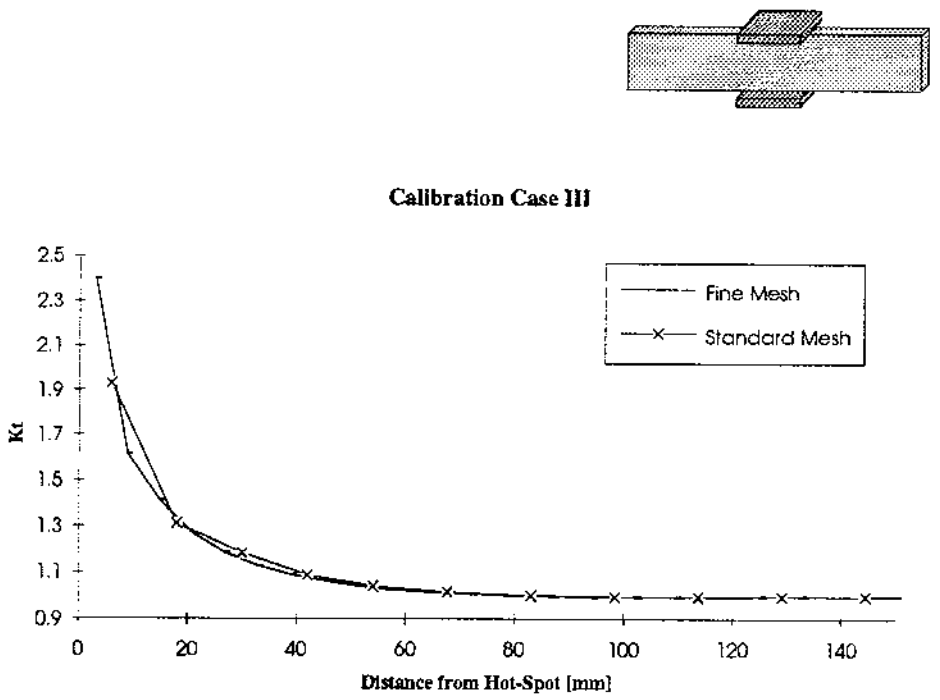

Figure 4.14: Distribution of Extrapolation Stresses for Calibration III

Calibration IV

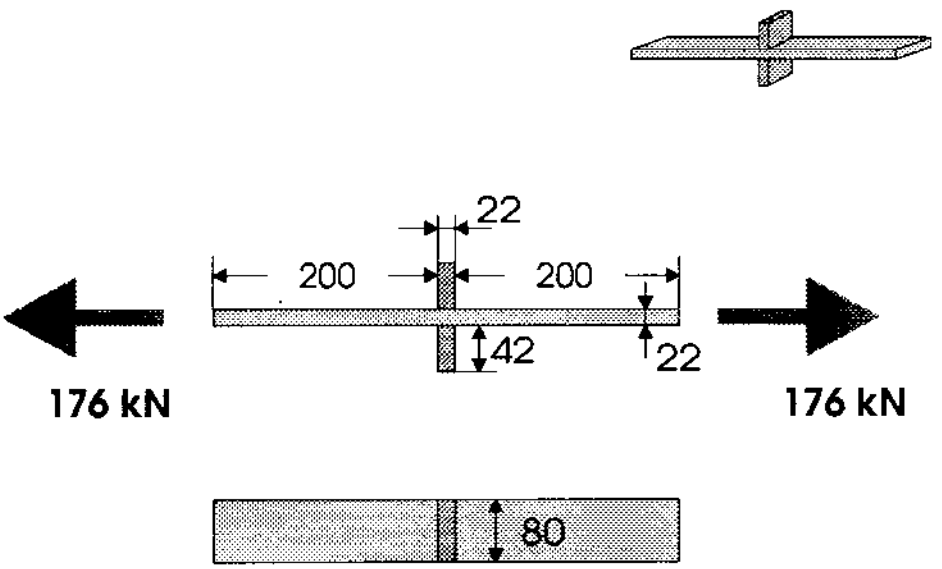

Figure 4.15: Geometry and Dimensions for Calibration IV

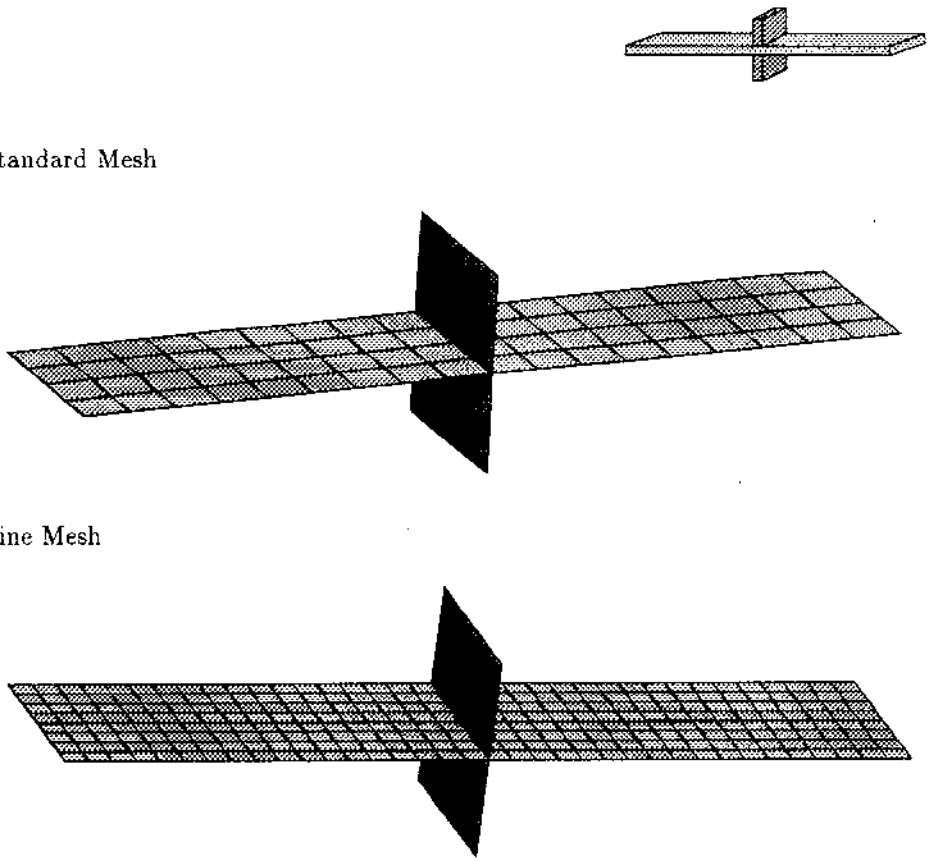

Figure 4.16: Finite Element Models for Calibration IV

111

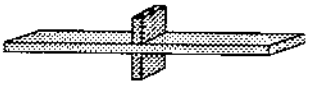

Standard Mesh

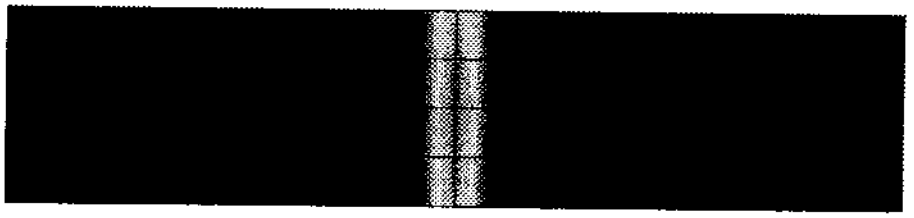

Fine Mesh

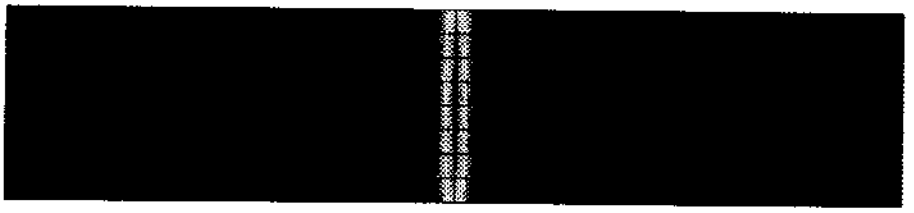

Figure 4.17: Stress Distributions for Calibration IV

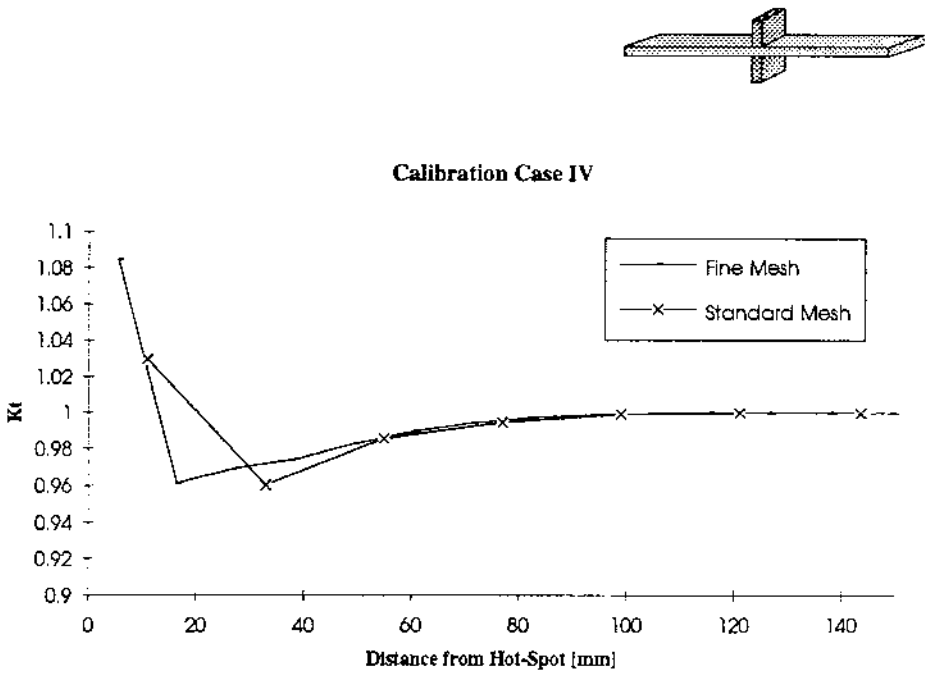

Figure 4.18: Distribution of Extrapolation Stresses for Calibration IV

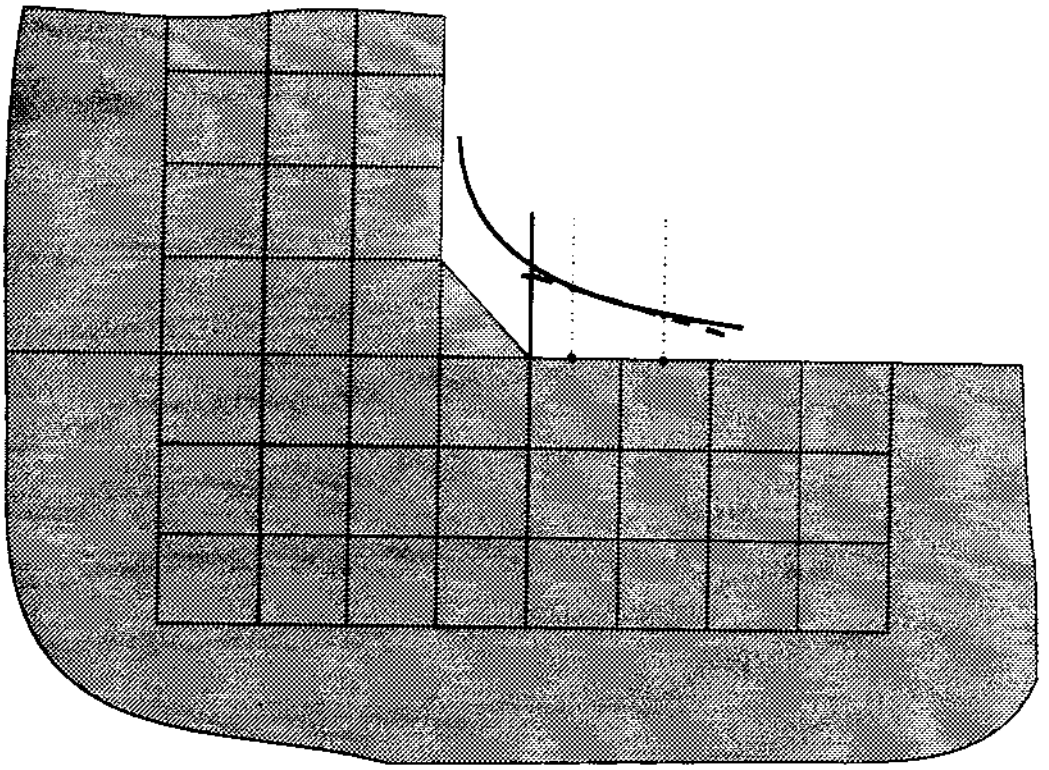

Figure 4.19: Alternative Extrapolation Procedure

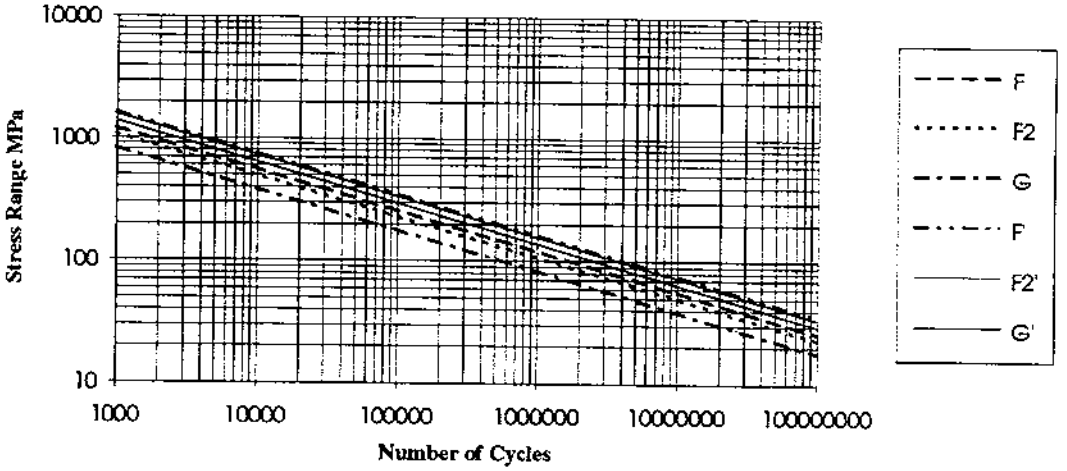

Figure 4.20: S-N Curves based on Alternative Calibration

spot. Since the stresses at 1/2 and 3/2 plate thickness are not directly available (no Gauss points at these locations), they have been interpolated using the stresses at the center points of the two adjacent elements.
The following stress concentration factor K_t has been calculated:

$$K_t = 2.339$$

4.3.4.3 Calibration

Based on the calibration procedure described in chapter 4.2.2 using the S-N curve parameters listed above the calibrated S-N curve with the following curve parameters has been obtained:

$$\begin{aligned} m &= 3.0 \\ \tilde{C} &= 7.32 \times 10^{12} \\ \log \tilde{C} &= 12.859 \end{aligned}$$

4.3.5 Calibration IV

4.3.5.1 Description of S-N Test Specimen

The test specimen used for Calibration IV has been investigated as part of a research project to develop thickness effect criteria for the fatigue strength evaluation of welded steel structures. This project is documented in [14]. The effects of weld improvements on the thickness effect were investigated. Overall profiling and toe-grinding were compared.

Nonload-carriying fillet-welded cruciform joints and T-joints were investigated. For Calibration IV a cruciform joint under tension load has been selected. Weld profiling has been used for this specimen.

Based on the test results for 7 specimen a S-N curve has been determined. This curve has the following parameters:

$$\begin{aligned} C &= 6.31 \times 10^{14} \\ m &= 4.05 \end{aligned}$$

The specimen dimensions and the applied tension load are shown in Fig. (4.15). The magnitude of the axial force has been chosen in order to produce a *nominal* stress of $100 N/mm^2$.

4.3.5.2 Finite Element Analysis

Based on the dimensions shown in Fig. (4.15) two finite element models of the test specimen have been generated. The first model has the minimum mesh size near the cutout that has been specified in chapter 3.4.4. The second model has a very fine mesh near the hot spot. A comparison of the stress concentration factors K_t obtained by the two meshes allows it to verify that mesh size has only an insignificant influence on the K_t values.

The results of the analysis with the fine mesh are used to judge the accuracy of the standard mesh. Fig. (4.16) shows the two models. Both models consist of 4-node shell elements. The actual stress distribution at the connection of the two

plates can not be obtained with shell elements since the elements are located on the centerlines of the two plates. Due to the fact that structural details are commonly analysed using shell elements the two models have been created and analysed to demonstrate these inadequacies.

Both models have been subjected to the same axial force. The resulting stress distributions are shown in Fig. (4.17). For both models the stress distribution along the centerline towards the hot spot has been plotted, see Fig. (4.18). It can be seen that the stress increases by about 10 % in the last element before the vertical plate.

Although even the stress distribution from the fine mesh is not very accurate close to the intersection of the two plates the determination of the stress concentration factor K_t has been based on the stresses obtained from the fine model.

The stress concentration factor K_t has been obtained using the stresses at 1/2 and 3/2 plate thickness from the hot spot and linearly extrapolating to the hot spot. Since the stresses at 1/2 and 3/2 plate thickness are not directly available (no Gauss points at these locations), they have been interpolated using the stresses at the center points of the two adjacent elements.
The following stress concentration factor K_t has been calculated:

$$K_t = 1.003$$

This indicates that for test specimen used in Calibration IV the hot spot stress and the nominal stress are virtually identical based on the extrapolation method used.

4.3.5.3 Calibration

Based on the calibration procedure described in chapter 4.2.2 using the S-N curve parameters listed above the calibrated S-N curve with the following curve parameters has been obtained:

$$\begin{aligned} m &= 3.0 \\ \tilde{C} &= 7.3210^{12} \\ \log \tilde{C} &= 12.859 \end{aligned}$$

Due to the fact that the stress concentration factor K_t is very close to 1.0 the curve parameters of the calibrated curve are almost identical to the original curve parameters.

4.4 Alternative Extrapolation and Calibration

The above performed calibration analyses use an extrapolation method that ignores the presence of the weld. In order to investigate the effects of a different extrapolation procedure, the calibration has been repeated using hot-spot stresses obtained by an alternative extrapolation procedure.

4.4.1 Stress Extrapolation

The stress extrapolation for the alternative calibration extrapolates the stresses at $1/2t$ and $3/2t$ to the toe of the weld. This is the method used by several classification societies. Fig. (4.19) shows the extrapolation procedure.

4.4.2 Alternative Calibration

For the first three calibration cases the hot-spot stresses have been re-calculated using the above defined extrapolation method. As to be expected the resulting stress concentration factors are lower than the ones obtained from the original calibration analyses.

The calibration has been performed for the three calibration cases based on the calculated stress concentration factors. Table (4.1) lists the stress concentration factors and the resulting calibrated S-N curves. Fig. (4.20) shows both the three calibrated curves (F', F2', G') and the three original S-N curves (F, F2, G).

For the F and F2 curve the resulting curve parameters of the calibrated curves (F', F2') are close together (4.33E+12 and 3.83E+12). However, the calibrated curve parameter for the G curve (2.59E+12) is distinctively different. The results of the calibration therefore do not allow it to combine the three calibrated curves into one S-N curve to be used for fatigue design based on hot-spot stresses obtained from finite element analyses.

4.5 Summary and Conclusion

Based on the approach developed in chapter 4.2.2 4 S-N test specimen have been analysed and the respective S-N curves have been calibrated for the use with hot spot stresses obtained through finite element analyses.

Three of the test specimen have been used to derive the UK Department of Energy S-N curves. The calibrated curves for these specimen are therefore especially useful for application purposes since they can be used in place of the standard curves.

The fourth calibration case is based on a test specimen consisting of a plate with plates welded perpendicular to the load on each side. For this configuration the use of shell elements cannot realisticly reproduce the stress distribution near the hot spot. The resulting stress concentration factor K_t was very close to 1.0. This calibration case was included to demonstrate both the limitations of shell elements for certain configurations and the limitations of the calibration procedure.

For each specimen two finite element models have been created. One model with the minimum mesh size defined in chapter 3.4.4 and the other one with element length decreased by a factor of 2. The analyses have shown that for all 4 test specimen the stress distribution could not be calculated with sufficient accuracy using the standard mesh size. The stress concentration factor K_t has therefore been calculated using the fine mesh.

In order to use the developed calibrated S-N curves for engineering applications precautions have to be taken to ensure that the stress distribution near the hot spot is calculated with sufficient accuracy. It is therefore recommended to verify the stress distribution obtained from using the minimum mesh size through a calculation with a model with a finer mesh.

Table (4.2) lists the original curve parameter (m, C), the calculated stress concentration factor K_t and the calibrated curve parameter ($\tilde{C}$) for the 4 calibration cases.

Most remarkable are the calibration results for the UK Department of Energy S-N curves (calibration cases 1 – 3). For the three test specimen that are related to the UKDEn F, G, F2 curves, respectively, the calibrated curve parameters $\tilde{C}$,

that have been obtained based on the calculated stress concentration factors K_t , are very close to each other.

This fact allows it to define one single S-N curve that can replace the UKDEn F, F2, G curves when used with hot spot stresses obtained from finite element analyses. The mean value of the three curve parameters $\tilde{C}$ has been chosen as the curve parameter $\tilde{C}_0$ for the calibrated design S-N curve. Together with the second curve parameter m that is not changed in the calibration process the proposed design S-N curve is defined as follows and is shown together with the three UKDEn curves in Fig. (4.21).

$$\begin{aligned} m &= 3.0 \\ \tilde{C}_0 &= 7.32 \times 10^{12} \\ \log \tilde{C}_0 &= 12.864 \end{aligned}$$

The calibration procedure used for the development of this curve assures that for the small-scale test specimen the use of this design S-N curve in combination with the hot spot stress obtained through finite element analysis in a specified manner will result in a fatigue damage equal to the mean value observed in the actual fatigue tests.

In order to use the developed calibrated curves for fatigue life evaluations of ship details, the influence of the scale effect on the stress distribution near the hot spot has to be evaluated. The stress recovery procedure defined in chapter 3 uses the plate thickness to determine the location of the stress sampling points. In many cases the stress distribution near the hot spot is not a function of the plate thickness

This curve can be used to replace the UKDEn F, F2, G S-N curves when the hot spot stress is used for the calculation of the fatigue damage. It is important to note that the hot spot stress has to be calculated using the procedure defined in chapter 3.

The problem of calculating the fatigue damage for ship details using hot-spot stresses obtained through finite element analyses can be viewed as a two-part process. A suitable S-N curve has to be defined and the scale difference between the small scale specimen and the ship detail has to be accounted for. The two parts can be clearly separated which makes the solution more transparent:

- The developed calibration process ensures that for the actual test specimen the calibrated S-N curve used to analyse the fatigue life for constant amplitude loading in combination with hot-spot stresses obtained from finite element analyses will result in the actually observed mean fatigue life.
- The second problem, the *dimension* problem is only approximately resolved. The definition of stress recovery procedures and minimum mesh sizes has the purpose to relate the small scale fatigue test specimen to the actual ship details. The use of the plate thickness as the governing dimension is somewhat misleading since in many cases the stress distribution is independent of the plate thickness. For ship details designed according to class rules the plate thickness is a function of the overall dimensions and its use as the governing dimension for the calculation of the hot-spot stress can be justified.

  In order to improve the understanding of the underlying processes it is desirable to take account for the size difference between test specimen and ship

Calibration I

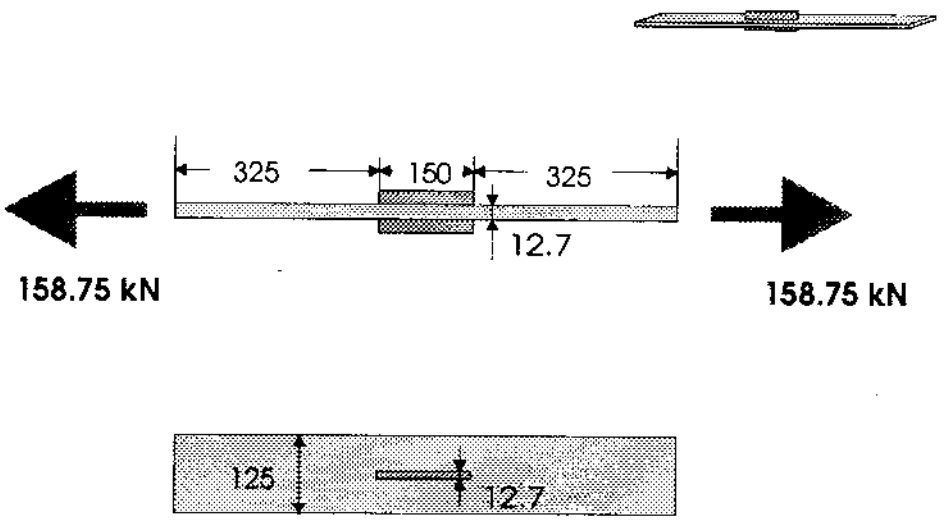

Figure 4.3: Geometry and Dimensions for Calibration I

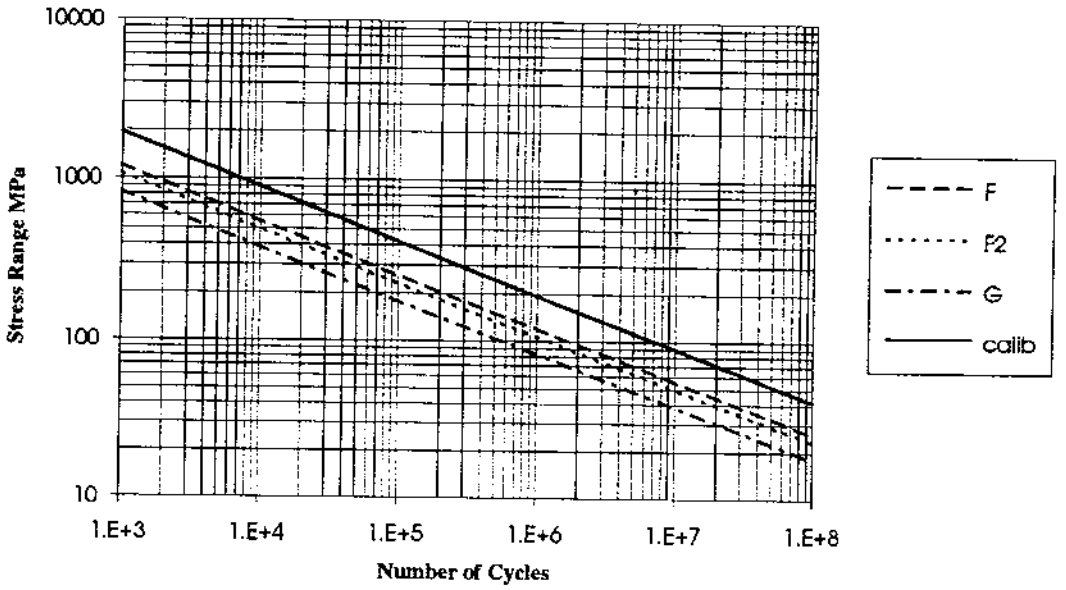

Figure 4.21: Original and Calibrated S-N Curves

Chapter 5

Re-Analysis of SMP Verification Cases

5.1 Introduction

As part of the Structural Maintenance for New & Existing Ships Project (SMP) the probability of fatigue failure has been analysed for Critical Structural Details (CSD) in two classes of tankers. The calculated failure probabilities were compared against failure probability estimates that were based on actual damage statistics for the two classes of tankers.

5.2 Modifications for SMP Fatigue Software

The Fatigue Life Evaluation Software allows it to calculate the fatigue life for a CSD at specified hot-spot locations. Hot-spots are distinguished by key-words. For the sideshell longitudinal to webframe connection hot-spots are defined both on the webframe and on the stiffening bracket. Fig. (5.1) shows the hot-spots and the key-words.

In the first version of the software S-N curves have been defined for each hot-spot location. This definition was based on the selection of a preliminary stress recovery procedure using the work on *Fatigue Classification of Ship Structural Details* that has been presented in [15] as a starting point.

Using this definition verification analyses were performed for two classes of tankers. The results of these analyses are documented in [1].

Based on the results of the FACTS project the originally defined S-N curves are replaced by the developed calibrated curves. It has to be noted that for the hot-spots that are located in parent material, e.g. at the cutout radius the S-N curve definitions are not changed.

Since the calibrated curves have been developed using finite element results that were based on shell elements the curves for lap-welded connections have to be modified. For the original definitions the fatigue strength has been down-graded from F to F2 for the case of a lap-joint. In order to adjust the calibrated curve parameter $\tilde{C}$ for the use with lap-welded connections, the ratio of the curve parameters of the

F and F2 curves is used. This ratio is given by

$$\frac{C_F}{C_{F2}} = 1.4028$$

The resulting curve parameter $\tilde{C}_L$ is obtained as follows:

$$\tilde{C}_L = \frac{\tilde{C}}{1.4028} = 5.218 \exp 12$$

5.2.1 Modifications of Data Files

In order to incorporate the calibrated results into the SMP software the file tt sn.smp has to be modified. This file contains the S-N curve information for all hot-spots that are identified for the chosen CSD, the sideshell longitudinal connection to the webframe.

The hot-spots are identified by their keywords. A flag is given that defines whether S-N information for two types of welded connections (lap weld or butt weld) is provided. In addition it is indicated wether the hot-spot is on a horizontal or vertical surface. This is important for the choice of the appropriate corrosion rate from the file `corosion.smp`. For each hot-spot additional S-N information can be provided for the case of weld improvements or other modifications that result in a different fatigue strength. For each hot-spot a maximum number of **15** S-N curves can be specified.

5.2.2 Format

The character strings in this files do not have to be preceded and followed by single quotation marks (')!. Special symbols are used to identify different parts of the file.

The S-n information of one hot-spot consists of a principal line containing the **keyword**, an identifier wether or not S-N information for both the butt-weld and the lap-weld case are present and the information whether the hot-spot is on a horizontal or vertical surface. The presence of S-N information for two types of weld is identified by adding a star (*) to the end of the keyword.

The principal line is identified by a **#**in the first column.

Two lines contain the information for one S-N curve. The first line is a comment line. The second line contains the necessary S-N information. The following 5 values have to be specified. No fixed format is required. The values have to be separated by blanks or a comma (,).

- $\log a$, cut of the $\log N$ axis by the mean S-N curve
- $\log \bar{a}$, $\log a - 2 \log s$
- $\log s$, standard deviation of $\log N$
- ρ, coefficient of variation
- m, negative inverse slope of the S-N curve

Up to **15** S-N curves can be specified. The S-N information for one hot-spot is complete, if an empty line is found or a line that starts with an exclamation mark (!) is found.

A line starting with an exclamation mark (!) symbolizes the start of the S-N information for the case of a lapweld. Following this line a set of S-N curves can be entered using the syntax described above.

5.2.2.1 Sample File

```
# COSS1                VER
Hot-Spot Curve:   Crack between Cutout and Sideshell (top)
12.8645 12.428 0.2183  .2  3.0

# COSS2                VER
Hot-Spot Curve:   Crack between Cutout and Sideshell (bottom)
12.8645 12.428 0.2183  .2  3.0

# COLUG1*              VER
Hot-Spot Curve:     Crack between Lug and WebFrame
12.8645 12.428 0.2183  .2  3.0
! Lapweld
Hot-Spot Curve for Lapweld:    Crack between Lug and WebFrame
12.7175 12.281 0.2183  .2  3.0

# COLUG2*              VER
Hot-Spot Curve:     Crack between Lug and WebFrame
12.8645 12.428 0.2183  .2  3.0
! Lapweld
Hot-Spot Curve for Lapweld:    Crack between Lug and WebFrame
12.7175 12.281 0.2183  .2  3.0

# CORAD1               VER
C-Curve, Basic Case:                      Crack at top Radius of Cutout
14.0342 13.630 .2041   .2  3.5

# CORAD2               VER
C-Curve, Basic Case:                      Crack at bottom Radius of Cutout
14.0342 13.630 .2041   .2  3.5

# COLOLUG1             VER
Hot-Spot Curve:     Crack between Lug and Longitudinal
12.8645 12.428 0.2183  .2  3.0

# COLOLUG2             VER
Hot-Spot Curve:     Crack between Lug and Longitudinal
12.8645 12.428 0.2183  .2  3.0

# BLONG1*              HOR
Hot-Spot Curve for Buttweld:   Crack between Brkt and Longl (Rathole)
12.8645 12.428 0.2183  .2  3.0
! Lapweld
Hot-Spot Curve for Lapweld:    Crack between Brkt and Longl (Rathole)
12.7175 12.281 0.2183  .2  3.0

# BLONG2*              HOR
Hot-Spot Curve for Buttweld: Crack between Brkt and Longl (Toe)
12.8645 12.428 0.2183  .2  3.0
```

```
! Lapweld
Hot-Spot Curve for Lapweld:    Crack between Brkt and Longl (Toe)
12.7175 12.281 0.2183  .2  3.0

# BWEB1              HOR
Hot-Spot Curve:        Crack between Brkt and Webframe (Rathole)
12.8645 12.428 0.2183  .2  3.0

# BWEB2              HOR
Hot-Spot Curve:        Crack between Brkt and Webframe (Toe)
12.8645 12.428 0.2183  .2  3.0

# BMIDRAD            HOR
C-Curve, Basic Case:              Crack at Midradius of Brkt
14.0342 13.630 .2041  .2  3.5
```

5.3 Analysis of Verification Cases

The background of the verification analysis including the derivation of the *target* failure probabilities and the description of the verification details is given in [1].

For each detail the original S-N curve is replaced by the appropriate calibrated curve. The hot-spot stresses are calculated according to the defined stress recovery procedures given in section 3.4.4 and the long-term loading parameters are calculated using these values.

For each detail in the two verification cases the resulting probability of failure is plotted once as a function of the median bias for several COV values and once as a function of the coefficient of variation of the bias for several bias values. As a comparison the original analysis results and the calibrated results are plotted in one graph.

5.3.1 Case I

5.3.1.1 Detail A

The results of the calibrated analysis are shown in Fig. (5.2). The comparison shown in Fig. (5.3) indicates that the calibrated analysis underestimates the target probability of failure.

5.3.1.2 Detail B

The results of the calibrated analysis are shown in Fig. (5.4). The comparison shown in Fig. (5.5) indicates that the calibrated analysis underestimates the target probability of failure.

5.3.1.3 Detail C

The S-N curve definition for detail C is identical to the original definition since the hot-spot is located at the radius of the cutout. Therefore the calculated failure probabilities are identical and are shown in Fig. (5.6).

5.3.2 Case II

5.3.2.1 Detail A

The results of the calibrated analysis are shown in Fig. (5.7). The comparison shown in Fig. (5.8) indicates that the calibrated analysis produces results that are closer to the *target* failure probability.

5.4 Conclusions

The calibrated S-N curves obtained throught the procedure described in chapter 4 have been used to replace the S-N curves originally used in the SMP Fatigue Life Evaluation Software.

Using these calibrated curves with the same long-term loading as in the original verification analyses, the details in the two verification cases have been re-analysed.

The original analysis showed good agreement between the calculated failure probability and the estimated target probability for Details A and B of verification case 1. Using the developed calibrated S-N curves that define a greater fatigue endurance than the originally used curves has resulted in significantly lower failure probabilities.

These results require a thorough examination in order to find explanations for the deviations in the failure probabilities. The results indicate that the inherent uncertainties in the load estimation are much larger than originally estimated.

However, it has to be mentioned that the accuracy of the estimated target failure probabilities is also very questionable, particularly for verification case 2 and for detail C of verification case 1.

Additional analysis using the calibrated S-N curves is necessary to verify the developed procedure and to get a better understanding of the underlying uncertainties.

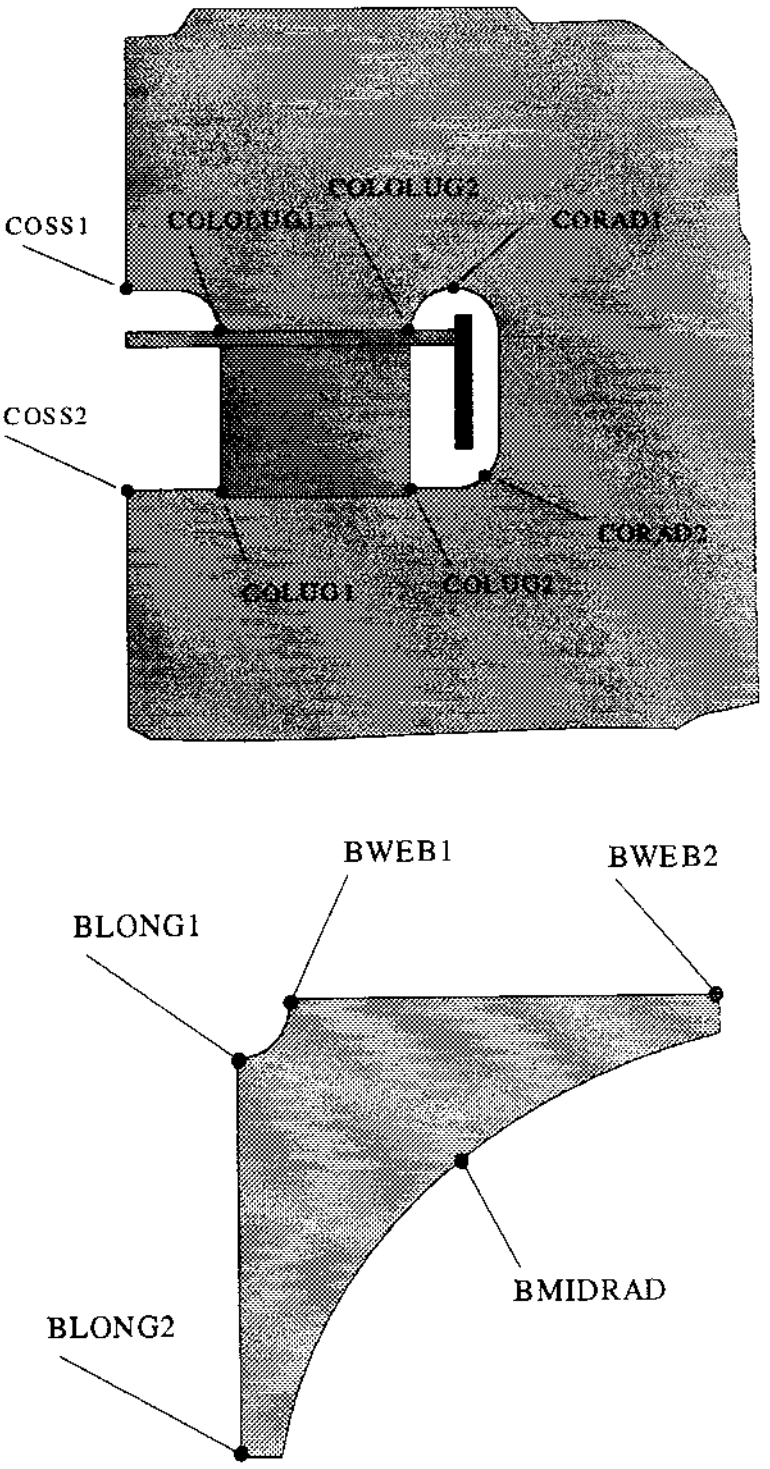

Figure 5.1: Hot-Spot Definition in Tanker CSD

Detail A:

Weibull Parameters from Loading Program		
Shape Parameter	Scale Parameter	Zero Crossing Rate
3.2969	0.7538	0.12041

Probability of Failure vs. Bias

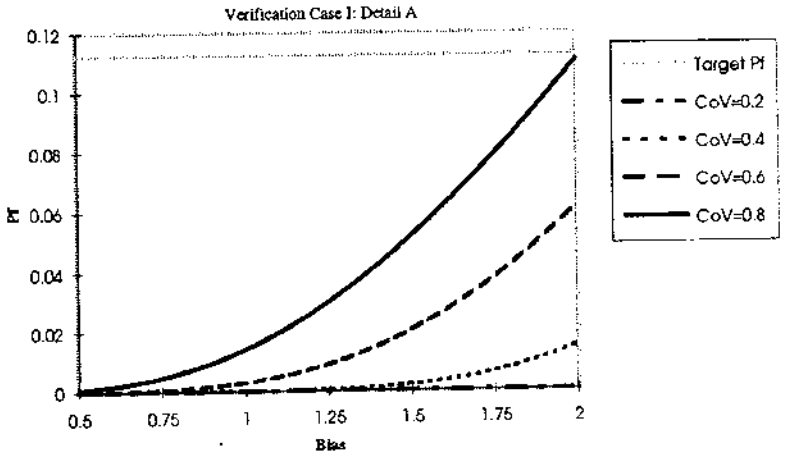

Probability of Failure vs. CoV of Bias

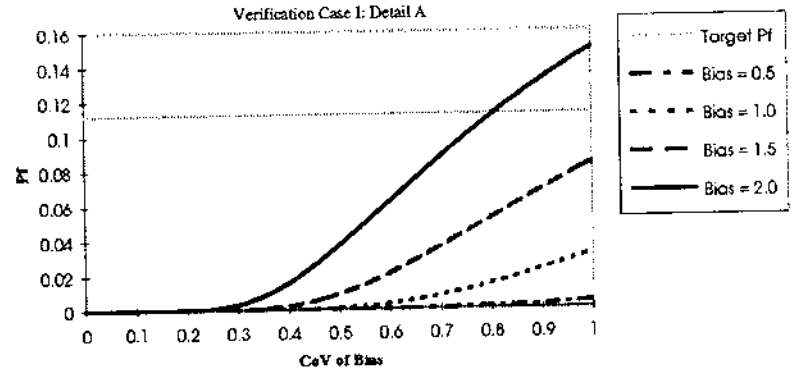

Figure 5.2: Case1: Calibrated Verification Results for Detail A

Detail A: Comparison of Original and Calibrated Results
Probability of Failure vs. Bias

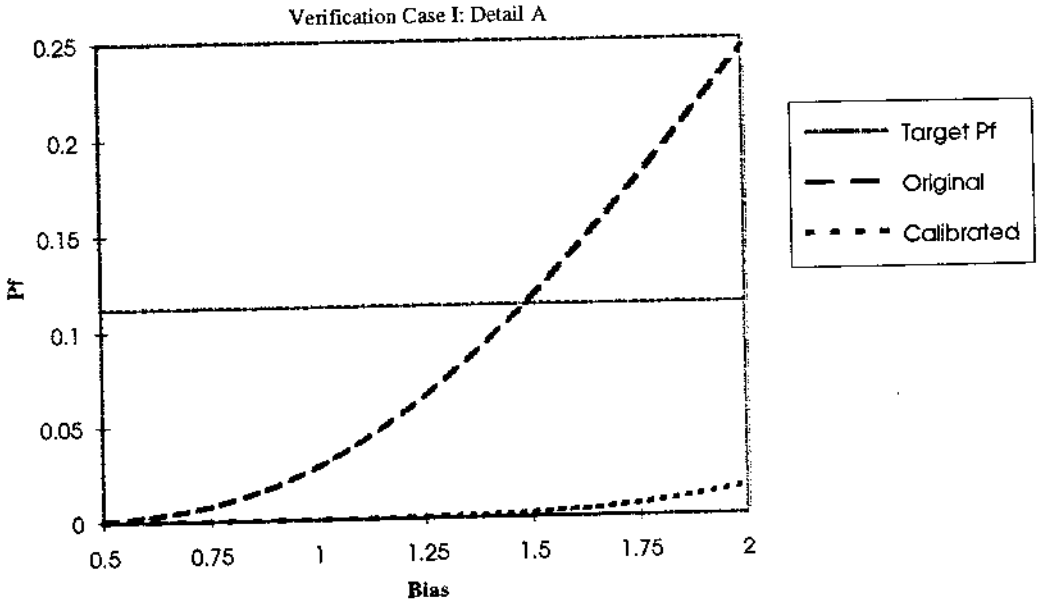

Probability of Failure vs. Bias

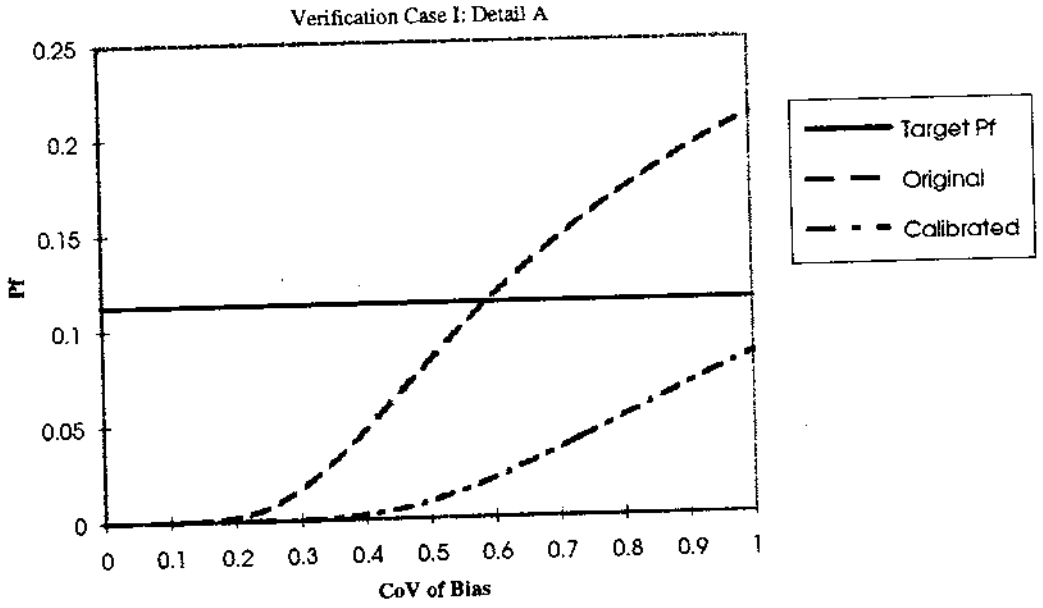

Figure 5.3: Case1: Comparison of Original and Calibrated Results for Detail A

123

Detail B:

Weibull Parameters from Loading Program		
Shape Parameter	Scale Parameter	Zero Crossing Rate
3.5716	0.7538	0.12041

Probability of Failure vs. Bias

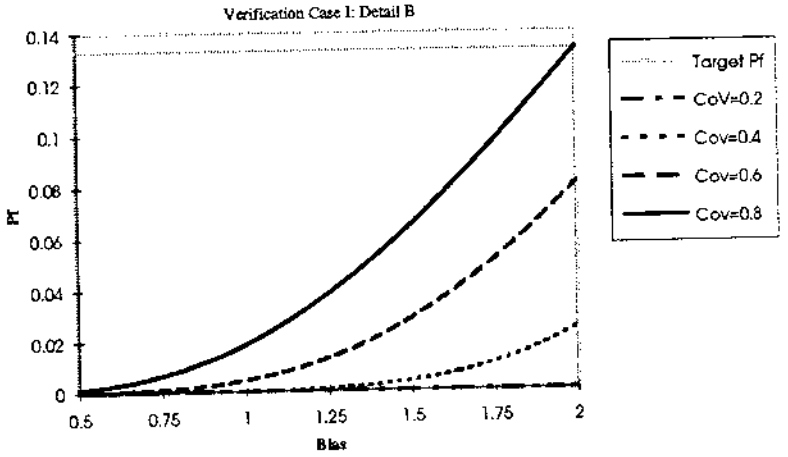

Probability of Failure vs. Bias

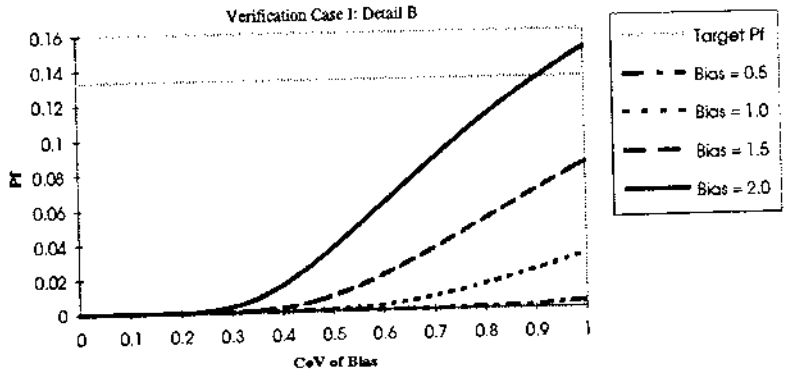

Figure 5.4: Case1: Calibrated Verification Results for Detail **B**

Detail B: Comparison of Original and Calibrated Results
Probability of Failure vs. Bias

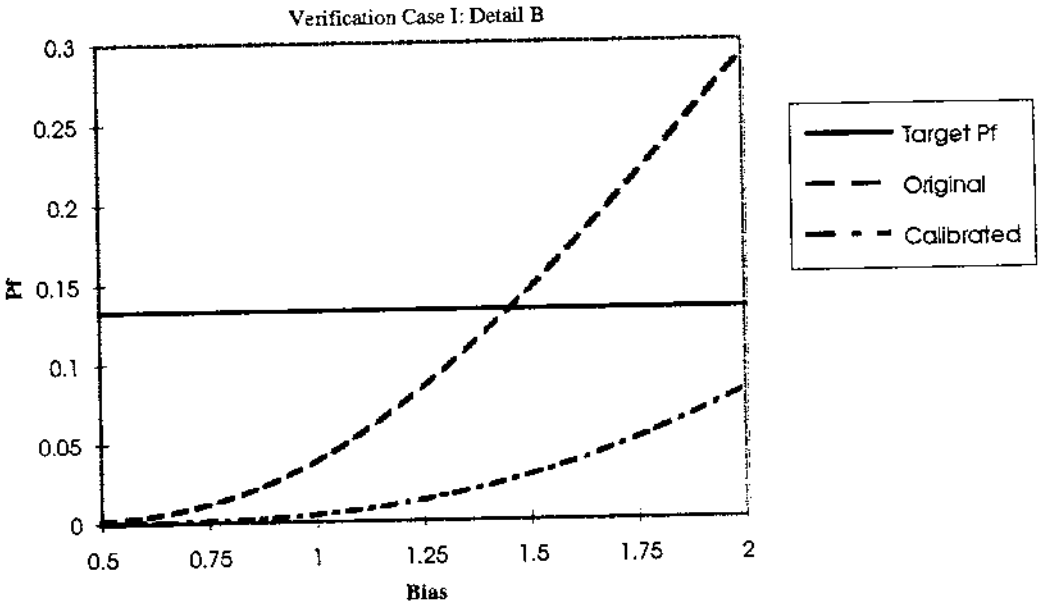

Probability of Failure vs. Bias

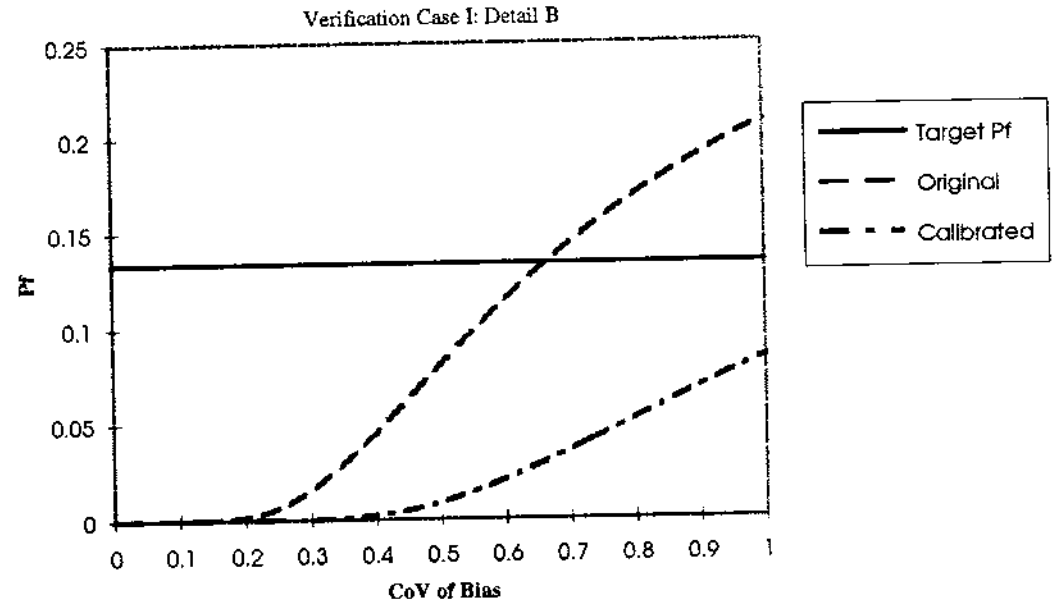

Figure 5.5: Case1: Comparison of Original and Calibrated Results for Detail B

Detail C:

Weibull Parameters from Loading Program		
Shape Parameter	Scale Parameter	Zero Crossing Rate
0.6896	0.7538	0.12038

Probability of Failure vs. Bias

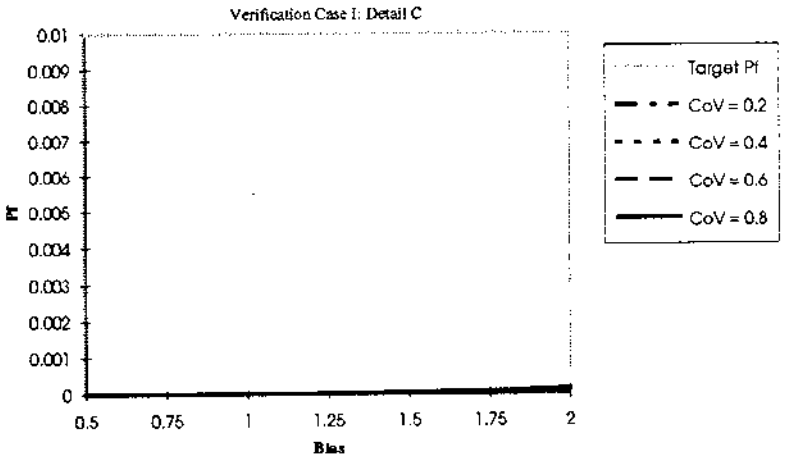

Probability of Failure vs. Bias

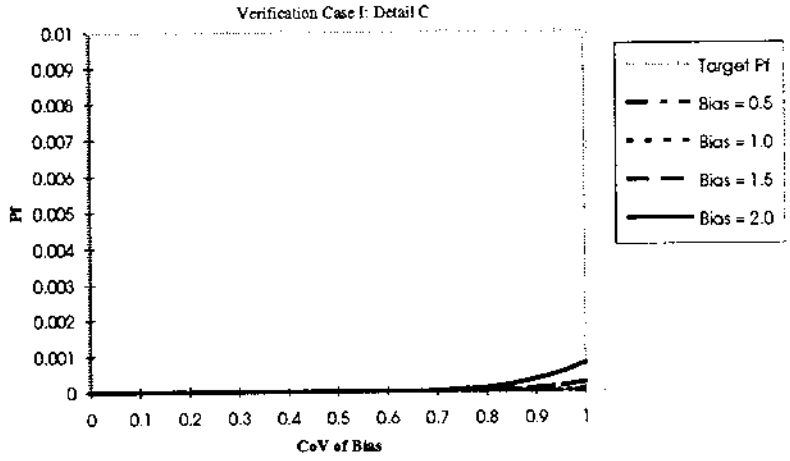

Figure 5.6: Case1: Calibrated Verification Results for Detail C

Detail A:
Probability of Failure vs. Bias

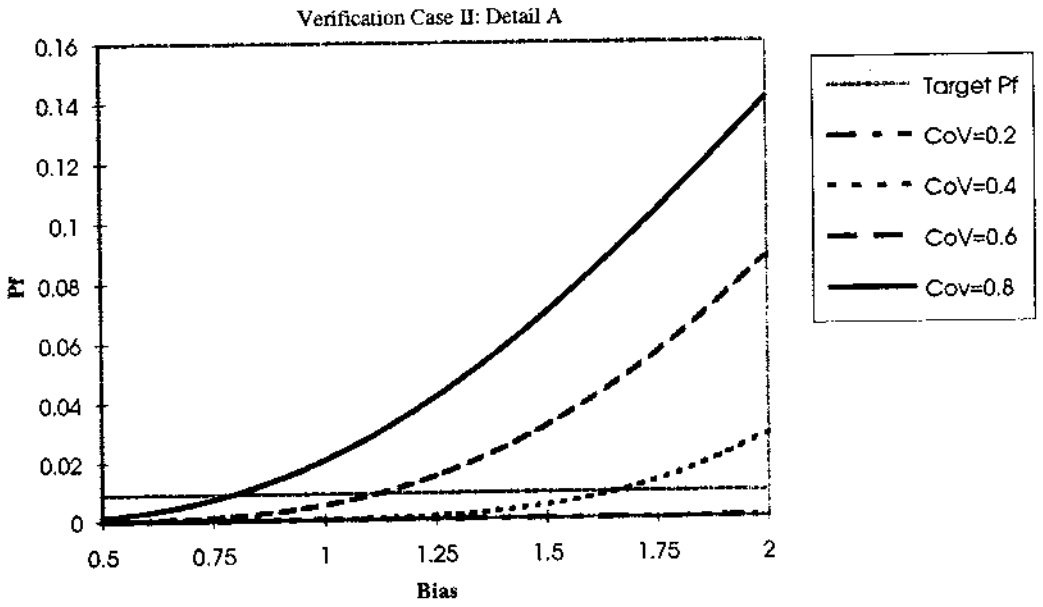

Probability of Failure vs. Bias

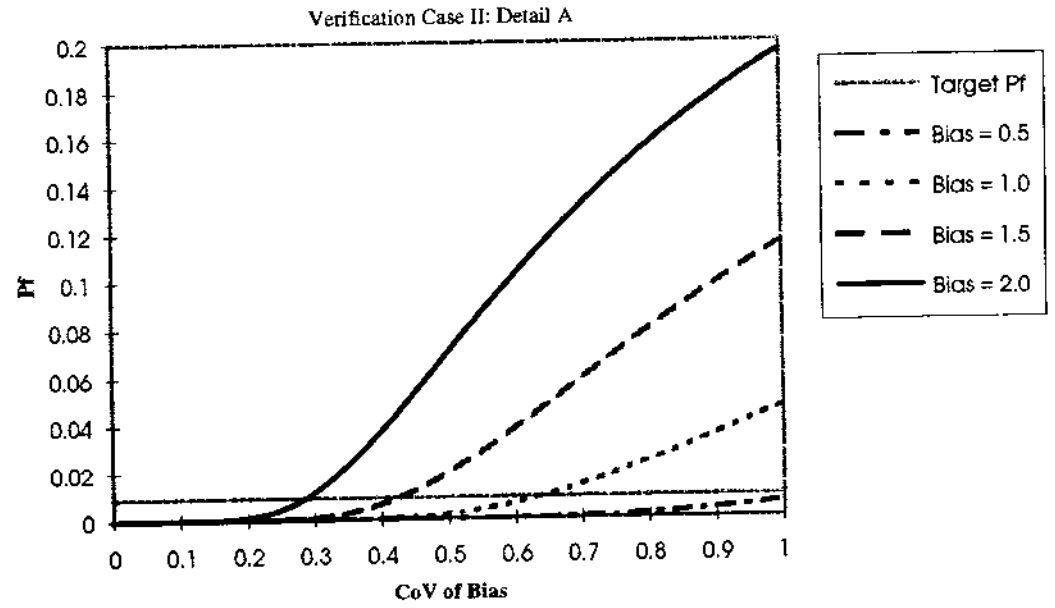

Figure 5.7: Case2: Calibrated Verification Results for Detail A

Detail A: Comparison of Original and Calibrated Results
Probability of Failure vs. Bias

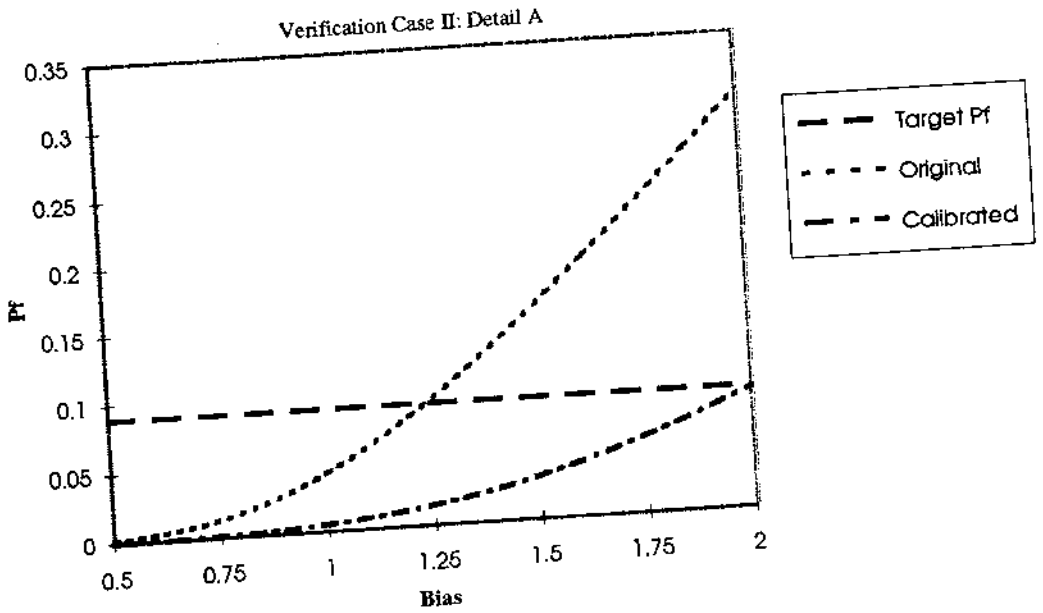

Probability of Failure vs. Bias

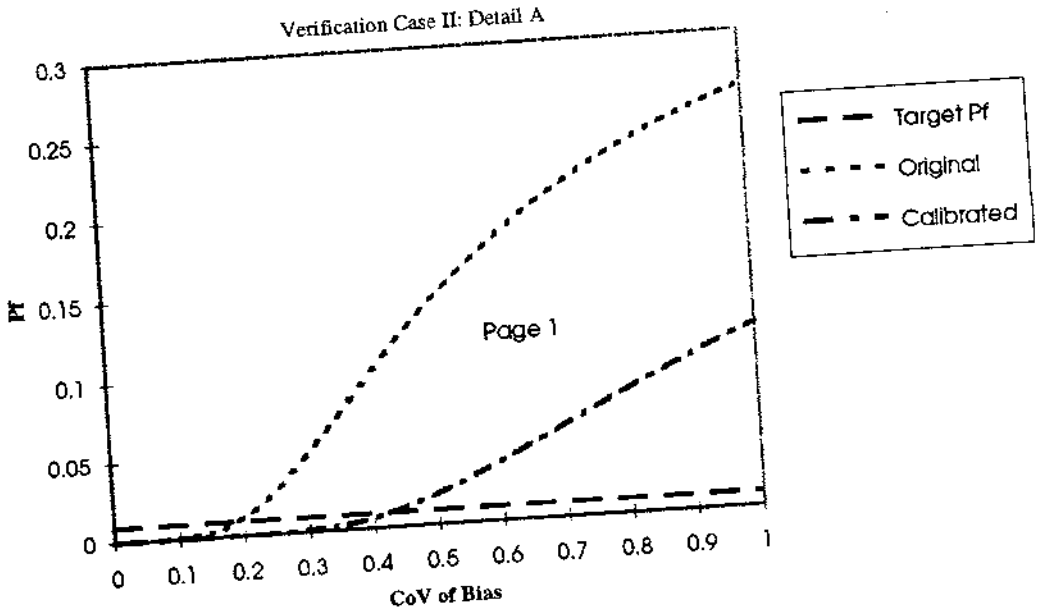

Figure 5.8: Case1: Comparison of Original and Calibrated Results for Detail A

Chapter 6

Management System for the Selection of S-N Curves

6.1 Introduction

The development of fatigue cracks due to cyclic loading is a phenomenon common to many engineering applications. It can be observed and is of particular concern in ships, bridges, cars, pressure vessels, aircraft and offshore installations.

The consequences of fatigue failure can range from simple nuisance cracks that are mainly a concern for maintenance and inspection to complete structural failure resulting in the loss of lifes and property. The accurate estimation of fatigue endurance is therefore of great importance for both design and maintenance purposes.

The fatigue life of a given structural component depends on several influencing factors:

- **Long-Term Cyclic Loading**: Since fatigue damage is a cumulative process the distribution of the cyclic stress components is the single most important factor that determines the fatigue life. In general the long-term load distribution has to be described on a statistical basis and depends strongly on the type of structure and the operating environment.
- **Material properties**: Different materials have in general different fatigue strength properties, which have to be determined experimentally.
- **Local stress concentrations**: The presence of local stress concentrations caused by a specific detail geometry or construction flaws such as misalignments magnifies the cyclic stress components and thus reduces the fatigue life. To some extent the influence of local stress concentration is determined experimentally.
- **Construction method**: Construction characteristics can greatly reduce the fatigue strength of a structural detail. The presence of welds in steel structures is the main cause for fatigue failures. The fatigue strength of welded connections has to be determined experimentally.

The experimentally obtained measures of fatigue strength are represented by stress range vs. number of cycles curves (S-N curves). The S-N curves are the direct

result of specific test series. Curves have been developed for plain material, simple welded geometries or even full-scale structural details including weld imperfections.

Many classification and regulatory organizations have developed sets of design S-N curves suitable for specific types of structural details. These curves again depend on the geometry and loading of the test specimen used in the fatigue test series.

The selection of the S-N curve appropriate for a given structural component and loading therefore requires a detailed knowledge of the available S-N curves and the respective test configurations, loading and the general background. Some of this information is given through design guidelines, which vary in format for the different sets of S-N curves.

For a design engineer facing the task to calculate the fatigue life of a given structural component the selection of the appropriate S-N curve is a difficult task since the knowledge base for this selection is not available in an easily accessible form.

It is therefore desirable to develop a format that allows it to classify different S-N curves and to retrieve the necessary information for the selection of the appropriate curve. This format can then be implemented in the form of a database, which can form the knowledge base for an electronic *Management System for the Selection of S-N Curves.*

6.2 Requirements for S-N Curve Selection

S-N curves have been developed for many different materials, detail configurations, manufacturing and construction methods. One of the main benefits of an electronic selection system is the ability to compare different types of S-N curves. The main emphasis in the development of the system is therefore the abilility to add new S-N curves or groups of S-N curves without the need to modify the developed data structure.

The definition of the data structure used to store the S-N curve information is therefore of the greatest importance. The structure has to include enough information to define all relevant curve parameters. In addition the rules for the selection of a curve have to be included in the data structure. This ensures that a management system for the selection of the S-N curves can be developed that is based on the defined data structure that does not have to be modified if additional curves are added.

In order to be useful for the selection of S-N curves the format for the selection rules has to be very specific and include categories to clearly describe detail geometries. This will require the use of graphical representations of the detail geometry.

Both the S-N curve representation and the rule definitions have to be formulated in a database format. This ensures a modular design of the selection system and makes the S-N information available to other applications without the need for modifications. This enhanced applicability is desirable in order to justify the effort of including many different S-N curve representations.

The use of a database to store the S-N information and the selection rules makes it necessary to develop the selection management system as an independent module that obtains the necessary information from the database through a query system, e.g. SQL.

The definition of the requirements for the *Management System for the Selection of S-N Curves* clearly indicates the structure of this system. The system consists of two main parts, a knowledge base and a functional shell. This allows the development of management systems with different levels of sophistication without modifications to the knowledge base that contains the S-N information.

6.3 Expert Systems in Engineering Applications

6.3.1 Definition of Expert Systems

Expert systems have moved from the Artificial Intelligence (AI) research into the mainstream of commercial computing. They represent a new approach to the design of software for intelligent decision support. The development of an expert system is based on knowledge engineering.

Although there is no universal agreement on the precise definition of an expert system, a typical expert system has in general four major components, [16]:

- the knowledge base
- the inference engine
- the acquisition module
- the explanatory interface

The knowledge base is by far the single most important component of any expert system. Knowledge can be represented in several ways, the most popular being *rules*, *frames* and *semantic nets*, [17].

Rule-based representation: In a rule-based system, knowledge is represented in terms of facts pertinent to a problem area and rules for manipulating the facts. Currently most expert system applications are rule-based. Most of these applications could also have been developed using traditional programming languages, [16].

Frame and semantic net based representations: Frame or semantic net schemes allow a deeper insight into underlying concepts and causal relationships. A frame is a record-like data structure for encoding information. Frames are usually organized into a hierarchy. The strength of frame-based systems derives from this hierarchical structure which enables frames to inherit attributes from others frames located above them in the hierarchy, [17].

6.3.2 Engineering Applications

The use of expert systems in engineering applications has increased significantly in recent years. This is partly due to the vast improvements in computing capabilities and the development of expert system shells that facilitate the design and implementation of expert system applications. In addition, the nature of many engineering problems makes the use of rule-based methods very attractive.

In [17] expert system applications are described for the five main branches of engineering, namely chemical, civil, electrical, mechanical and manufacturing engineering.

The basis for an expert system for the *assessment of the safety of existing steel jacket platforms* is outlined in [18]. The after describing the main components of an expert system, the development process is outlined, focusing especially on the development of the knowledge base.

Knowledge trees have been developed for the major criteria to determine the likelihood of significant increase in wave load or of significant reducion in strength for a steel jacket offshore platform.

6.4 Database Theory

6.4.1 Introduction

The storage and management of information and operational data has always been one of the most important tasks for all types of organizations. Data is in general contained in a database. In [19], the term *database* is defined as

> A database is a collection of stored operational data used by the application systems of some particular enterprise

It has to be noted that the storage method for the data is not defined. In the following only the development of electronic database systems is outlined.

A database system is characterized by the data model it supports. Early systems were developed based on the established file system. These *hierarchical* or *network* models have in general low level data manipulation languages and require users to optimize the access to the data by carefully navigating in hierarchies or networks [20].

Almost all of the database systems developed over the past few years are based on the *relational* model. In addition, almost all current database research is also based on relational ideas. Many non-relational systems are often described, for commercial purposes, as supporting relational features. Currently, the *relational model* is the single most important development in the entire history of the database field, [19].

6.4.2 The Relational Model

The *relational model* was introduced by E.F. Codd in 1970, [21], including the following definition of the model's first objectives:

- To allow a high degree of data independence. The application programs must not be affected by modifications to the internal data representation, particularly by the changes to file organizations, record orderings, and access paths.
- To provide substantial grounds for dealing with data semantics, consistency, and redundancy problems.

In a relational system data is perceived by the user as two-dimensional tables or relations. A relation is defined in [20] as

> Subset of the Cartesian product of a list of domains characterized by a name

where a *domain* is the set of possible atomic data items. A relation contains a time-variant number of unique records. Each record is uniquely defined by a *primary key*, where the key can consist of a combination of several data items.

Relations are manipulated by the use of a set of operators defined as *relational algebra* and an assignment operation. The most important property of each of the algebraic operations is the fact that the output of each operation results in another relation. In the original definition, Codd [22] defined eight operators, two groups of four each. One group contains the operations **union**, **intersection**, **difference** and **Cartesian product** and the other group consists of the special relational operations **select** **project**, **join** and **divide**.

The fundamental intent of *relational algebra* is to allow the *writing of expressions* for data retrieval, updating, the definition of access rights and many other possible applications.

6.4.3 Database Design: Normalization Theory

While the *relational model* has led to the development of powerful database systems, it does not free the user from the task of defining the database structure and organizing the required information content into different relations.

A badly designed database structure can lead to data inconsistencies due to data reduncancy, i.e. the same information is stored in several places.

Normalization Theory has been developed to formalize the requirements for an effective database design. Originally, Codd defined the first, second and third normal form (1NF, 2NF, 3NF), [23]. Later the third normal form was re-defined as the Boyce-Codd normal form (BCNF), [24] and a fourth (4NF) and fifth (5NF) normal form were proposed, [25],[26].

The definition of the different normal forms is intended to serve as guidelines for the design of efficient databases. A relation is only required to be in the first normal form (1NF). The first normal form (1NF) requires that a relation only contains atomic values.

Definitions for the higher normal forms are given in [20], [19]. In general it is desirable to develop relations that satisfy the conditions of the higher normal forms. However, for a particular database design it is possible that a relation that is not of a higher normal form can advantagous.

6.5 Database for S-N Curves

As outlined in section 6.2 the most important component of the S-N selection system is the *knowledge base* that contains all necessary curve information in combination with the *rules* that govern the curve selection.

This knowledge base will be implemented as a database using the *relational data model*. Section 6.4 contains a short overview over the development of database theory with special regard to the relational model.

The first step in the development of the S-N selection knowledge base is the definition of the requirements imposed on the system. Based on these requirements the format for the *selection rules* will be defined. The developed format will be implemented for several sets of S-N curves from different organizations.

6.5.1 Requirements

The requirements for the S-N curve knowledge base fall into two categories:

- Representation of all relevant curve information.
- Representation of selection rules in a format suitable for the development of the *S-N selection system.*

The database is intended to be versatile enough that it can contain a wide range of different S-N curves in order to justify the development of applications based on the database. In addition it will be possible to compare S-N curves from different organizations.

In order to easily develop applications based on the database it is necessary to use a consistent set of units for all information. This will require that some of the S-N data is converted to the chosen system. In addition a standard representation for the S-N curves has to be defined.

The representation of the selection rules in a database has to be versatile enough to cover a wide range of materials, construction methods, stress conditions, etc.It is desirable to include graphic representations of some of the selection rules in order to enable the development of user friendly applications that represent information such as specimen geometries and crack location in a graphical form.

6.5.2 Lehigh University: Fatigue Test Data Management System

As part of a research project to develop advanced double hull concepts, *Fleet of the Future Program (FFP)*, large scale fatigue tests for beam type specimen have been conducted, [27]. A computerized database containing the fatigue test results for large scale beam specimen has been developed. In addition to the fatigue test data obtained from the experiments, data from several other laboratories has been included in the database. The database development is described in citelehigh:fatigue:dbase.

The database has been developed primarily for the storage and statistical analysis of S-N test data. For data obtained from other laboratories the database contains for each fatigue test information regarding to the type of load, stress range, cycles to failure, min. stress, max. stress, and steel and geometry of the beam.

For the fatigue tests conducted as part of the *Fleet of the Future Program (FFP)* additional information regarding the actual crack observations has been documented.

All information is stored in the database tables in the form of keywords. Some of these keywords consist of a combination of multiple code words describing the test data source, detail type, etc. . The keyword and code words are defined in the *User's Guide* that is published as an appendix to [27].

The use of keywords that represent multiple pieces of information violates the concept of relational database theory, see section 6.4. The Lehigh database does not contain information regarding to the design S-N curves that have been developed based on the individual test results. Although the design S-N curves are in general based on a statistical analysis of the test results, the curve parameters are often modified to conform with theoretical results or to be compatible with previous curves.

The definition of the *fatigue detail types* is limited to details related to welded beams. The different details are described using keywords that are described in the *User's Guide* and contain information regarding the detail geometry, loading, weld type, etc.Nevertheless, the methodology used to describe the different fatigue details can be used as a starting point for the development of the appropriate data structure of the S-N curve database.

6.5.3 Representation of S-N Curve Information

The core of the S-N database is the information with regard to the actual S-N curves. This information has to completely represent the respective S-N curves. This allows it to use the database both for the management of the different sets of curves and also as the base for the development of the *System for the Selection of S-N curves*.

For each S-N curve the following information has to be represented in the database:

- **Curve**: For each **Curve** the **Class** it belongs to has to be stated. Finally, the **Curve Parameters** have to be included. These The curve parameter include a reference stress range for the *design* and the *mean* curve, two main curve parameters, two slope parameters and the number of cycles for the *reference value*, the slope change and the constant amplitude fatigue limit. In addition the standard deviation of $\log N$ and the multiplier used for the definition of the *design* curve are included.
- **Class**: The class of S-N curve a particular curve belongs to. As part of the **Class** information the name of the class, the **Environment**, the **Material**, the type of **Stress** used to define the S-N curve, a bibliographic reference and a possible additional memo have to be provided.

The actual implementation, which has to create several different *relations* for the different pieces of information will be described in section 6.5.5.

6.5.4 Definition and Representation of Selection Rules

In order to develop applications for the selection of S-N curves based on the S-N curve database it is necessary to include all information that defines the usage for each curve.

The format has to be flexible enough to allow for the input of a wide variety of different S-N curves. Since each S-N curve can in general be used for several different configurations of details, weld type, etc. , the selection information will be implemented in the form of *rules*, where each rule consists of a combination of the different influencing factors and the S-N curve that has to be used for this combination of factors.

Each *rule* has to contain the following information:

- **Curve**: The S-N curve that has to be used for a detail that satisfies that particular rule
- **Class**: The class the S-N curve belongs to.
- **Detail Type**: The type of specimen defined by a description and a graphical representation. For each type of specimen is has to be identified, which of the additional rule components are applicable for this type of detail.

- **Weld Type**: If applicable, the type of weld has to be defined. This includes the post-weld treatment, if applicable.
- **Defects**: The type of defects that can not be present in the detail.
- **Inspection**: The type of weld inspection and the percentage of the weld that has to be inspected.
- **Dimensions**: The limiting values for part dimensions or edge distances that are required for a specific S-N curve.
- **Loading**:The type of loading (axial, bending, etc.)
- **Location**: The location of the crack initiation site.

6.5.5 Datastructure for S-N Curve Database

The information requirements that have been defined in the two preceding sections have to be combined in one database structure. This structure has to follow the relational data model as described in section 6.4. This requires that all the information is grouped into relations, where each data item only contains atomic values.

As a general rule for the development of the data structure, all information that is relevant for the selection process is input with the help of additional relations that contain a unique identification and a description of the particular information. Fig. (6.1) shows the database structure. In the following sections each relation contained in the database structure is described in detail including the data fields, the primary and foreign keys and the links to other relations.

The relevant dimensions for a particular rule constitute a *many-to-many* relationship. This is implemented with the help of an additional relation that combines the rules and the dimension.

The sections are named according to the relation name. Each data item that has a # in the first column is represents a *foreign key*. The first data item(s) separated from the rest of the relation by a horizontal line serves as the *primary key* for the relation.

6.5.5.1 Relation: CURVE

The relation **CURVE** contains the S-N curve information for the different curves. This includes the curve parameters and the class the curve belongs to.

CURVE		
	Curve_ID	Num
#	Class_ID	Num
	Name	Char
	σ_D	Num
	σ_M	Num
	C1	Num
	C2	Num
	m1	Num
	m2	Num
	N1	Num
	N2	Num
	N3	Num
	StdDev	Num
	DevMult	Num

Key:
The key of this relation is the combination of `Curve_ID` and `Class_ID`. This combination has to be unique. Curves from different classes can therefore have identical identification numbers.

Links:
One data item is linked to an other relation:

Data Item	Linked Relation
Class_ID	**CLASS**

6.5.5.2 Relation: CLASS

The relation **CLASS** contains the information pertaining to the class of S-N curves. Uniquely identified by an identification number the name of the class, a bibliographic reference, the operating environment, the material, the definition of the stress that has to be used in conjunction with the curve, and an additional memo are contained in the relation.

CLASS		
#	Class_ID	Num
	Name	Char
	Reference	Char
#	Environment_ID	Num
#	Material_ID	Num
#	Stress_ID	Num
	Class_Memo	Char

Key:
The key of this relation is the `Class_ID`. This simple numeric value has to be

unique.

Links:
Three data items are linked to an other relation:

Data Item		Linked Relation
Material_ID	———	**MATERIAL**
Environment_ID	———	**ENVIRONMENT**
Stress_ID	———	**STRESS**

The `Class_ID` is used as a *foreign key* in the **CURVE**, the **RULE** and the **DIMENSIONS_IN_RULE** relation.

6.5.5.3 Relation: RULE

The relation **RULE** contains the necessary information to enable the selection of an S-N curve for a given detail. With the exception of the graphical representation of the specific configuration all data items are linked to other relations.

RULE		
	Rule_ID	Num
#	Curve_ID	Num
#	Class_ID	Num
#	Joint_ID	Num
#	Weld_ID	Num
#	Defects_ID	Num
#	Inspection_ID	Num
#	Loading_ID	Num
#	Location_ID	Num
	Picture	Num

Key:
The key of this relation is the combination of the three data items `Rule_ID`, `Curve_ID` and `Class_ID`.

Links:
Nine data items are linked to an other relation:

Data Item		Linked Relation
Curve_ID	———	**CURVE**
Class_ID	———	**CLASS**
Joint_ID	———	**JOINT**
Weld_ID	———	**WELD**
Defects_ID	———	**DEFECTS**
Inspection_ID	———	**INSPECTN**
Loading_ID	———	**LOADING**
Location_ID	———	**LOCATION**

6.5.5.4 Relation: MATERIAL

The relation **MATERIAL** contains the information pertaining to the material for a particular S-N curves. Uniquely identified by an identification number the name of the material and an additional memo are contained in the relation.

MATERIAL		
#	Material_ID	Num
	Name	Char
	Material_Memo	Char

Key:
The key of this relation is the `Material_ID`. This simple numeric value has to be unique.

Links:
No data item is linked to another relation. The `Material_ID` is used as a *foreign key* in the **CURVE** relation.

6.5.5.5 Relation: ENVIRONMENT

The relation **ENVIRONMENT** contains the information about the operating environment for a particular S-N curve, e.g. air or seawater. Uniquely identified by an identification number the name of the environment and an additional memo are contained in the relation.

ENVIRONMENT		
#	Envrironment_ID	Num
	Name	Char
	Memo	Char

Key:
The key of this relation is the `Environment_ID`. This simple numeric value has to be unique.

Links:
No data item is linked to another relation. The `Environment_ID` is used as a *foreign key* in the **CURVE** relation.

6.5.5.6 Relation: STRESS

The relation **STRESS** contains the information, which type of stress has to be used in connection with a particular S-N curve. Uniquely identified by an identification number the name of the stress, the definition, a graphical representation, a bibliographic reference and an additional memo are included in the relation.

STRESS		
#	Stress_ID	Num
	Name	Char
	Definition	Char
	Picture	Char
	Reference	Char
	Memo	Char

Key:
The key of this relation is the `Stress_ID`. This simple numeric value has to be unique.

Links:
No data item is linked to another relation. The `Stress_ID` is used as a *foreign key* in the **CURVE** relation.

6.5.5.7 Relation: JOINT

The relation **JOINT** contains the information to identify the principal joint configuration. Uniquely identified by an identification number the name of the joint, a graphical representation and a memo describing general failure modes are contained in the relation.

JOINT		
#	Joint_ID	Num
	Name	Char
	Picture	Char
	Failure_Memo	Char

Key:
The key of this relation is the `Joint_ID`. This simple numeric value has to be unique.

Links:
No data item is linked to another relation. The `Joint_ID` is used as a *foreign key* in the **CURVE** relation.

6.5.5.8 Relation: WELD

The relation **WELD** contains the information that defines the type of weld for the particular detail. Uniquely identified by an identification number the name of the weld, a description of the required post-weld treatment and an additional memo are contained in the relation.

WELD		
#	Weld_ID	Num
	Name	Char
	Reference	Char
	Memo	Char

Key:
The key of this relation is the `Weld_ID`. This simple numeric value has to be unique.

Links:
No data item is linked to another relation. The `Weld_ID` is used as a *foreign key* in the **RULE** relation.

6.5.5.9 Relation: DEFECTS

The relation **DEFECTS** contains the information that defines the defects in a detail that can not be present. Uniquely identified by an identification number the defect that is not allowed and an additional memo are contained in the relation.

DEFECTS		
#	Defects_ID	Num
	Not_Allowed	Char
	Memo	Char

Key:
The key of this relation is the `Defects_ID`. This simple numeric value has to be unique.

Links:
No data item is linked to another relation. The `Defects_ID` is used as a *foreign key* in the **RULE** relation.

6.5.5.10 Relation: INSPECTION

The relation **INSPECTION** contains the information defining the inspection method and the relative amount of material to be inspected. Uniquely identified by an identification number the name of the inspection method, the percentage of material to be inspected and an additional memo are contained in the relation.

INSPECTION		
#	Inspection_ID	Num
	Testmethod	Char
	%_of_Material	Char
	Memo	Char

Key:
The key of this relation is the `Inspection_ID`. This simple numeric value has to be unique.

Links:
No data item is linked to another relation. The `Inspection_ID` is used as a *foreign key* in the **RULE** relation.

6.5.5.11 Relation: DIMENSIONS

The relation **DIMENSIONS** contains the information regarding the dimensions of the detail that govern the choice of the S-N curve. Uniquely identified by an identification number descriptions for two parts and the dimensions are contained in the relation.

DIMENSIONS		
#	Dimensions_ID	Num
	Part_1	Char
	Smaller_Than	Num
	Larger_Than	Num
	Part_2	Char

Key:
The key of this relation is the `Dimensions_ID`. This simple numeric value has to be unique.

Links:
No data item is linked to another relation. The `Dimensions_ID` is used as a *foreign key* in the **DIMENSIONS_IN_RULE** relation.

6.5.5.12 Relation: DIMENSIONS_IN_RULE

The relation **DIMENSIONS_IN_RULE** links the two relations **RULE** and **DIMENSIONS** and thus establishes a *many-to-many* relationship between these two tables. This makes it possible that one rule can contain several dimensions and each dimension can be used in several rules. The relation consists of the *primary keys* of the **RULE** relation and the **DIMENSIONS** relation.

DIMENSIONS_IN_RULE		
	Rule_ID	Num
	Curve_ID	Num
	Class_ID	Num
	Dimensions_ID	Num

Key:
The key of this relation is the combination of the four data items `Rule_ID`, `Curve_ID`, `Class_ID` and `Dimensions_ID`.

Links:
No data item is linked to another relation. The `Rule_ID` `Curve_ID` and `Class_ID` are used as foreign keys in the **RULE** relation. The `Dimensions_ID` is used as a foreign key for the **DIMENSIONS** relation.

6.5.5.13 Relation: LOADING

The relation **LOADING** contains the information with regard to the loading in the detail. Uniquely identified by an identification number the name of the loading and an additional memo are contained in the relation.

LOADING		
#	Loading_ID	Num
	Name	Char
	Memo	Char

Key:
The key of this relation is the `Loading_ID`. This simple numeric value has to be unique.

Links:
No data item is linked to another relation. The `Loading_ID` is used as a *foreign key* in the **RULE** relation.

6.5.5.14 Relation: LOCATION

The relation **LOCATION** contains the information with regard to the location of the crack initiation in the detail. Uniquely identified by an identification number the name of the location and an additional memo are contained in the relation.

LOCATION		
#	Location_ID	Num
	Name	Char
	Memo	Char

Key:
The key of this relation is the `Location_ID`. This simple numeric value has to be unique.

Links:
No data item is linked to another relation. The `Location_ID` is used as a *foreign key* in the **RULE** relation.

6.5.6 Implementation Examples

In order to test the developed data structure and to provide the knowledge base for the working model of the *System for the Selection of S-N curves* S-N curves and usage information from three different organizations have been evaluated. Data from the following three sources has been used:

- **UK Department of Energy**
- **American Association of State Highway and Transportation Officials (AASHTO)**
- **Germanischer Lloyd**

In the following sections the three data sources are described.

6.5.6.1 UK Department of Energy: Guidance Manual for Offshore Installations

The current fatigue design guidance manual for steel welded joints in offshore structures [28], contains a section on fatigue design. It includes definitions of the required analysis scope, the fatigue loading, the basis for fatigue analysis, a definition of fatigue life and a list of factors] influencing fatigue life.

For the purpose of fatigue design, welded joints are divided into several classes, each with a corresponding design S-N curve. With the exception of nodal joints, which are assumed to be in class T, the fatigue classification depends on

- the geometrical arrangement of the detail
- the direction of the fluctuating stress relative to the detail
- the method of manufacture and inspectino of the detail

The basic design S-N curves for joints that are in air or in seawater with adequate corrosion protection are shown in Fig. (6.2). For unprotected joints in sea water the basic S-N curve is reduced by a factor of 2 on life for all joint classes. The basic S-N curves are of the form:

$$\log N = \log(K_1) - d\sigma - m\log(S_B)$$

where:

N = predicted number of cycles to failure
S_B= Stress range
d = number of standard deviations below mean
σ = standard deviation of $\log N$
m inverse slope of the S-N curve

In the guidance manual details are grouped into 7 joint classifications. For each joint class several specific configuration examples are given These classifications have been used for the development of the S-N database and are therefore listed here together with the figure numbers for the detail configurations:

1. **Plain Material**: The different configurations for this joint class are shown in Figs. (6.4, 6.5).
2. **Continuous Welds essentially parallel to the direction of Applied Stress**: The different configurations for this joint class are shown in Figs. (6.6, 6.7, 6.8).
3. **Transverse Butt Welds in Plates**: The different configurations for this joint class are shown in Figs. (6.9, 6.10, 6.11, 6.12, 6.13).
4. **Welded Attachments on the Surface or Edge of a Stressed Member**: The different configurations for this joint class are shown in Figs. (6.14, 6.15, 6.16).
5. **Load-Carrying Fillet and T Butt Welds**: The different configurations for this joint class are shown in Figs. (6.17, 6.18, 6.19, 6.20).
6. **Details in Welded Girders**: The different configurations for this joint class are shown in Figs. (6.21, 6.22, 6.23, 6.24, 6.25).
7. **Details in Tubular Members**: The different configurations for this joint class are shown in Figs. (6.26, 6.27, 6.28, 6.29, 6.30, 6.31).

6.5.6.2 AASHTO - Standard Specifications for Highway Bridges

The current AASHTO Specifications [29] contain provisions for the fatigue design of steel bridge details. These provisions are based on a set of fatigue resistance curves which define the strength of different classes of details. The curves were developed from an extensive research program sponsored by the Natinal Cooperative Highway Research Program (NCHRP) under th direction of the Transportation Research Board. The program, conducted over a periond of 6 years from 1966 to 1972, involved the fatigue testing of 800 full sized, welded steel bridge details. The test data was reported in two reports, [30], [31].

The statistically designed experimental program was conducted under controlled conditions so that analysis of the test data would reveal the parameters that

were significant in describing fatigue behavior. The result was the quantification of th efatigue strength of welded bridge details and the development of comprehensive design and specification provisions.

In an additional project, documented in [32], new fatigue test data from a variety of sources has been analysed to determine if changes to the original set of curves were required. As a result of this project several minor adjustments have been made to the original AASHTO fatigue design curves. Table (6.1) lists the curve parameters for the lower bound fatigue design curves.

6.5.6.3 Germanischer Lloyd: Fatigue Design Requirements

The Rules of Germanischer Lloyd for the hull contain requirements for the assessment of fatigue strength of hull structural elements since the 1978 edition. These requirements were based on the German Industrial Standard for Cranes (DIN 15018).

In the 1992 edition of the hull rules completely revised fatigue strength requirements have been issued. These new requirements are based on the latest national and international development in the field of fatigue design (IIW, Eurocode).

Germanischer Lloyd requires a fatigue strength analysis for all structures, which are predominantly subjected to cyclic loads such as side framing and side longitudinals.

The design S-N curves for the calculation of the cumulative damage ratio are shown in Fig. (6.3). The S-N curves represent the lower limit of the scatter band of 95% of all test results available (corresponding to 97.5% survivial probability).

6.6 Implementation of Selection System

6.6.1 Purpose

With the implementation of the S-N curve database, all information necessary for the development of a system for the selection of S-N curves is available. Since the selection rules are also included in the database it is only necessary to develop a set of database queries that are invoked based on user input that evaluate the available *rules*.

The selection system is primarily intended to simplify the choice of the appropriate S-N curve for a given structural detail. The information contained in the S-N curve database can in general be used to develop applications for the following purposes:

- Selection of the appropriate S-N curve for a given purpose. For a given detail the user selects the S-N curve based on the detail configuration, e.g. type of joint, type of weld, etc.
- Choice of a *known* S-N curve. The S-N curve database can be used to perform the input of a required S-N curve into an analysis software. This will prohibit input errors and allows easy updating.
- Comparison of S-N curves from different sources. Having S-N curves from many different sources included in the database makes it possible to compare individual curves from different organizations.

In general the use of a centralized database for S-N curves is very beneficial and will facilitate the use of the different S-N curves. In this project only the implementation of the system for the selection of S-N curves is described.

6.6.2 Implementation

The implementation of the system for the selection of S-N curves is based on the representation of the selection *rules* contained in the S-N database. The rules contain information or requirements for the following detail characteristics:

- Joint type
- Weld
- Defects
- Inspections
- Loading
- Location
- Dimensions

By using the build-in *query* capabilities of commercial database systems, it is possible to analyse the S-N curve database and select the appropriate curve for a given configuration.

The implementation of the selection system is in principle nothing more than the formalization of a query pattern. The advantage of a selection system is that it is not necessary for the user to know details about the underlying database system. In addition unautorized or accidental alterations of the S-N database can be prevented.

However, the implementation of the selection system does not have the flexibility that the use of direct database queries has. In practice, a combination of the two approaches is desirable, where the access to the actual database is limited to authorized users.

In the following the structure of a basic selection procedure is described. This procedure will be implemented in the *working model* described in section 6.7. Fig. (6.32) shows a flow diagram of the selection process.

The user will have the choice to select an S-N curve from one specific class or from all classes available in the database. Based on this choice a list of available *joint* types will be displayed. One *joint* type has to be selected.

For the selected *joint* type the user has to select a specific *weld* type from the list of available *weld* types. This process continues for the choice of *defects*, *Inspections*, *Loadings*, *Locations* and *Dimensions*.

In general, this process will result in one or more S-N curves that match the selected criteria. In the case that the user does not find a suitable choice in one of the selection criteria, no appropriate S-N curve is contained in the database.

In a second level of development, alternative selection procedures have to be implemented that allow more flexibility in the selection process.

6.7 Working Model

6.7.1 Software

The S-N database has been implemented based on the data structure shown in Fig. (6.1) using a commercially available database development software, **Microsoft Access 1.1** [1] . The software requires an IBM compatible PC with a minimum of 2MB of RAM (4MB recommended) running Microsoft Windows 3.1.

Usage information for **Microsoft Access 1.1** can be found in [33], [34]. A language reference is contained in [35]. Information about programming in **Microsoft Access Basic** is contained in [36].

The implementation of the working model is to a large extent based on the use of *Forms*, *Queries*, *Tables* and *Macros*.

6.7.2 Database Input

The S-N curve information for each of the three sources has been input into the database. In addition the selection rules have been implemented based on the usage guidance given for the three sets of S-N curves.

The input data for the **CURVE** relation is shown in Table (6.2. Table (6.3 contains the input for the **CLASS** relation. The joint descriptions, which are based on the joint classification found in the UKDEn guidance manual, are contained in relation **JOINT** and are listed in Table (6.4.

The input for the **WELD**, **DEFECTS**, **MATERIAL** and **INSPECTIONS** relations are shown in Tables (6.5,6.6,6.9, 6.14) respectively. The input for the **DIMENSIONS** relation is shown in Table (6.10). The data that links the dimensions and the rules, which is contained in relation **DIMENSIONS_IN_RULE**, is shown in Tables (6.11, 6.12, 6.13).

The input data for the **RULE** relation is shown for the individual classes. Tables (6.15, 6.16, 6.17, 6.18) show the rule input for the four UKDEn S-N curve classes. Tables (6.19, 6.20) show the rule input for the Germanischer Lloyd S-N curves. Finally, Table (6.21) contains the rule input for the AASHTO S-N curves.

This data forms the *knowledge base* for the implemented working model.

6.7.3 Program Capabilities

The program has been designed for the dual use as a database management system and as a system for the selection of S-N curves. The program allows it to enter data for all the relations of the S-N database.

The selection system is implemented based on the flow diagram shown in Fig. (6.32). In addition it is possible to simply choose one of the S-N curves of a particular class of curves.

The implementation is mainly intended as a demonstration of the advantages and benefits of the S-N curve database. The program allows it to manipulate data directly using the built-in query and data editing capabilities of **Microsoft Access**.

[1] Microsoft Access 1.1, Relational Database Management System for Windows, Microsoft Corporation, 1992

6.7.4 Program Documentation and Usage

The software is based on the data contained in the S-N curve database. The user interface and the selection system have been developed with the help of `forms` and `queries`.

All necessary components are contained in the file **SNDBASE.MDB** that is contained on the disk, which is enclosed with this report. In order to use the program it is necessary that `Microsoft Access 1.1` is installed on the computer.

In order to use the built-in query and data editing capabilities it is strongly advised to review the basic commands and concepts of `Microsoft Access`.

The main screen of the program displays four buttons that perform different tasks:

- `Enter Data`: Displays the Enter Data switchboard that allows it to enter new data for each of the relations used in the database.
- `Select S-N Curve`: Displays the Select S-N curve switchboard that offers different choices for the selection of S-N curves
- `Database Window`: Display the Microsoft Access user interface
- `Exit Microsoft Access`: Exit Microsoft Access and return to Windows

6.8 Conclusions

As part of the FACTS project a system for the selection of S-N curves has been developed. The basis for this system is a database for S-N curves. The data structure for this database has been developed and S-N data from three sources has been entered in order to test and validate the developed structure.

The the development of the S-N database was necessary for the implementation of the *system for the selection of S-N curves*. This system uses the S-N database as the *knowledge base*. Therefore the rules that govern the choice of a particular S-N curve for a specific configuration have been included in the database.

A working model of the selection system has been defined and implemented. The purpose of the implementation was to demonstrate the advantages of the selection system and to provide a core system suitable for further development.

The experience gained designing, implementing and testing the *System for the Selection of S-N Curves* makes it possible to draw the following conclusions:

- A centralized database for S-N curves from different sources greatly enhances the availability of fatigue strength information and makes it possible to easily compare curves from different sources. Using the database as the input source for the fatigue strength information that is required input for most fatigue life calculation ensures that consistent and up-to-date data is used for calculations.
- The data input for the three distinct groups of S-N curves indicates that it is possible to categorize the rules for the S-N curve selection using the developed data structure.
- The developed data structure is flexible enough to allow S-N curves from various sources to be entered.

- The implementation of the selection rules as part of the database makes it possible to use the built-in *query* capabilities of the commercial database software (**Microsoft Access**) for selection requirements that are currently not implemented.

that has been designed to developed.

Table 6.1: General Equation and Coefficients for AASHTO lower Bound Fatigue Design Curves

General Equation:

$$N = A \times S_r^{-3.0}$$

where:

N estimated minimum number of cycles to failure
S_r allowable stress range, ksi
A constant as listed below

Category	Constant A
A	2.510^{10}
$\bar{B}$	1.19110^{10}
$\bar{B}'$	6.10910^{9}
$\bar{C}$	4.44610^{9}
$\bar{D}$	2.18310^{9}
$\bar{E}$	1.07210^{9}
$\bar{E}'$	3.90810^{8}

Table 6.2: Data for CURVE relation

Curve	Class	Name	σ_D	σ_M	C1	C2	m1	m2	N1	N2	N3	SDev	a
1	7	AA_A	160.02	224.65	13.36	13.36	3	3	2E6	5E6		0.22	2
2	7	AA_B	124.98	156.61	12.89	12.89	3	3	2E6	5E6		0.14	2
3	7	AA_B1	100.04	125.37	12.6	12.6	3	3	2E6	5E6		0.14	2
4	7	AA_C	89.99	99.12	12.29	12.29	3	3	2E6	5E6		0.06	2
5	7	AA_D	70.99	83.8	12.07	12.07	3	3	2E6	5E6		0.10	2
6	7	AA_E	56.01	65.4	11.75	11.75	3	3	2E6	5E6		0.10	2
7	7	AA_E1	40.01	46.72	11.31	11.31	3	3	2E6	5E6		0.10	2
1	5	GL160	160	217.5	13.31	17.46	3	5	2E6	5E6		0.2	2
2	5	GL140	140	190.31	13.14	17.17	3	5	2E6	5E6		0.2	2
3	5	GL125	125	169.92	12.99	16.92	3	5	2E6	5E6		0.2	2
4	5	GL112	112	152.25	12.85	16.68	3	5	2E6	5E6		0.2	2
5	5	GL100	100	135.94	12.7	16.44	3	5	2E6	5E6		0.2	2
6	5	GL90	90	122.34	12.56	16.21	3	5	2E6	5E6		0.2	2
7	5	GL80	80	108.75	12.41	15.95	3	5	2E6	5E6		0.2	2
8	5	GL71	71	96.51	12.25	15.69	3	5	2E6	5E6		0.2	2
9	5	GL63	63	85.64	12.1	15.43	3	5	2E6	5E6		0.2	2
10	5	GL56	56	76.12	11.95	15.18	3	5	2E6	5E6		0.2	2
11	5	GL50	50	67.97	11.8	14.93	3	5	2E6	5E6		0.2	2
12	5	GL45	45	61.17	11.66	14.7	3	5	2E6	5E6		0.2	2
13	5	GL40	40	54.37	11.51	14.45	3	5	2E6	5E6		0.2	2
14	5	GL36	36	48.94	11.37	14.22	3	5	2E6	5E6		0.2	2
1	2	UKDEN_B	150.01	185	15.07	15.07	4	4	2E6	1E7	1E15	0.18	2
2	2	UKDEN_C	123.84	161.99	13.73	13.73	3.5	3.5	2E6	1E7	5E13	0.20	2
3	2	UKDEN_D	91.25	125.86	12.3	12.3	3	3	2E6	1E7	2E12	0.21	2
4	2	UKDEN_E	80.3	118.02	12.22	12.22	3	3	2E6	1E7	2E12	0.25	2
5	2	UKDEN_F	68.1	95.2	11.94	11.94	3	3	2E6	1E7	9E11	0.22	2
6	2	UKDEN_F2	59.94	85.05	11.79	11.79	3	3	2E6	1E7	6E11	0.23	2
7	2	UKDEN_G	49.85	65.64	11.45	11.45	3	3	2E6	1E7	3E11	0.18	2
8	2	UKDEN_W	42.85	56.89	11.27	11.27	3	3	2E6	1E7	2E11	0.18	2
1	3	UKDEN_B	150.01	185	15.37	15.37	4	4	2E6	1E7	2E8	0.18	2
2	3	UKDEN_C	123.84	161.99	14.03	14.03	3.5	3.5	2E6	1E7	2E8	0.20	2
3	3	UKDEN_D	91.25	125.86	12.6	12.6	3	3	2E6	1E7	2E8	0.21	2
4	3	UKDEN_E	80.3	118.02	12.52	12.52	3	3	2E6	1E7	2E8	0.25	2
5	3	UKDEN_F	68.1	95.2	12.24	12.24	3	3	2E6	1E7	2E8	0.22	2
6	3	UKDEN_F2	59.94	85.05	12.09	12.09	3	3	2E6	1E7	2E8	0.23	2
7	3	UKDEN_G	49.85	65.64	11.75	11.75	3	3	2E6	1E7	2E8	0.18	2
8	3	UKDEN_W	42.85	56.89	11.57	11.57	3	3	2E6	1E7	2E8	0.18	2
1	1	UKDEN_B	150.01	185	15.37	17.01	4	5	2E6	1E7	2E8	0.18	2
2	1	UKDEN_C	123.84	161.99	14.03	16.47	3.5	5	2E6	1E7	2E8	0.20	2
3	1	UKDEN_D	91.25	125.86	12.6	15.63	3	5	2E6	1E7	2E8	0.21	2
4	1	UKDEN_E	80.3	118.02	12.52	15.37	3	5	2E6	1E7	2E8	0.25	2
5	1	UKDEN_F	68.1	95.2	12.24	15	3	5	2E6	1E7	2E8	0.22	2
6	1	UKDEN_F2	59.94	85.05	12.09	14.72	3	5	2E6	1E7	2E8	0.23	2
7	1	UKDEN_G	49.85	65.64	11.75	14.32	3	5	2E6	1E7	2E8	0.183	2
8	1	UKDEN_W	42.85	56.89	11.57	14	3	5	2E6	1E7	2E8	0.18	2
15	5	GL120PL	120	127.68	16.83	24.62	5	9	2E6	5E6		0.2	2
16	5	GL100PL	100	106.4	16.44	23.91	5	9	2E6	5E6		0.2	2
1	4	UKDEN_HT	116.51	154.08	12.86	12.86	3	3	2E6	1E7	2E8	0.18	2

Table 6.3: Data for CLASS relation

ID	Name	Reference	Mat	Stress	Env	Memo
1	UKDEN_Air	[28]	1	1	1	
2	UKDEN_Cor_Noprotect	[28]	1	1	1	
3	UKDEN_Cor_Protect	[28]	1	1	1	
4	UKDEN_HotSpot	[28]	1	2	1	
5	GL_Nominal	[37]	1	1	1	
7	AASHTO	[32]	1	1	1	

Table 6.4: Data for JOINT relation

ID	Name	Picture	Memo
1	Plain Material		
2	Continuous Longitudinal Weld		
3	Transvers Butt Welds		
4	Welded Attachments		
5	Load-Carrying Fillet and T Butt Welds		
6	Details in Welded Girders		
7	Details in Tubular Members		

Table 6.5: Data for WELD relation

ID	Name	Type	Process	Position	Location	Memo
1	Full Pen. Butt Weld	on permanent backing	n/a	n/a	n/a	
2	Full Pen. Butt Weld	not submerged arc	manual	Flat Pos	shop	
3	Full Pen. Butt Weld	submerged arc	n/a	n/a	n/a	
4	Full Pen. Butt Weld	not submerged arc	n/a	not Flat Pos	n/a	
5	Full Pen. Butt Weld	n/a	n/a	n/a	not shop	
6	Full Pen. Butt Weld	submerged arc	auto	n/a	n/a	
7	Full Pen. Butt Weld	open arc	auto	n/a	n/a	
8	Fillet Weld	submerged arc	auto	n/a	n/a	
9	Fillet Weld	open arc	auto	n/a	n/a	
10	Fillet Weld	n/a	n/a	n/a	n/a	
11	Full Pen. Butt Weld	not submerged arc	auto	Flat Pos	shop	
12	Tack Weld	n/a	n/a	n/a	n/a	
13	No Weld	n/a	n/a	n/a	n/a	
14	Full Pen. Butt Weld	one-sided (no backing)	n/a	n/a	n/a	
15	Full Pen. Butt Weld	n/a	auto	n/a	n/a	
16	Fillet Weld	n/a	auto	n/a	n/a	
17	Full Pen. Butt Weld	n/a	manual	n/a	n/a	
18	Fillet Weld	n/a	manual	n/a	n/a	
19	Intermittent Fillet Weld	n/a	n/a	n/a	n/a	
20	Full Pen. Groove Weld	n/a	n/a	n/a	n/a	
21	Partial Pen. Groove Weld	n/a	n/a	n/a	n/a	

153

Table 6.6: Data for DEFECTS relation

ID	Required	Machining	Not_Allowed	Memo
1	As rolled w/o flame-cut edges	n/a	stress concentrations	
2	As rolled w/ flame-cut edges	ground	visible signs of drag lines	
3	As rolled w/ machine flame-cut edges	n/a	cracks in surface	
4	weld overfill dressed flush	finish-machined	significant defects in weld	
5	n/a	n/a	stop-start positions	
6	n/a	n/a	n/a	
7	weld overfill dressed flush	n/a	significant defects in weld	
8	smooth profile at the weld toe of stressed element	n/a	n/a	
9	weld ends ground to specified radius	n/a	n/a	
10	n/a	ground	undercutting	
11	Ar rolled w/ flame-cut edges	n/a	cracks and severe notches	

Table 6.7: Data for LOADING relation

ID	Name	Memo
1	Axial	
2	Bending	
8	Bending and Shear	
9	Axial (any direction)	

Table 6.8: Data for LOCATION relation

ID	Name	Memo
1	Plate edge	
2	Parent metal	
3	Weld metal	
4	Parent or weld metal	
5	Parent metal at weld toe	
9	Parent metal at cope hole	
10	Weld throat	

Table 6.9: Data for MATERIAL relation

ID	Name	Memo
1	Steel	

Table 6.10: Data for DIMENSIONS relation

Dim	Part_1	≤	≥	Part_2
5	Edge Distance		10 mm	
6	Member 1	1.15 * Thickness		Member 2
7	Attachment Length		150 mm	
8	Attachment Length	150 mm		
9	Edge Distance	10 mm		
10	Weld End Radius		1.25 * thickness	
11	Slope	1:5		
12	Slope	1:3		
13	Slope	1:2		
14	Cope Hole	30% of Web		
15	Cope Hole		30% of Web	
16	Attachment Length	300 mm	150 mm	
17	Attachment Length		300 mm	
18	Cover Plate thickness	0.7 web thickness		
19	Cover Plate thickness	1.5 web thickness	0.7 web thickness	
20	Cover Plate thickness		1.5 web thickness	
21	Diameter	50 mm		
22	Diameter		50 mm	
23	Slope	1:2.5		
24	Distance from Flange		4 * web thickness	
25	Attachment Length	50 mm		
26	Attachment Length	100	50	
27	Attachment Length		100	
28	Flange Thickness	20 mm		
29	Flange Thickness		20 mm	

Table 6.11: Data for DIMENSIONS_IN_RULE relation

Rule	Curve	Class	Dimensions
42	3	1	5
43	3	1	5
44	3	1	5
45	3	1	5
49	4	1	6
54	5	1	5
54	5	1	7
55	5	1	8
55	5	1	9
57	5	1	5
58	5	1	5
60	5	1	8
63	6	1	10
64	6	1	7
64	6	1	9
65	6	1	7
65	6	1	5
67	6	1	5
69	7	1	9
70	7	1	9
71	7	1	9
73	7	1	9
74	7	1	9
81	5	5	11
82	6	5	12
83	7	5	13
84	7	5	11
85	8	5	12
86	9	5	13
87	4	5	11
88	5	5	12
94	8	5	14
95	8	5	15
96	8	5	8
97	9	5	16
98	10	5	17
99	11	5	8
100	12	5	16
101	13	5	17
108	10	5	18
109	11	5	19

Table 6.12: Data for DIMENSIONS_IN_RULE relation (cont.)

Rule	Curve	Class	Dimensions
110	12	5	20
112	8	5	21
113	9	5	22
127	2	7	23
128	4	7	23
129	2	7	23
130	4	7	23
131	4	7	24
133	5	7	26
134	6	7	27
136	6	7	28
137	7	7	29
330	3	2	5
331	3	2	5
332	3	2	5
333	3	2	5
337	4	2	6
342	5	2	5
342	5	2	7
343	5	2	8
343	5	2	9
345	5	2	5
346	5	2	5
348	5	2	8
351	6	2	10
352	6	2	7
352	6	2	9
353	6	2	5
353	6	2	7
355	6	2	5
357	7	2	9
358	7	2	9
359	7	2	9
361	7	2	9
362	7	2	9
379	3	3	5
380	3	3	5
381	3	3	5
382	3	3	5
386	4	3	6

Table 6.13: Data for DIMENSIONS_IN_RULE relation (cont.)

Rule	Curve	Class	Dimensions	
391	5	3	5	
391	5	3	7	
392	5	3	8	
392	5	3	9	
394	5	3	5	
395	5	3	5	
397	5	3	8	
400	6	3	10	
401	6	3	7	
401	6	3	9	
402	6	3	5	
402	6	3	7	
404	6	3	5	
406	7	3	9	
407	7	3	9	
408	7	3	9	
410	7	3	9	
411	7	3	9	
439	1	4	5	
439	1	4	7	
440	1	4	8	
440	1	4	9	
442	1	4	5	
443	1	4	5	
445	1	4	8	
448	1	4	10	
449	1	4	7	
449	1	4	9	
450	1	4	5	
450	1	4	7	
452	1	4	5	
454	1	4	9	
455	1	4	9	
456	1	4	9	
458	1	4	9	
459	1	4	9	

Table 6.14: Data for INSPECTION relation

ID	Testmethod	%of_Material	Memo
1	Nondestructive Testing	100	
2	Visual	100	
3	n/a	0	

Table 6.15: Data for RULE relation (Class 1

ID	Curve	Class	Joint	Weld	Defects	Insp	Load	Loc	Pic
27	1	1	1	13	1	3	1	2	
28	1	1	1	13	2	3	1	2	
29	1	1	1	13	3	3	2	2	
30	2	1	1	5	4	1	1	4	
31	2	1	1	13	3	3	2	2	
32	2	1	1	13	3	3	1	2	
33	2	1	2	7	5	3	1	4	
34	2	1	2	6	5	3	1	4	
35	2	1	2	8	5	3	1	4	
36	2	1	2	9	5	3	1	4	
37	2	1	3	5	4	1	1	4	
40	2	1	3	5	4	1	1	4	
41	2	1	7	5	7	1	1	2	
42	3	1	2	6	6	1	1	4	
43	3	1	2	7	6	3	1	4	
44	3	1	2	8	6	3	1	4	
45	3	1	2	9	6	3	1	4	
46	3	1	3	11	6	3	1	4	
47	3	1	7	5	6	3	1	4	
48	4	1	3	5	6	3	1	4	
49	4	1	3	6	6	3	1		
50	4	1	6	5	6	3	8	4	
51	4	1	6	12	6	3	1	2	
52	4	1	7	5	6	3	1	2	
53	5	1	3	1	6	3	1	4	
54	5	1	4	10	6	3	1	2	
55	5	1	4	5	6	3	9	2	
56	5	1	5	5	10	3	1	2	
57	5	1	6	10	6	3	2	2	
58	5	1	6	10	6	3	1	2	
59	5	1	6	12	6	3	1	9	
60	5	1	7	10	6	3	1	5	
61	5	1	7	5	6	3	1	5	
62	5	1	7	1	6	3	1	5	
63	6	1	3	5	6	3	1	4	
64	6	1	4	10	6	3	1	5	
65	6	1	4	5	6	3	9	5	
66	6	1	5	10	10	3	1	10	
67	6	1	5	10	9	3	1	5	
68	6	1	7	14	9	3	2	5	
69	7	1	4	5	6	3	1	5	
70	7	1	4	5	6	3	9	5	
71	7	1	5	10	6	3	1	5	
72	7	1	5	10	6	3	1	5	
73	7	1	6	10	6	3	1	5	
74	7	1	6	10	6	3	1	5	
75	7	1	6	10	6	3	2	5	
76	8	1	7	5	6	3	1	10	

Table 6.16: Data for RULE relation (Class 2)

ID	Curve	Class	Joint	Weld	Defects	Insp	Load	Loc	Pic
317	1	2	1	13	1	3	1	2	
318	1	2	1	13	2	3	1	2	
319	1	2	1	13	3	3	2	2	
320	2	2	1	5	4	1	1	4	
321	2	2	1	13	3	3	2	2	
322	2	2	1	13	3	3	1	2	
323	2	2	2	7	5	3	1	4	
324	2	2	2	6	5	3	1	4	
325	2	2	2	8	5	3	1	4	
326	2	2	2	9	5	3	1	4	
327	2	2	3	5	4	1	1	4	
328	2	2	3	5	4	1	1	4	
329	2	2	7	5	7	1	1	2	
330	3	2	2	6	6	1	1	4	
331	3	2	2	7	6	3	1	4	
332	3	2	2	8	6	3	1	4	
333	3	2	2	9	6	3	1	4	
334	3	2	3	11	6	3	1	4	
335	3	2	7	5	6	3	1	4	
336	4	2	3	5	6	3	1		
337	4	2	3	6	6	3	8	4	
338	4	2	6	5	6	3	1	2	
339	4	2	6	12	6	3	1	2	
340	4	2	7	5	6	3	1	4	
341	5	2	3	1	6	3	1	2	
342	5	2	4	10	6	3	9	2	
343	5	2	4	5	6	3	1	2	
344	5	2	5	5	10	3	2	2	
345	5	2	6	10	6	3	1	2	
346	5	2	6	10	6	3	1	9	
347	5	2	6	12	6	3	1	5	
348	5	2	7	10	6	3	1	5	
349	5	2	7	5	6	3	1	5	
350	5	2	7	1	6	3	1	4	
351	6	2	3	5	6	3	1	5	
352	6	2	4	10	6	3	9	5	
353	6	2	4	5	6	3	1	10	
354	6	2	5	10	10	3	1	5	
355	6	2	5	10	9	3	2	5	
356	6	2	7	14	9	3	1	5	
357	7	2	4	5	6	3	9	5	
358	7	2	4	5	6	3	1	5	
359	7	2	5	10	6	3	1	5	
360	7	2	5	10	6	3	1	5	
361	7	2	6	10	6	3	1	5	
362	7	2	6	10	6	3	2	5	
363	7	2	6	10	6	3	1	10	
364	8	2	7	5	6	3			

Table 6.17: Data for RULE relation (Class 3)

ID	Curve	Class	Joint	Weld	Defects	Insp	Load	Loc	Pic
2366	1	3	1	13	1	3	1	2	
367	1	3	1	13	2	3	1	2	
368	1	3	1	13	3	3	2	2	
369	2	3	1	5	4	1	1	4	
370	2	3	1	13	3	3	2	2	
371	2	3	1	13	3	3	1	2	
372	2	3	2	7	5	3	1	4	
373	2	3	2	6	5	3	1	4	
374	2	3	2	8	5	3	1	4	
375	2	3	2	9	5	3	1	4	
376	2	3	3	5	4	1	1	4	
377	2	3	3	5	4	1	1	4	
378	2	3	7	5	7	1	1	2	
379	3	3	2	6	6	1	1	4	
380	3	3	2	7	6	3	1	4	
381	3	3	2	8	6	3	1	4	
382	3	3	2	9	6	3	1	4	
383	3	3	3	11	6	3	1	4	
384	3	3	7	5	6	3	1	4	
385	4	3	3	5	6	3	1	4	
386	4	3	3	6	6	3	1		
387	4	3	6	5	6	3	8	4	
388	4	3	6	12	6	3	1	2	
389	4	3	7	5	6	3	1	2	
390	5	3	3	1	6	3	1	4	
391	5	3	4	10	6	3	1	2	
392	5	3	4	5	6	3	9	2	
393	5	3	5	5	10	3	1	2	
394	5	3	6	10	6	3	2	2	
395	5	3	6	10	6	3	1	2	
396	5	3	6	12	6	3	1	9	
397	5	3	7	10	6	3	1	5	
398	5	3	7	5	6	3	1	5	
399	5	3	7	1	6	3	1	5	
400	6	3	3	5	6	3	1	4	
401	6	3	4	10	6	3	1	5	
402	6	3	4	5	6	3	9	5	
403	6	3	5	10	10	3	1	10	
404	6	3	5	10	9	3	1	5	
405	6	3	7	14	9	3	2	5	
406	7	3	4	5	6	3	1	5	
407	7	3	4	5	6	3	9	5	
408	7	3	5	10	6	3	1	5	
409	7	3	5	10	6	3	1	5	
410	7	3	6	10	6	3	1	5	
411	7	3	6	10	6	3	1	5	
412	7	3	6	10	6	3	2	5	

Table 6.18: Data for RULE relation (Class 4

ID	Curve	Class	Joint	Weld	Defects	Insp	Load	Loc	Pic
438	1	4	3	1	6	3	1	4	
439	1	4	4	10	6	3	1	2	
440	1	4	4	5	6	3	9	2	
441	1	4	5	5	10	3	1	2	
442	1	4	6	10	6	3	2	2	
443	1	4	6	10	6	3	1	2	
444	1	4	6	12	6	3	1	9	
445	1	4	7	10	6	3	1	5	
446	1	4	7	5	6	3	1	5	
447	1	4	7	1	6	3	1	5	
448	1	4	3	5	6	3	1	4	
449	1	4	4	10	6	3	1	5	
450	1	4	4	5	6	3	9	5	
451	1	4	5	10	10	3	1	10	
452	1	4	5	10	9	3	1	5	
453	1	4	7	14	9	3	2	5	
454	1	4	4	5	6	3	1	5	
455	1	4	4	5	6	3	9	5	
456	1	4	5	10	6	3	1	5	
457	1	4	5	10	6	3	1	5	
458	1	4	6	10	6	3	1	5	
459	1	4	6	10	6	3	1	5	
460	1	4	6	10	6	3	2	5	

Table 6.19: Data for RULE relation (Class 5

ID	Curve	Class	Joint	Weld	Defects	Insp	Load	Loc	Pic
277	3	5	3	5	4	1	1	5	
78	5	5	3	2	6	1	1	5	
79	7	5	3	3	6	1	1	5	
80	8	5	3	1	6	3	1	3	
81	5	5	3	2	6	1	1	5	
82	6	5	3	2	6	1	1	5	
83	7	5	3	2	6	1	1	5	
84	7	5	3	3	6	3	1	5	
85	8	5	3	3	6	3	1	5	
86	9	5	3						
87	4	5	3	2	4	1	1	5	
88	5	5	3	2	4	1	1	5	
89	3	5	2	15	5	3	1	4	
90	4	5	2	16	5	3	1	4	
91	5	5	2	15	6	3	1	4	
92	5	5	2	18	6	3	1	4	
93	7	5	2	19	6	3	1	5	
94	8	5	2	19	6	3	1	9	
95	8	5	2	19	6	3	1	9	
96	8	5	4	10	6	3	1	5	
97	9	5	4	10	6	3	1	5	
98	10	5	4	10	6	3	1	5	
99	11	5	4	10	6	3	1	5	
100	12	5	4	10	6	3	1	5	
101	13	5	4	10	6	3	1	5	
102	7	5	6	10	6	3	1	5	
103	7	5	6	10	6	3	2	5	
104	7	5	6	10	6	3	1	5	
105	8	5	5	5	6	3	1	5	
106	9	5	5	10	6	3	1	5	
107	12	5	5	10	6	3	1	10	
108	10	5	6	10	6	3	1	5	
109	11	5	6	10	6	3	1	5	
110	12	5	6	10	6	3	1	5	
111	8	5	5	10	6	3	1	5	

Table 6.20: Data for RULE relation (Class 5) cont.

ID	Curve	Class	Joint	Weld	Defects	Insp	Load	Loc	Pic
112	8	5	7	18	6	3	1	5	
113	9	5	7	17	6	3	1	5	
114	15	5	1	13	3	3	1	1	
115	16	5	1		2	3	1	1	
188	5	5	3	2	6	1	1	5	
189	7	5	3	3	6	1	1	5	
190	8	5	3	1	6	3	1	3	
191	5	5	3	2	6	1	1	5	
192	6	5	3	2	6	1	1	5	
193	7	5	3	2	6	1	1	5	
194	7	5	3	3	6	3	1	5	
195	8	5	3	3	6	3	1	5	
197	4	5	3	2	4	1	1	5	
198	5	5	3	2	4	1	1	5	
199	3	5	2	15	5	3	1	4	
200	4	5	2	16	5	3	1	4	
201	5	5	2	15	6	3	1	4	
202	5	5	2	18	6	3	1	4	
203	7	5	2	19	6	3	1	5	
204	8	5	2	19	6	3	1	9	
205	8	5	2	19	6	3	1	9	
206	8	5	4	10	6	3	1	5	
207	9	5	4	10	6	3	1	5	
208	10	5	4	10	6	3	1	5	
209	11	5	4	10	6	3	1	5	
210	12	5	4	10	6	3	1	5	
211	13	5	4	10	6	3	1	5	
212	7	5	6	10	6	3	1	5	
213	7	5	6	10	6	3	2	5	
214	7	5	6	10	6	3	1	5	
215	8	5	5	5	6	3	1	5	
216	9	5	5	10	6	3	1	5	
217	12	5	5	10	6	3	1	10	
218	10	5	6	10	6	3	1	5	
219	11	5	6	10	6	3	1	5	
220	12	5	6	10	6	3	1	5	
221	8	5	5	10	6	3	1	5	
222	8	5	7	18	6	3	1	5	
223	9	5	7	17	6	3	1	1	
224	15	5	1	13	3	3	1	1	
225	16	5	1		2	3	1	1	

Table 6.21: Data for RULE relation (Class 7)

ID	Curve	Class	Joint	Weld	Defects	Insp	Load	Loc	Pic
2116	1	7	1	13	1	3	1	1	
118	2	7	3	5	4	1	1	4	
121	2	7	2	10	6	3	1	4	
122	2	7	2	20	6	3	1	4	
125	3	7	2	21	6	3	1	4	
126	4	7	3	5	6	1	1	4	
127	2	7	3	5	4	1	1	4	
128	4	7	3	5	6	1	1	4	
129	2	7	3	5	7	1	1	4	
130	4	7	3	5	6	1	1	4	
131	4	7	6	20	6	3	1	4	
132	4	7	6	10	6	3	1	5	
133	5	7	4	20	6	3	1	5	
134	6	7	4	20	6	3	1	5	
135	6	7	4	20	6	3	1	5	
136	6	7	6	20	6	3	1	5	
137	7	7	6	20	6	3	1	5	
138	6	7	6	19	6	3	1	5	
226	1	7	1	13	1	3	1	1	
228	2	7	3	5	4	1	1	4	
229	2	7	2	10	6	3	1	4	
230	2	7	2	20	6	3	1	4	
231	3	7	2	21	6	3	1	4	
232	4	7	3	5	6	1	1	4	
233	2	7	3	5	4	1	1	4	
234	4	7	3	5	6	1	1	4	
235	2	7	3	5	7	1	1	4	
236	4	7	3	5	6	1	1	4	
237	4	7	6	20	6	3	1	4	
238	4	7	6	10	6	3	1	5	
239	5	7	4	20	6	3	1	5	
240	6	7	4	20	6	3	1	5	
241	6	7	4	20	6	3	1	5	
242	6	7	6	20	6	3	1	5	
243	7	7	6	20	6	3	1	5	
244	6	7	6	19	6	3	1	5	

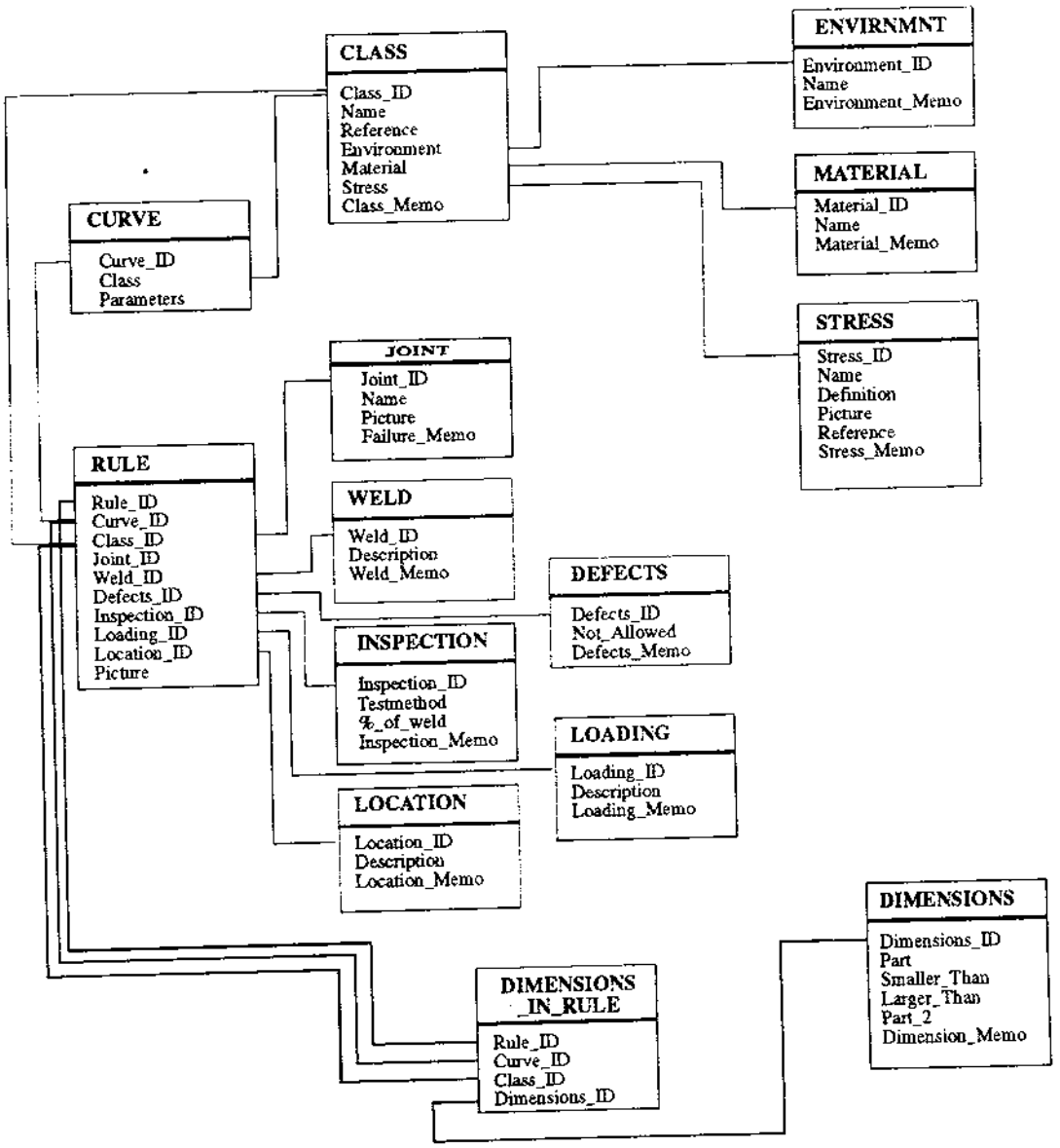

Figure 6.1: Structure of S-N Database

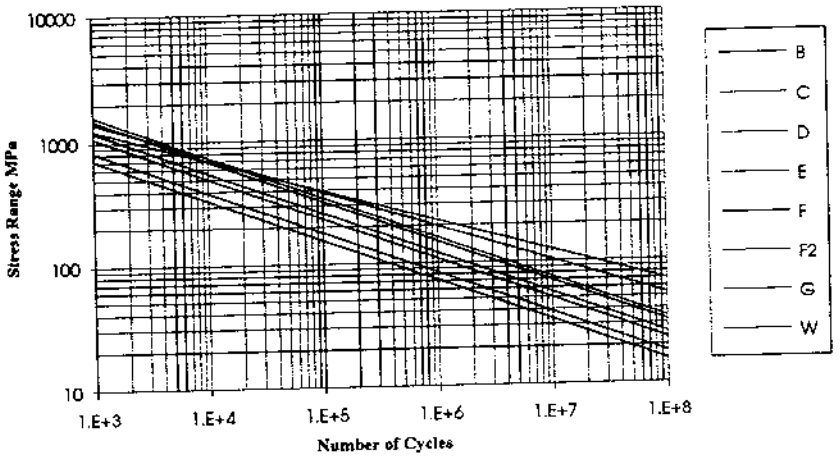

Figure 6.2: UKDEn Fatigue design S-N curve for planar welded joints

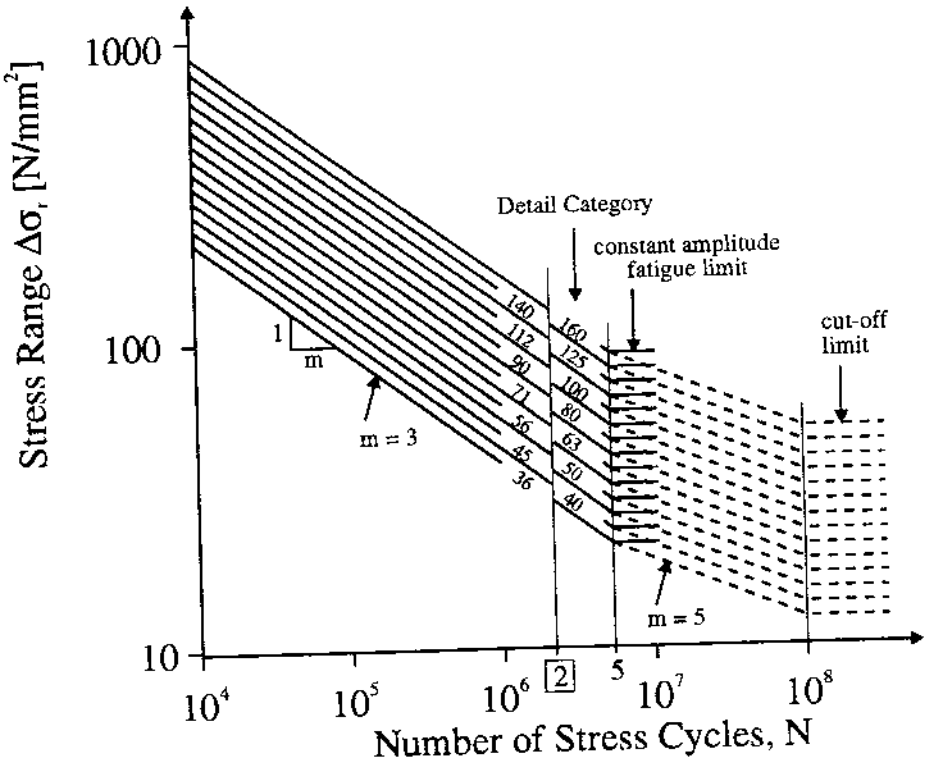

Figure 6.3: Fatigue design S-N curve for planar welded joints, IIW/ECCS

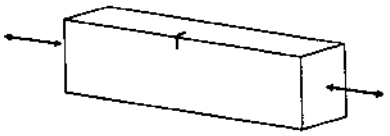

Figure 6.4: UKDEn Plain Material 1

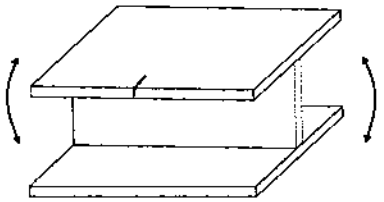

Figure 6.5: UKDEn Plain Material 2

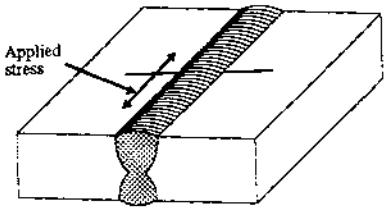

Figure 6.6: UKDEn Continous Weld 1

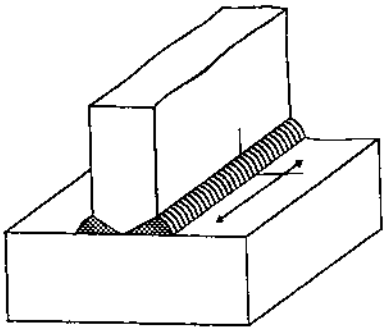

Figure 6.7: UKDEn Continous Weld 2

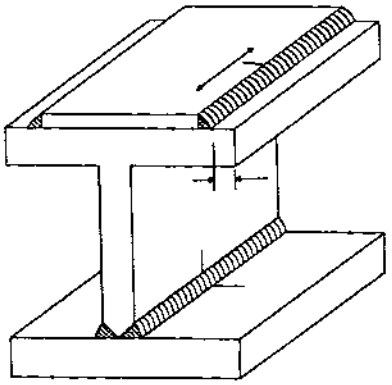

Figure 6.8: UKDEn Continous Weld 3

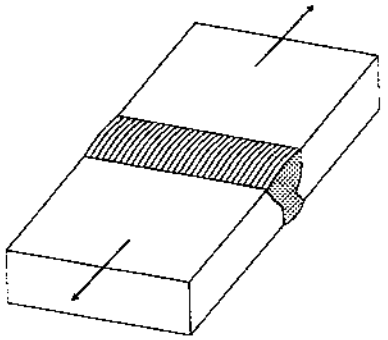

Figure 6.9: UKDEn Transverse Butt Weld 1

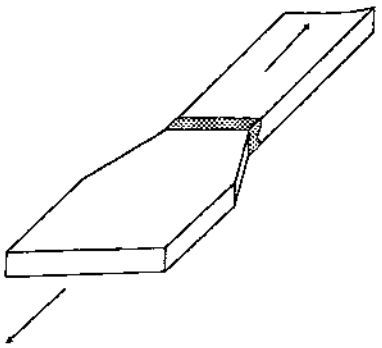

Figure 6.10: UKDEn Transverse Butt Weld 2

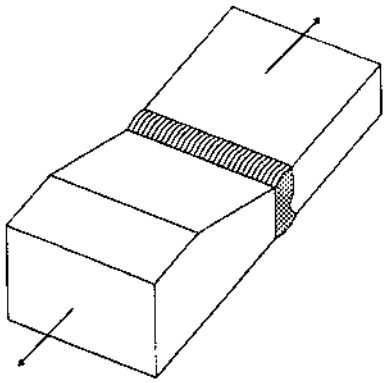

Figure 6.11: UKDEn Transverse Butt Weld 3

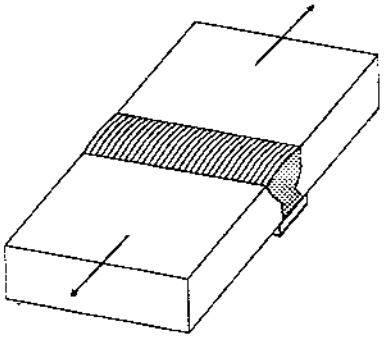

Figure 6.12: UKDEn Transverse Butt Weld 4

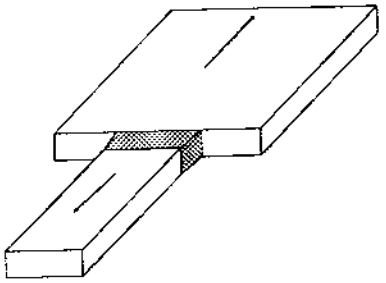

Figure 6.13: UKDEn Transverse Butt Weld 5

Figure 6.14: UKDEn Welded Attachment 1

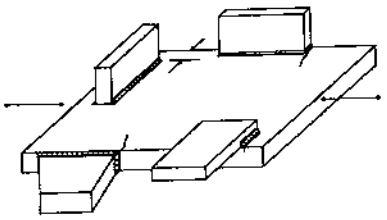

Figure 6.15: UKDEn Welded Attachment 2

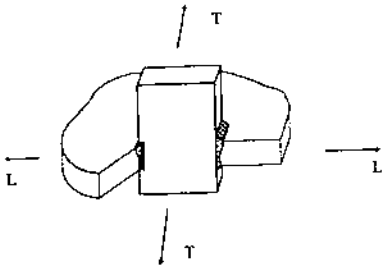

Figure 6.16: UKDEn Welded Attachment 3

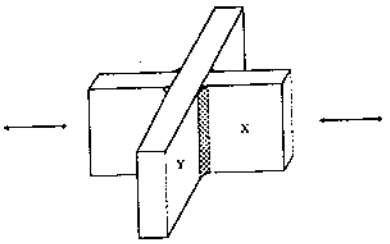

Figure 6.17: UKDEn Load Carrying Fillet and T Butt Weld 1

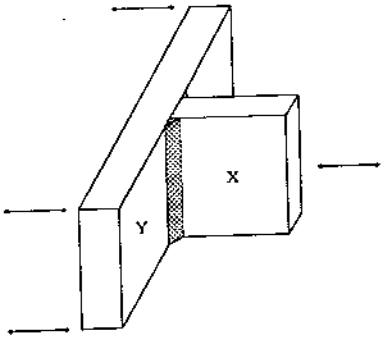

Figure 6.18: UKDEn Load Carrying Fillet and T Butt Weld 2

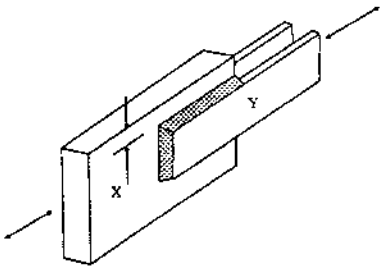

Figure 6.19: UKDEn Load Carrying Fillet and T Butt Weld 3

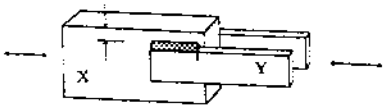

Figure 6.20: UKDEn Load Carrying Fillet and T Butt Weld 4

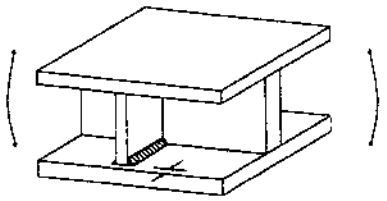

Figure 6.21: UKDEn Detail in Welded Girders 1

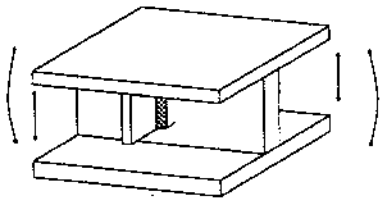

Figure 6.22: UKDEn Detail in Welded Girders 2

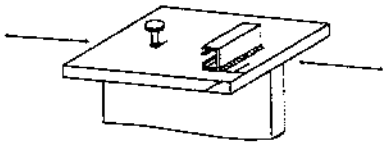

Figure 6.23: UKDEn Detail in Welded Girders 3

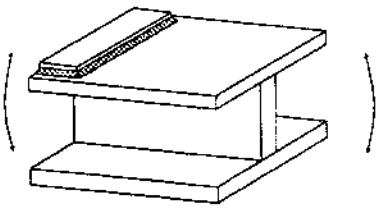

Figure 6.24: UKDEn Detail in Welded Girders 4

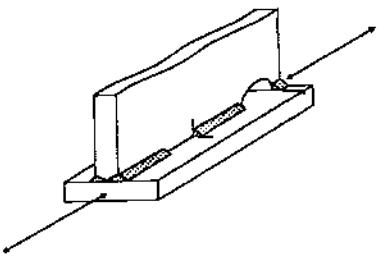

Figure 6.25: UKDEn Detail in Welded Girders 5

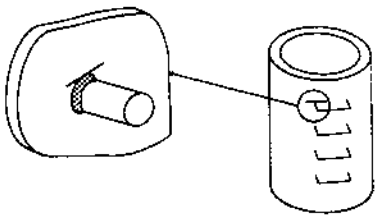

Figure 6.26: UKDEn Detail related to Tubular Members 1

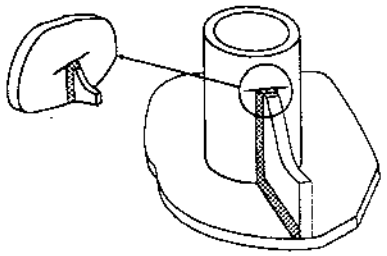

Figure 6.27: UKDEn Detail related to Tubular Members 2

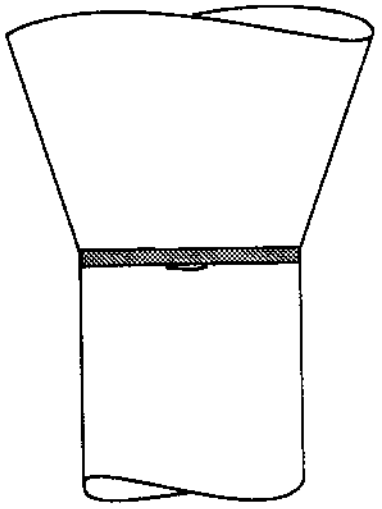

Figure 6.28: UKDEn Detail related to Tubular Members 4

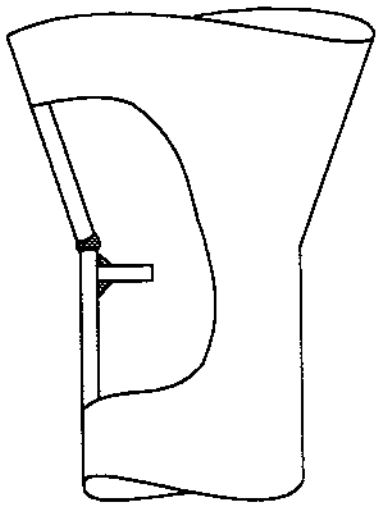

Figure 6.29: UKDEn Detail related to Tubular Members 5

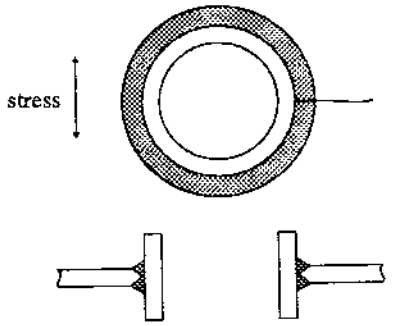

Figure 6.30: UKDEn Detail related to Tubular Members 6

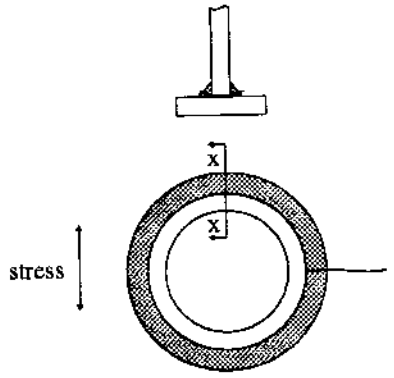

Figure 6.31: UKDEn Detail related to Tubular Members 7

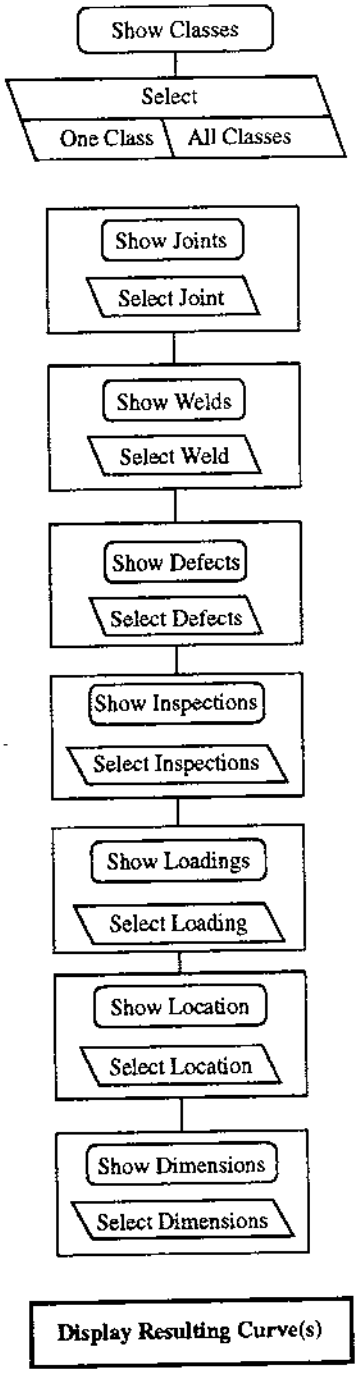

Figure 6.32: Flow Diagram of Selection Process

Bibliography

[1] R. Schulte-Strathaus and R. G. Bea. Verification study for tanker csd evaluation software. Technical Report SMP 1-8, Structural Maintenance for New and Existing Ships, 1992.

[2] M.A. Miner. Cumulative damage in fatigue. *Journal of Applied Mechanics - ASME*, (12), 1945.

[3] A. Palmgren. Die lebensdauer von kugellagern. *Zeitschrift des Vereins Deutscher Ingenieure*, (68(4)):339-341, 1924.

[4] C. Lindley, P.H. Bateson, S.E Webster, B. Lian, and F. Knight. Fatigue endurance under constant and variable amplitude loading of a welded quenched and tempered structural steel. In *Int. Conf. 'Welding -90'*, GKSS Research Center Geesthacht, Germany, 1990.

[5] S. Machida, H. Yajima, and M. Matoba. On the use of high tensile steels in marine structures. Technical Report Draft, International Ship Ship Structures Comitee (ISSC), 1991.

[6] E. Niemi. Recommendations concerning stress determination for fatigue analysis of welded components. Technical Report IIW - Doc. XIII-1458-92, International Institute of Welding, 1992.

[7] R. Schulte-Strathaus and R. G. Bea. Fatigue database development and analysis. Technical Report SMP 1-1, Structural Maintenance for New and Existing Ships, 1991.

[8] R.E. Peterson. *Stress Concentration Design Factors.* J. Wiley & Sons, 1974.

[9] G.P. Tilly and D.E. Nunn. Variable amplitude fatigue in relation to highway bridges. In *Vol. 194*, page 550. Proc. Institution of Mechanical Engineers, 1981.

[10] J.W Fisher, D.R. Mertz, and A. Zhong. Steel bridge members under variable amplitude long life fatigue loading. Technical report, National Cooperative Highway Research Program, 1983. Report 267.

177

PROJECT TECHNICAL COMMITTEE MEMBERS

The following persons were members of the committee that represented the Ship Structure Committee to the Contractor as resident subject matter experts. As such they performed technical review of the initial proposals to select the contractor, advised the contractor in cognizant matters pertaining to the contract of which the agencies were aware, performed technical review of the work in progress and edited the final report.

Chairman

Paul Cojeen	U. S. Coast Guard

Members

LT Robert Holzman	U. S. Coast Guard
Fred Seibold	Maritime Administration
Dr. Walter MacLean	U. S. Merchant Marine Academy
Chao Lin	Maritime Administration
Dr. Y-k Chen	American Bureau of Shipping
William Siekierka	Naval Sea Systems Command, Contracting Officer's Technical Representative
Dr. Robert Sielski	National Academy of Science, Marine Board Liaison
CDR Steve Sharpe	U.S. Coast Guard, Executive Director Ship Structure Committee

[11] U.K. Department of Energy, London. *Offshore Installations: Guidance on Design, Construction and Certification; Section 21:Steel*, fourth edition edition, January 1990.

[12] T.R. Gurney. Fatigue tests on fillet welded joints under variable amplitude loading. Technical report, The Welding Institute, 1985. Research Report 293.

[13] J.G. Wylde. Application of fatigue design rules for welded steel joints. Technical report, The Welding Institute, 1986. Research Report 298.

[14] J. Yagi, S. Machida, M. Matoba, Y. Tomita, and I. Soya. Thickness effect criterion for fatigue strength evaluation of welded steel structures. In *Vol. 115*, pages 58–65. Transaction of the ASME, 1993.

[15] Yung kuang Chen. Fatigue classification of ship structural details. Technical Report SMP 1-4, Structural Maintenance for New and Existing Ships, 1992.

[16] R. Forsyth, editor. *Expert Systems: Principles and case studies.* Chapman and Hall Computing, New York, 1984.

[17] D.T. Pham, editor. *Expert Systems in Engineering.* Springer Verlag, Berlin, 1988.

[18] R.K. Aggarwal. *Methodology for Assessment by Regulatory Bodies of the Safety of Existing Steel Offshore Platforms.* PhD thesis, Dept. of Civil Engineering, University of California, Berkeley, Berkeley, CA, 1991.

[19] C.J. Date. *An Introduction to Database Systems*, volume Vol. 1. Addison-Wesley, Reading,MA, 1987.

[20] G. Gardarin and P. Valduriez. *Relational Databases and Knowledge Bases.* Addison-Wesley, Reading,MA, 1989.

[21] E.F. Codd. A relational model of data for large shared data banks. In *CACM, V13, N6*, pages 377 – 87, June 1970.

[22] E.F. Codd. Relational completeness of data base sublanguages. In *Data Base Systems*, volume Vol. 6 of *Courant Computer Science Symposia Series.* Prentice-Hall, Englewood Cliffs, N.J., 1972.

[23] E.F. Codd. Further normalization of the data base relational model. In *Data Base Systems*, volume Vol. 6 of *Courant Computer Science Symposia Series.* Prentice-Hall, Englewood Cliffs, N.J., 1972.

[24] E.F. Codd. Recent investigations into relatinal data base systems. In *Proc. IFIP Congress*, 1974.

[25] R. Fagin. Multivalued dependencies and a new normal form for relational databases. In *ACM TODS 2*, Sept. 1977. No. 3.

[26] R. Fagin. Normal forms and relational database operators. In *Proc. ACM SIGMOD International Conference on Management of Data*, Sept. 1979.

[27] J.W. Fisher, R.J. Dexter, R. Roberts, B.T. Yen, G. Decorges, S.P. Pessiki, A.C. Nussbaumer, J.E. Tarquinio, G.R. Kober, M.L. Gentilcore, and S.M. Derrah. Structural failure modes for advanced double hull: Fatigue and fracutre failure modes. Technical report, Lehigh University, Bethlehem, Pennsylvania, 1993. Final Report for cooperative agreement N00014-91-CA-0001 TDL 91-01 Phase I.3(a).

[28] U.K. Department of Energy, London. *Offshore Installations: Guidance on Design, Construction and Certification; Section 21:Steel*, fourth edition edition, January 1990.

[29] American Association of State Highway and Transportation Officials (AASHTO). *AASHTO Standard Specifications for Highway Bridges*, thirteenth edition edition, 1983.

[30] J.W Fisher, K.H. Frank, M.A. Hirt, and B.M McNamee. Effects of weldments on the fatiuge trength of steel beams. Technical report, National Cooperative Highway Research Program, 1970. Report 102.

[31] J.W Fisher, P.A. Albrecht, B.T. Yen, D.J. Klingerman, and B.M. McNamee. Fatigue strength of steel beams with welded stiffeners and attachments. Technical report, National Cooperative Highway Research Program, 1974. Report 147.

[32] P.B. Keating and J.W Fisher. Evaluation of fatigue tests and design criteria on welded details. Technical report, National Cooperative Highway Research Program, 1986. Report 286.

[33] Microsoft Corporation. *Microsoft Access: User's Guide*, version 1.1 edition, 1992.

[34] C.N. Prague and M.R. Irwin. *Microsoft Access Bible.* IDG Books Worldwide, 1993.

[35] Microsoft Corporation. *Microsoft Access: Language Reference*, version 1.1 edition, 1992.

[36] N.C. Shammas. *Microsoft Access Programming.* Windcrest Books, 1993.

[37] Germanischer Lloyd. Germanischer lloyd: Fatigue strength requirements. In *Tanker Structures Cooperative Forum (TSCF)*, 1991.